Investigation of Flexible Bridge Deck Overlays in Kansas

by

Nahreen Mobasharah

B.S., Military Institute of Science and Technology, 2022

A THESIS

submitted in partial fulfillment of the requirements for the degree

MASTER OF SCIENCE

Department of Civil Engineering
Carl R Ice College of Engineering

KANSAS STATE UNIVERSITY
Manhattan, Kansas

2026

Approved by:

Major Professor
Mustaque Hossain

Copyright

Abstract

In Kansas, the bridges continuously deteriorate due to frequent freeze-thaw cycles and repeated traffic loads. Therefore, the bridge decks need to be overlaid intermittently. A hot-mix asphalt (HMA) overlay for bridge decks requires to be impermeable, friction-improved, and rut-resistant. This research focuses on determining whether modified Reflective Cracking Interlayer (RCI) mixtures, used on highways, can function effectively as a thin-bridge-deck overlay while also protecting the deck from moisture infiltration. This study used primary aggregates from the RCI mixtures, a gradation band based on the New Jersey Bridge Deck Wearing Surface Course, and a PG 70-28 RCI binder. Friction data from a freshly paved RCI overlay project showed an average Mean Profile Depth (MPD) of 0.021 in. (0.54 mm) and a mean British Pendulum Number of 82. While the RCI mixture meets the minimum MPD required by FHWA for highways, higher friction would be needed for an RCI-based HMA bridge deck overlay mix. In this study, the target design air voids at 50 gyrations for the HMA mix were 2.5±0.5% and an MPD of 0.039 in. (1 mm) or higher. Thirty-five trial gradations were assessed using the Laser Texture Scanner for friction, the falling-head permeability test for permeability, and the IDEAL-RT test for rutting. Concurrent Hamburg Wheel Tracking Device (HWTD) rutting tests were also conducted. The results showed that the initial fine-graded primary aggregate mixtures were impermeable but lacked sufficient friction. Adding calcined bauxite slightly increased the MPD. Subsequently, the study introduced secondary coarse aggregates in the mix design. Based on their volumetrics and MPD, five mix designs were selected. These mix designs achieved an MPD of 0.039 in. (1.0 mm) or higher, while all mixtures except one showed the nearly impermeable coefficient of permeability (k) of 0 to 1.97 $\times 10^{-5}$ in./s (0 to 5×10^{-5} cm/s). Although none of the mixtures met the target of 15,000 wheel passes at a 0.5 in. (12.5 mm) rut depth in the HWTD test, two mixtures exhibited higher rutting resistance.

Statistical analysis using Response Surface Methodology and constrained multi-response optimization quantified the relationships between mix design variables (air voids, dust content, and coarse aggregate and coarse sand contents) and the three performance responses. Only one mixture satisfied all three performance thresholds (MPD ≥ 0.039 in. (1.0 mm), $k \leq 1.97 \times 10^{-5}$ in./s (5×10^{-5} cm/s), RT Index ≥ 65), confirming it as the best-balanced mixture for bridge deck overlay

applications. The mathematical optimum identified within the design space indicated that achieving all three performance targets simultaneously requires a coarse, near-gap-graded mixture with low fines and low air voids.

Table of Contents

List of Figures

List of Tables

Acknowledgments

First, I would like to thank Almighty Allah for giving me strength, patience, and the opportunity to complete this thesis.

I want to express my sincere gratitude to my advisor, Dr. Mustaque Hossain, for his guidance, expertise, patience, encouragement, and continuous support throughout this research. His advice and mentorship were very important in completing this work.

I am grateful to my advisory committee members, Dr. Christopher A. Jones and Dr. Cen Wu, for their valuable suggestions, feedback, and support during my graduate study.

I would like to sincerely thank Dr. Xingdong Wu, Dr. Ya Gao, and Gibson Yu for their help, guidance, and support in different stages of this research. Their assistance was very valuable to me. I also appreciate the help of the undergraduate students Ayleen Gonzalez, Miles Cusick, and Ashley Xayyasaeng, who assisted during the project. I also acknowledge KSU Civil Engineering Department Research Technologist Clifford Temple, who assisted in this project whenever needed.

My sincere gratitude goes to Blair Heptig, P.E., from the Kansas Department of Transportation (KDOT), for his support and mentorship throughout this research. I am also thankful to the Kansas Department of Transportation (KDOT) for supporting this project.

I want to thank Flint Hills Resources (FHR) for providing the binder used in this study. I also sincerely acknowledge Dolese Bros. Co., Ideker, Inc., Hamm Olathe, Iron Mountain, Williams Diversified Materials, and Venture Corporation for providing the coarse aggregates used in this research.

Finally, I would like to thank my parents, my siblings, my family, my roommate, and everyone who supported, encouraged, and helped me throughout my graduate studies. Their support means a great deal to me.

List of Abbreviations

AADT	- Annual Average Daily Traffic
AV	- Air Voids (%)
ANOVA	- Analysis of Variance
AIC	- Akaike Information Criterion
BDWSC	- Bridge Deck Wearing Surface Course
BIC	- Bayesian Information Criterion
CTM	- Circular Texture Meter
Cp	- Mallows' Cp statistic
CCD	- Central Composite Design
DF	- Degrees of Freedom
ETD	- Estimated Texture Depth (mm)
FO	- First-Order (linear terms)
HWTD	- Hamburg Wheel Tracking Device
IDEAL-RT	- Indirect Tensile Asphalt Cracking Resistance (Rutting Index)
LTS	- Laser Texture Scanner
LOF	- Lack of Fit
MPD	- Mean Profile Depth (mm)
MSE	- Mean Squared Error
NMAS	- Nominal Maximum Aggregate Size (mm)
PQ	- Pure Quadratic (terms)
RCI	- Reflective Cracking Interlayer
RSM	- Response Surface Methodology
RMSE	- Root Mean Square Error
SS	- Sum of Squares
R^2	- Coefficient of determination
Adj. R^2	- Adjusted coefficient of determination
Ra	- Arithmetic mean roughness
Rq	- Root mean square roughness
RMS	- Root mean square deviation of surface profile

Rsk	- Skewness of surface texture profile
Rku	- Kurtosis of surface texture profile
SO	- Second-Order (model)
TWI	- Two-Way Interaction
VMA	- Voids in Mineral Aggregate (%)
VFA	- Voids Filled with Asphalt (%)
VIF	- Variance Inflation Factor
F	- F-statistic (ratio of variances)
K	- Coefficient of permeability
p	- p-value (probability of observed or more extreme result)
t	- t-statistic (coefficient divided by standard error)
r	- Pearson correlation coefficient
ρ	- Spearman rank correlation coefficient
k	- Permeability coefficient (cm/s)
d	- Equivalent pore diameter (mm)
σ_m	- Maximum contact stress between tire and pavement
v	- Vehicle speed (m/s)
λ	- Wavelength of surface texture (mm)
A	- Amplitude (height) of surface texture (mm)
D	- Overall desirability score
d	- Individual desirability score (per response)

Chapter 1: Introduction

1.1 Background

The United States has more than 617,000 bridges. Recently, 7.5% of the country's bridges were rated as structurally defective or in poor condition (ASCE, 2021). Forty-two percent (42%) of all bridges are now at least 50 years old. Unfortunately, these structurally challenged bridges are used by 178 million people daily. The current nationwide estimate for bridge repairs is $125 billion. According to estimates (ASCE, 2021), to improve conditions, annual bridge restoration investment needs to be raised from $14.4 billion to $22.7 billion, a 58% increase. At the current rate of spending on bridge rehabilitation, repairs would not be completed until 2071, and the additional deterioration over the following 50 years would become unmanageable. Therefore, the country needs a systematic approach to bridge preservation. Several states are focusing on preventive maintenance and prioritizing repairs to existing damage (ASCE, 2021). Furthermore, freeze-thaw weather and increasing traffic accelerate the deterioration of aged bridges. Many factors cause bridge deterioration, but corrosion alone has been identified as one of the most significant ones. The most recent bridge failure in the United States (US) (Fern Hollow Bridge in Pittsburgh) occurred in 2022 due to unaddressed corrosion of the transverse tie plate (NTSB, 2024). Studies estimate that the annual cost of corrosion in the US is approximately $137.9 billion, which represents about 3.1% of the 1998 gross domestic product (Koch et al., 2002). In the transportation sector, corrosion-related costs for highway bridges amount to approximately $8.3 billion per year (Koch et al., 2002).

Figure 1.1: Fern Hollow Bridge collapse in Pittsburgh, Pennsylvania (2022) (NTSB, 2024)

Kansas has 24,891 bridges (ARTBA, 2024). Approximately 5.2% of these bridges (1,301) are structurally deficient. Every day, more than 538,000 people cross these deficient bridges. A study found that approximately 4,516 bridges needed repairs in 2025 (ARTBA, 2024). The owner-based bridge tables of the Federal Highway Administration (FHWA) also show that there are more unsafe bridges in the county-owned system than in the state-owned system. About 1,172 of these bridges are owned by the county, 69 by the state, and 43 by cities (ARTBA, 2024). Besides these, most Kansas bridges undergo an average of 60 or more freeze-thaw cycles each year (Bukovatz, 1984). Kansas's adverse weather and its geographical location pose significant challenges for the Kansas Department of Transportation (KDOT) in maintaining these aging bridges. According to a Kansas study, since the mid-1950s, the use of chloride deicing salts has increased, leading to increased corrosion of structural steel and bridge decks (TRB, 1974). Although Kansas uses many corrosion-protection techniques for bridge decks, ongoing deterioration indicates that these methods are not entirely effective due to deicing salt exposure and freeze-thaw cycles. According to Sprinkel and Ozyildirim (2007), thin-bonded concrete overlays tested only for Kansas bridge decks reduced chloride permeability for specific combinations. However, it remained extremely susceptible to cracking. According to KDOT's experience, polymer overlays are effective preventive treatments on sound decks. Still, when applied to more distressed structures or late in the season, they have caused cracking, debonding, and construction-timing problems (Reed, 2013). High molecular weight methacrylate and epoxy resins used in crack-sealing systems initially improved crack conditions. After about 15 months, they lost much of their flexibility, limiting their long-term ability to handle movement under Kansas traffic and climate conditions (Meggers, 1998).

Therefore, KDOT needs an urgent solution for alternative bridge deck overlaying. The ideal solution is an overlay that serves as both an interlayer barrier and a surfacing layer. One such option will be a somewhat modified version of the most practical option: the New Jersey idea, a version of the Bridge Deck Wearing Surface course (BDWSC) developed by the New Jersey Department of Transportation (NJDOT). NJDOT developed a highly modified asphalt overlay with a very fine-graded aggregate mixture. BDWSC is designed as a thin bridge deck surface layer that provides waterproofing, durability, and adequate friction while protecting the underlying deck (NJDOT, 2018). Therefore, the main objective of this research is to investigate the modified RCI concept (based on BDWSC gradation) to determine whether it is suitable for Kansas, given local materials and weather conditions.

1.2 Problem Statement

The bridge deck is the most critical element in a highway-bridge system. The reason is that the bridge deck is directly exposed to traffic loading and harsh environmental conditions. The joints and microcracks in the deck create pathways for chloride ions. Chloride ions react with reinforcing bars, leading to corrosion. Bridge deck overlays create a barrier, fill microcracks, and prevent chloride ions from penetrating. But if the bridge deck has reflective cracking, it reduces the effectiveness of deck overlays. Reflective cracking occurs in bridge deck overlays when there is active cracking in the deck, and they propagate upwards to the overlays.

The reflective cracking creates pathways for moisture infiltration again. Consequently, the overlays fail to fulfill the primary waterproofing function. Reflective Cracking Interlayer (RCI) systems have been developed to delay crack propagation and reduce moisture infiltration. RCI consists of highly polymer-modified asphalt mixtures. They are designed to absorb the strain under traffic load and create an impermeable layer. These are mainly used as interlayers. However, in most conventional applications, the RCI layer must be used with a surface overlay because RCI cannot restore friction. This composite system increases the total overlay thickness, which may be impractical for bridges with strict dead-load and vertical-clearance limitations. However, limited research has evaluated whether an RCI-type mixture can simultaneously provide waterproofing, rutting resistance, and sufficient surface friction when used as a primary bridge deck overlay layer.

1.3 Research Objectives

This study aims to address the practical challenges KDOT faces with bridge deck overlay by developing a hot-mix asphalt (HMA) mix that improves friction, reduces permeability, and provides adequate rutting resistance. The research focuses on determining whether RCI-based mixtures can function effectively as a thin-bridge-deck overlay while also protecting the deck from moisture infiltration.

The specific research objectives of this study include the following:

1. To develop an HMA-mix that has adequate friction for the bridge deck overlay by ensuring that the mix has a minimum Mean Profile Depth (MPD) value of 0.039 in. (1.00 mm) without using any high-friction surface treatment;
2. To investigate whether the mixture works as an impermeable layer when it is placed as a bridge deck overlay; and
3. To determine the rutting resistance using the IDEAL-RT test and validate IDEAL-RT Index results with the Hamburg Wheel Tracking Device test results.

1.4 Thesis Outline

This thesis is organized into five chapters. Chapter 1 presents the research background, problem statement, and study objectives. Chapter 2 provides a comprehensive literature review about bridge deck deterioration mechanisms, overlay systems, reflective cracking interlayers, and performance test methods used for HMA mixtures, including permeability, surface texture, and rutting resistance. Chapter 3 describes the research methodology, including materials selection, mixture design, specimen preparation, and laboratory testing procedures used in this study. Chapter 4 presents the experimental results and discusses the performance of the evaluated mixtures based on the laboratory test results. Finally, the key findings of this research present conclusions and recommendations for future research on RCI-based bridge deck overlay systems.

Chapter 2: Literature Review

2.1 Introduction

According to the FHWA's Long-Term Bridge Performance (LTBP) Program, the bridge deck has two fundamental roles in a highway bridge system. First, it distributes traffic loads to the supporting girders, and second, it provides sufficient friction for the riders (Chavel, 2022). The bridge deck is the most vulnerable element of the bridge, as it is directly exposed to adverse environmental conditions and heavy traffic (FHWA, 2014). Deck deterioration occurs due to water and traffic, including moisture infiltration and the entry of deicing chemicals through cracks and joints. This accelerates reinforcement corrosion and loss of flexural and shear capacity of the deck (FHWA, 2014). These problems eventually lead to more frequent maintenance and rehabilitation, as well as higher life-cycle costs (Babaei & Hawkins, 1987; Hu et al., 2013; Russell, 2012).

According to the modern Bridge Management System, engineers focus on preventive techniques rather than major rehabilitation or deck replacement (Ahmad, 2011). Bridge deck overlay is a popular and cost-effective preventive maintenance method. Overlays not only create an impermeable layer between the traffic and the deck but also restore ride quality and rutting resistance. Overlays can seal existing cracks and surface pores in a distressed deck (Lane & Jalinoos, 2017). The effectiveness of overlays depends on material properties and construction quality. Therefore, permeability, surface texture, long-term friction, rutting resistance under traffic, cracking resistance, and interface bond durability with the bridge deck are used to evaluate the overlay's performance.

This chapter reviews (i) major bridge deck deterioration mechanisms and how overlay can solve this issue, (ii) commonly used overlay system types, including polymer-based overlays, cementitious overlays, asphalt overlays with and without waterproofing membranes, and the BDWSC concept developed by NJDOT and its application, and (iii) key performance requirements and testing methods used to evaluate potential bridge deck overlay suitability. The chapter concludes by summarizing research gaps and establishing motivation for the experimental and statistical evaluation framework used in this thesis.

2.2 Bridge Deck Failure Mechanism and Overlay Needs

In the frost belt, bridges freeze before pavement since they are exposed to cold air from above and below (Bollendorf, 2021). The bridges lack ground heat, leading to frost formation, a dangerous condition for drivers and pedestrians (Bollendorf, 2021). As a result, deicing salts are widely used on bridges to prevent ice and slippery conditions. A deicer salt prevents ice formation by lowering the freezing point of water and preventing ice from bonding to paved surfaces (Bollendorf, 2021). However, these deicing salts produce chloride ions (Gode & Paeglitis, 2014). The chloride ion can penetrate through cracks and joints of the reinforced concrete bridge deck. It moves through capillary action, causing the steel to corrode (Gode & Paeglitis, 2014; Zhuo et al., 2019). Additionally, the trapped water in concrete pores forms ice in cold weather. When ice forms, its volume increases by 9% compared to water, placing severe stress on the concrete and leading to delamination, cracking, and eventual spalling (FHWA, 2006).

To address this issue, researchers use a well-bonded overlay, which creates a barrier between the weather and the bridge deck (NCHRP, 1987). The bridge is also subject to stresses from repeated loading, which can cause structural distress (Gao & Fam, 2024). The bridge deck experiences millions of truck traffic and frequent bending over its service life, leading to fatigue cracks (Gao & Fam, 2024). Typically, fatigue cracking initially appears as microcracks in the tensile zone of the concrete section or at weak interfaces, such as the paste-reinforcement interface and the paste-aggregate transition zone (Okada et al., 1978). However, due to repeated stress, microcracks coalesce into visible cracks that appear as transverse, longitudinal, or patterned on the concrete deck (National Academies of Sciences, 2017). While longitudinal cracks typically develop parallel to traffic, transverse cracks are perpendicular to traffic. Transverse cracks occur due to restrained shrinkage of the concrete deck as it cures and dries (National Academies of Sciences, 2017). Longitudinal cracks occur when concrete experiences shrinkage stress, structural overloading, or thermal stress (FHWA-NJDOT, 2008; National Academies of Sciences, 2017). As the crack width increases due to repeated loading, it weakens the interlocking bond of aggregates, reducing shear transfer and stiffness by separating aggregates from the paste (Okada et al., 1978). Water in cracks interacts with fine particles, forming a slurry. Repeated loading can cause slurry to pump out through cracks or joints, leading to spalling (Okada et al., 1978). Furthermore, leaking expansion joints, inadequate drainage slopes, and clogged drains may worsen these conditions.

Over the years, researchers have proposed solutions to this issue. For instance, the use of low-permeability concrete with a low water-to-cement (w/c) ratio and other cementitious materials, sufficient concrete cover, and careful detailing of joints and drainage are common practices (FHWA, 2017; NCHRP, 1987). Additionally, stainless steel, galvanized steel, or epoxy-coated steel reinforcement bars are used in bridge decks to prevent corrosion (FHWA, 2004, 2022, 2023, 2024). However, these methods have a high initial cost (Darwin et al., 2020; FHWA, 2017). Also, some methods work well for small-scale repairs or preventive measures but may not be satisfactory for severely damaged or aging decks (ElBatanouny et al., 2022; FHWA, 2004, 2022, 2023).

The bridge deck maintenance techniques are effective when engineers need to address only one deterioration mechanism (e.g., permeability or corrosion) and do not need to improve ride quality or work with a highly distressed deck. Thus, researchers offered another effective preservation and rehabilitation option: overlay systems. Overlays are widely considered one of the most effective single interventions because they simultaneously address structural, durability, and functional demands (FHWA, 2017, 2022).

Figure 2.1: Underside view of a reinforced concrete bridge deck showing concrete spalling and exposed corroded reinforcement (Salina Journal, 2015)

2.3 Types of Overlays

Bridge deck overlay systems are commonly classified into polymer-based overlays, cementitious (concrete) overlays, and hot-mix asphalt (HMA) overlays (often used with waterproofing membranes) (FHWA, 2017).

HMA overlays are among the most widely used bridge deck wearing courses in the US, applied either directly to the deck or, more commonly, over a waterproofing membrane system by the state departments of transportation (DOTs). These overlays are more common because they are easy to install, relatively low cost, and improve rideability (smoothness) (FHWA, 2017). However, this type of overlay increases the dead load on the bridge and may sometimes get deboned from the concrete deck, allowing water to be trapped beneath the overlay.

Latex-Modified Concrete (LMC) overlay is another waterproofing overlay. FHWA describes LMC as a concrete system containing latex (commonly styrene-butadiene polymers) (FHWA, 2017). LMC overlays typically have lower chloride permeability than conventional concrete, as the latex polymer admixture in concrete reduces permeability (FHWA, 2017). However, LMC overlays often take longer to achieve the strength required for opening to traffic and are more costly. Another common type of overlay is epoxy polymer concrete overlays. In polymer overlays, polymers serve as the binder, with aggregates embedded in the resin system to form a thin protective wearing surface. The main advantage is rapid curing, allowing relatively fast reopening to traffic. The cured epoxy binders resist penetration of water and deicing chemicals (FHWA, 2017). These overlays are commonly thin (about 0.25–0.5 in) and may have limited service life under very high traffic volumes or severe weather.

Waterproofing membranes are frequently used by the state departments of transportation (DOTs) primarily to waterproof decks, often in combination with an HMA wearing course. While membranes are effective at waterproofing, FHWA also implies that they are highly installation-sensitive, particularly around joints and drains (FHWA, 2017). Silica fume overlays are conventional concrete overlays that are modified by adding silica fume, either as a cement supplement or a partial cement replacement. Silica fume is typically added to reduce permeability by refining the pore structure. FHWA identifies it as a very-low-permeability solution (FHWA, 2017).

There are other special types of bride deck overlays available. High-Molecular-Weight Methacrylate (HMWM) resin systems are used as surface sealers, crack sealers, and initial prime/bond coats for some polymer overlays (FHWA, 2017). Although HMWM systems can be effective for bonding and preventing the infiltration of deicing solutions into both wide and hairline cracks, HMWM is temperature-sensitive and may generate airborne emissions. Polyester polymer overlays are polymer concrete overlays in which polyester resin works as the binder. The biggest advantage of these overlays is that they require less curing time, which supports rapid construction and reopening (FHWA, 2017). Polyester systems require primers with safety considerations; in addition, polyester polymer overlays are usually thicker than epoxy polymer overlays, which can support longer service life but also increase material use and deadload (FHWA, 2017).

In Kansas, multi-layer polymer overlays have become the primary deck preservation practice for KDOT. A KDOT bridge management presentation reports the first polymer overlay placement in Kansas in the late 1990s (Reed, 2013). It describes a gradual increase in the use of polymer overlays through the 2000s, followed by a more rapid increase after 2010 (Reed, 2013; Kulseth, 2015). A 2015 study showed that KDOT had used polymer-based overlays on primary highway bridge decks for many years, with more than 200 decks overlaid, predominantly with epoxy-based materials, followed by later trials with methacrylates and polyesters (Meggers, 2016).

2.4 Overlay-Related Failure Modes and Reflective Cracking

While overlays are widely used as preservation treatments, they sometimes fail to perform properly. Reflective cracking is a common failure mode in overlays (Peshkin et al., 2011; VTRC, 2018). Due to frequent bending, thermal movement, and differential stiffness, cracks in the underlying deck (or at joints and repaired areas) may propagate upward over the overlay (VTRC, 2018; WisDOT, 2017). Reflective cracking can reduce the waterproofing performance by reestablishing direct infiltration paths through the overlay (VTRC, 2018). If the overlay lacks sufficient crack resistance and the deck has an active crack pattern, reflective cracking in the overlay may occur rapidly, reducing its effectiveness (Asphalt Institute, 2024; Peshkin et al., 2011).

To address this issue, reflective cracking interlayers are commonly used as an intermediate layer between the deck (or a base asphalt layer) and the surface overlay (Asphalt Institute, 2024). The purpose of an interlayer is to delay crack propagation by (i) reducing stress concentration at the crack area, (ii) accommodating movement through a more flexible or energy-dissipating layer, and (iii) creating an impermeable layer for the underlying deck that experiences alligator cracking. In practice, interlayers can also act as a moisture barrier and improve overall system durability by limiting water intrusion along the interface (Asphalt Institute, 2024).

RCI is made from highly polymer-modified asphalt (often placed as a thin, flexible layer) designed to provide crack relief and waterproofing on highway pavements (Asphalt Institute, 2024; Caltrans, 2013). The RCI layer is intended to absorb and redistribute strains caused by crack movement and thermal cycling. Thus, the interlayer also reduces the rate of cracking on new overlays (Asphalt Institute, 2024; Russell, 2012). At the same time, by creating a dense, well-bonded intermediate layer, the RCI layer can reduce permeability and improve the corrosion protection (NCHRP, 1987; Peshkin et al., 2011; Russell, 2012).

The RCI interlayer can serve as a barrier between the overlay and the deck, but it cannot provide a riding surface or carry traffic because it is thin (Asphalt Institute, 2024). For these reasons, RCI and an overlay need to be used together. However, in many bridge deck rehabilitation projects, placing both an RCI interlayer and an overlay is not always practical. Pavement has no dead-load restrictions, and there is no issue with vertical clearance. However, many bridges lack sufficient clearance or load-bearing capacity to support that added HMA thickness (Caltrans, 2013).

According to Caltrans policy, live load capacity must be checked whenever an overlay is considered for an existing bridge deck due to changes in dead load (Caltrans, 2013). A highly elastic, polymer-modified asphalt interlayer (RCI) is typically placed at a thickness of 1 inch (25.4 mm). But it requires a minimum overlay thickness above them to provide friction (Asphalt Institute, 2024). The overlay thickness is typically 1.5 to 2 inches (38 to 51 mm). The combined thickness of RCI and overlay can exceed 2.5 in. (63.5 mm). According to AASHTO LRFD, for bituminous wearing surfaces with an estimated unit weight of 140 pcf (22.0 kN/m^3), a 2.5-inch (63.5-mm) overlay increases the superimposed dead load by approximately 29 lb/ft^2 (1.39 kPa) (AASHTO, 2020). Thus, these layers add dead load to the existing superstructure, and the situation becomes more constrained when vertical clearance is limited in underpasses, interchanges, and tunnels (AASHTO, 2020; Caltrans, 2013). Research from the National Center for Asphalt Technology (NCAT) confirms that while thicker overlays generally delay reflective cracking, increasing thickness is often the least cost-effective approach and may not be structurally feasible on load-restricted bridges (NCAT, 2012). Therefore, this study aims to develop a practical bridge-deck solution in which a modified RCI interlayer-based system serves as the primary overlay, providing improved waterproofing while addressing traditional limitations in surface friction and texture, as well as rutting resistance.

2.5 Bridge Deck Wear Surfacing Course (BDWSC)

As mentioned earlier, to address the competing requirements, NJDOT developed BDWSC. BDWSC is a bridge deck surface layer that serves as both an impermeable layer and a deck overlay for ride quality. NJDOT first created BDWSC to meet the permeability criteria for bridge deck pavements that traditional asphalt mixtures could not meet (Bennert & Pezeshki, 2015; NJDOT, 2018). NJDOT BDWSC has four criteria to meet: 1. Rut resistance, 2. Fatigue resistance, 3. Ability to achieve high density without vibratory compaction, and 4. Extremely low permeability.

To meet all these targets simultaneously, the BDWSC relies on a Styrene-Butadiene-Styrene (SBS) polymer-modified binder. NJDOT stated that older SBS mixes became difficult to work with above about 4% polymer. However, newer SBS formulations could exceed 7% while still being workable, helping the surface remain both rut- and fatigue-resistant. The BDWSC is a dense-graded HMA mixture with a nominal maximum aggregate size (NMAS) of 3/8 in. (9.5 mm). It is a rut-resistant and fatigue-resistant overlay system that NJDOT engineered specially to protect structural concrete from moisture infiltration and chloride-induced corrosion (Bennert & Pezeshki, 2015; Corun, 2020). NJDOT recognized that bridge decks must be highly durable under extreme loading conditions while maintaining minimal thickness to accommodate vertical clearance constraints. The Route 80 ACROW steel panel bridge in New Jersey suffered significant distress within two weeks when using a traditional ½ in. (12.5 mm) NMAS Superpave mix overlay. That overlay was replaced with BDWSC and showed no distress after 1.5 years of heavy traffic (Bennert et al., 2015; Rashid, 2015).

The BDWSC specification also sets strict volumetric requirements to guarantee mechanical stability and impermeability. These requirements include a minimum binder content of 7% with stone sand to ensure polish resistance, a minimum Voids in Mineral Aggregate (VMA) of 18%, a Voids Filled with Asphalt (VFA) of 90–100%, and a dust proportion controlled within 0.3 to 0.9 (Corun, 2020). The coarse aggregates are argillite, gneiss, granite, quartzite, or trap rock with no Reclaimed Asphalt Pavement (RAP). The BDWSC report states that the blend should have a minimum sand equivalent of 45% (AASHTO T 176) and a minimum uncompacted void content of 45% (AASHTO T 304, Method A). At a gyratory design level of 50 using the Superpave Gyratory Compactor (SGC), NJDOT aims to achieve approximately 99% of the theoretical maximum density. The mix design requires a flexural beam fatigue life (AASHTO T-321) of greater than 100,000 cycles at 59°F (15°C) and 1,500 microstrains, and an Asphalt Pavement Analyzer rutting of less than or equal to 0.12 in. (3 mm) at 8,000 cycles at 147.2°F (64°C) (Corun, 2020). Over seven years, the BDWSC mix has worked effectively on the world's busiest bridge (Annual Average Daily Traffic, AADT of approximately 280,000–300,000 vehicles per day) in

New Jersey, which has an orthotropic steel deck with substantial vertical movement (Corun, 2020; Willis et al., 2016).

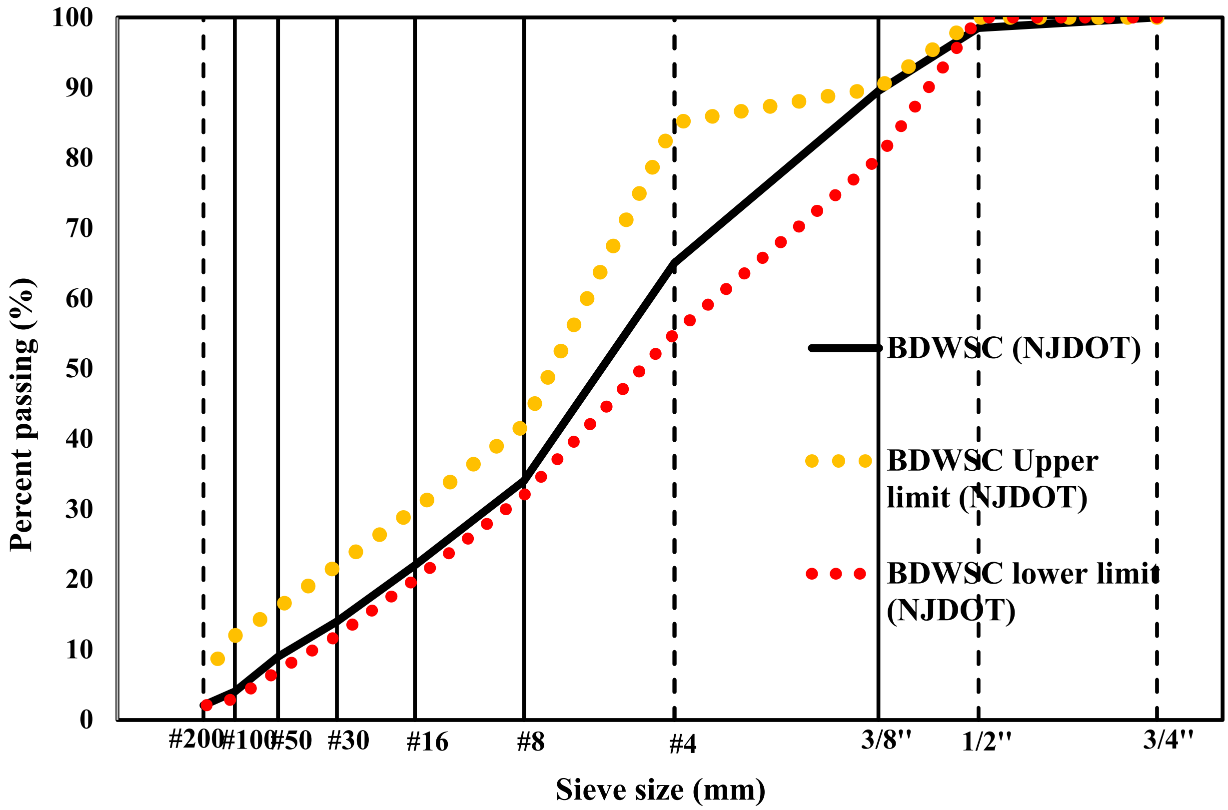

Figure 2.2: BDWSC Gradation Curve (Corun, 2020)

2.6 Agencies that have adopted BDWSC

Based on the NJDOT BDWSC approach, Oregon DOT (ODOT) researched an impermeable asphalt bridge deck surface mixture with a higher asphalt content and finer gradation to optimize the waterproofing performance (Haynes et al., 2020). ODOT used a PG 76-22 polymer-modified binder and a PG 70-22ER extended resin (ER) binder and followed the NJDOT gradation range with 20% RAP. The mix design targeted extremely low air voids at 50 design gyrations, and trials were conducted at binder contents of 7.5%, 8.0%, and 8.5% (Haynes et al., 2020). ODOT study showed that a mixture with 8.0% PG 76-22 was the optimal mix design, achieving 3.2% air voids with zero rainfall infiltration over 120 hours while maintaining adequate rutting resistance (5,208 flow number) and baseline cracking performance. The study also used a PG 70-22ER binder, which did not achieve the very low air-void target (Haynes et al., 2020).

The study also showed that the mix with 8.5% binder content had approximately a 75.8% reduction in rutting resistance compared with the 8.0% mix (1,262 at 8.5% flow number vs. 5,208 at 8.0%). Surface texture (Mean Texture Depth, MTD) decreased with increasing asphalt content, with an 8.5% asphalt content achieving an MTD of only 0.020 in. (0.508 mm) (Haynes et al., 2020).

Table 2.1 ODOT Results Based on BDWSC (Haynes et al., 2020)

Asphalt Content (%) (PG 76-22)	7.5%	8.0%	8.5%
Air Voids at N=50 (%)	4.9	3.2	1.0
Rutting (Flow Number ())	5,736	5,208	1,262
Rainfall Infiltration (120 h)	Initial infiltration starts after 34 hours	None observed	None observed
Cracking (FI (rel. to 8.0%)	Lower	Baseline (1.0)	1.95×Baseline
Bond (OFTT (F/T effect))	No significant change	No significant change	No significant change
Texture (MTD (mm))	0.559	0.533	0.508

The New York State DOT (NYSDOT) has a similar concept for their bridge deck overlay called the Waterproofing Bridge Deck Overlay (WBDO) (NYSDOT, 2024, 2025). The concept involved using a highly modified asphalt bridge deck surface course to create an impermeable layer. The WBDO requires PG 76E-28 elastomeric-modified binder (meeting AASHTO M 332 with a minimum elastic response of 55% at 168.8°F (76°C)). NYSDOT's specification specifies a nominal maximum aggregate size of 3/8” (9.5 mm) and a minimum binder content of 7.25%. The binder content is higher than NJDOT's minimum requirement for BDWSC. The gradation maintains strict production limitations of ±2% on the US No. 200 sieve (0.075 mm). The use of RAP is highly restricted (NYSDOT, 2024, 2025). The air voids at 50 design gyrations should be 1.5 ± 0.5%, and the VMA should be at least 15.5%. The WBDO is mainly used to prevent water and salt infiltration. NYSDOT uses this technique on both new and old bridges where the deck must be resurfaced and reopened to traffic quickly. WBDO is placed in a single lift with a thickness of 1 to 2.5 inches (25 to 60 mm) (NYSDOT, 2024, 2025).

2.7 Performance Tests of RCI-based Bridge Deck Overlay

Performance testing of RCI-based bridge deck overlays is essential because they must function simultaneously as a protective waterproofing layer and provide sufficient friction and rutting resistance under heavy traffic and harsh environmental exposure (FHWA, 2017, 2023; Tabatabai et al., 2016). In this study, the performance of the bridge deck overlay mix was evaluated for friction, permeability, and rutting resistance.

2.7.1 Friction

The shear resistance that develops when tire and surface contact each other is called friction (Gillespie, 1992; Hall et al., 2009). Friction arises from two mechanisms: adhesion and hysteresis (Giles, 1969; Hall et al., 2009). Adhesion developed due to micro-scale bonding. The interlocking between tire rubber and pavement surface irregularities develops adhesion. Hysteresis is produced when the tire deforms, and energy is dissipated. The most critical friction occurs in wet conditions, as water creates a thin layer between the tire and the surface. A study showed that texture is more important in wet conditions because it determines (i) how quickly water can escape the contact voids and (ii) how much "mechanical interlock" and rubber deformation happen at the interface (Hall et al., 2009; Henry, 2000). FHWA divided the texture into microtexture and macrotexture (Hall et al., 2009; Henry, 2000). Microtexture controls adhesion at low speeds, while macrotexture controls water drainage, splashes/spray, and the speed-dependence of friction (i.e., how quickly friction drops as speed increases) (Henry, 2000).

FHWA defines microtexture as surface wavelengths ranging from 0.00002 to 0.020 in. (0.5 μm to 0.5 mm), and macrotexture as wavelengths ranging from 0.020 to 1.97 in. (0.5 mm to 50 mm) (Henry, 2000; see Figure 2.4). Microtexture is mainly provided by the roughness of aggregate particles (which dominate friction at low speeds or in dry weather). At the same time, macrotexture is driven by gradation of the mixture, aggregate size/shape, and surface finishing, which create pathways and voids or pores that facilitate water infiltration. Macrostructure is important for RCI-type mixtures because their fine gradation and higher binder content can reduce surface texture depth. Adequate macrotexture improves wet-weather friction by allowing water to escape from the tire-pavement interface even when microtexture is sufficient under dry conditions (Hall et al., 2009).

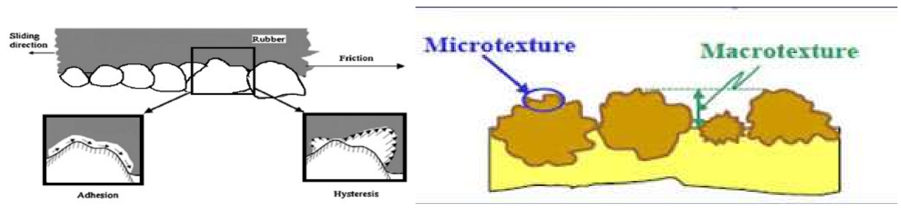

(a) (b)

Figure 2.3: Pavement surface texture and friction mechanisms: (a) friction generation through adhesion and hysteresis between tire rubber and pavement surface (World Road Association, 2015), and (b) illustration of pavement microtexture and macrotexture contributing to skid resistance (Hall et al., 2009)

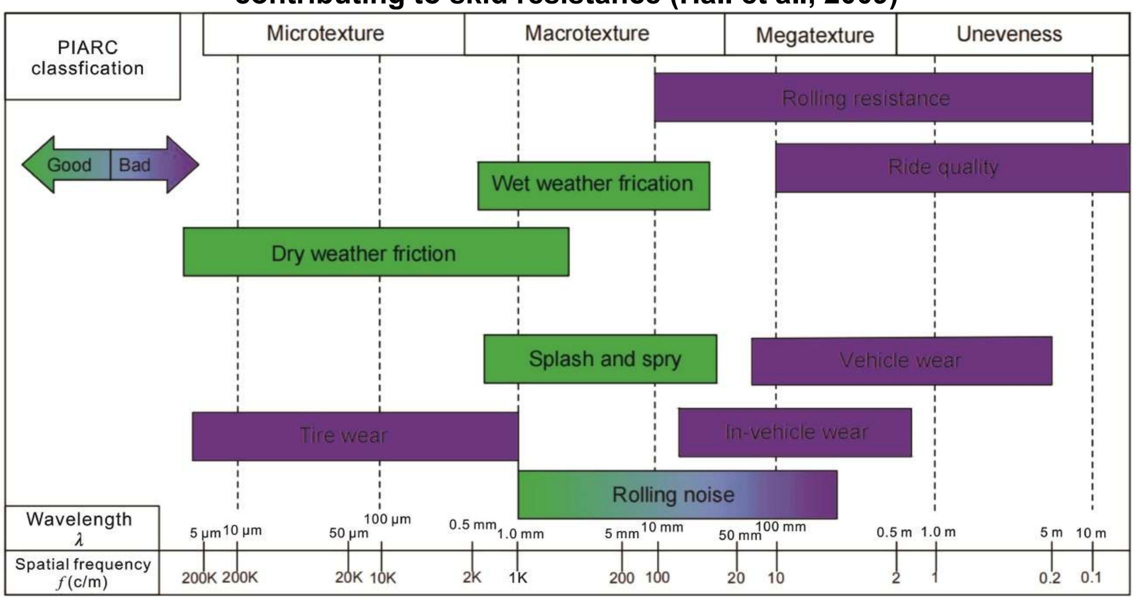

Figure 2.4: PIARC classification for pavement surface characteristics according to wavelength (Chen et al., 2022)

MTD and MPD are two methods for quantifying pavement macrotexture. MTD is obtained from the volumetric sand patch method (ASTM E965). At the sand patch test, a known volume of sand is spread into a circular patch, and the measured diameter is converted to an average texture depth. Conversely, MPD is derived from a profile measurement using laser-based texture scanners and represents the computed texture depth from the surface elevation profile rather than a volumetric fill. MPD is commonly calculated over standardized 4-in (100-mm) profile segments (per ASTM E1845/ISO 13473-1 practice) and can be converted to an estimated texture depth. MTD is a traditional volumetric macrotexture measure. In this study, MPD was measured using a Laser Texture Scanner (LTS) because it provides rapid, repeatable, non-contact texture measurement suitable for dense bridge-deck overlay surfaces (ASTM, 2023; ASTM, 2024; FHWA, 2019; ISO, 2019).

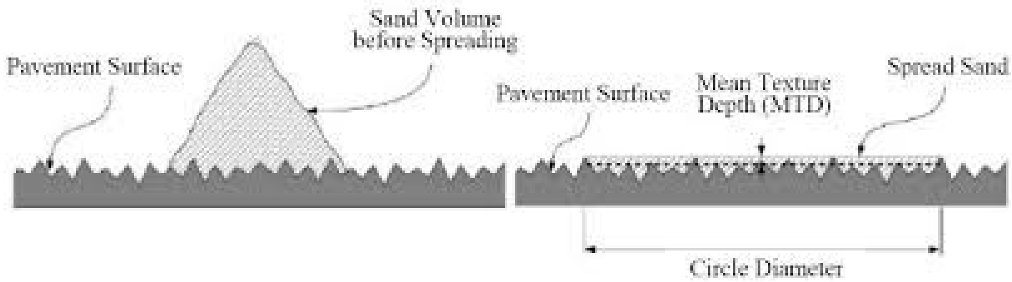

Figure 2.5: Illustration of the sand patch method used to measure pavement surface macrotexture (ASTM, 2015)

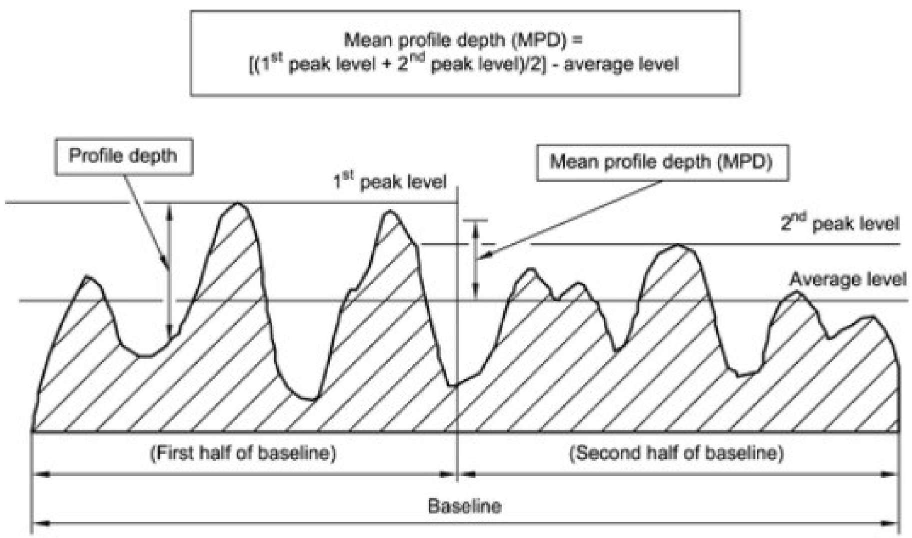

Figure 2.6: Illustration of Mean Profile Depth (MPD) calculation from pavement surface profile measurements (ISO, 2019)

An LTS is a portable, non-contact, high-resolution optical device that measures surface macrotexture. The LTS scans a defined area with a laser and records the surface elevation profile at a vertical resolution of 0.00012 in. (0.003 mm). The LTS passes a laser over a 4 in. x 4 in. (100 mm x 100 mm) surface area in about 90 seconds, then automatically computes macrotexture metrics. The LTS passes a laser line over the surface and records elevations at many points. The software computes the texture parameter MPD, as defined in ASTM E1845, and related indices, such as Estimated Texture Depth (ETD) and Texture Profile Index. The profile is divided into segments of length typically 2 in. (50 mm). For each segment, the software automatically fits a linear average reference line and computes the average height of profile peaks above that line. Then, Mean Segment Depth (MSD) is computed for each segment (ASTM International, 2023; FHWA, 2022; ISO, 2019). MPD is the average of all MSD values across the scanned length or circle. Because agencies have long used the sand patch test to report Mean Texture Depth (MTD), ISO-based practices commonly convert MPD to an Estimated Texture Depth (ETD). A widely cited relation is (ASTM International, 2023; ISO, 2019):

$$ETD = 0.02 + 0.8 \times MPD \tag{2.1}$$

where ETD = Estimated Texture Depth, and MPD = Mean Profile Depth.

The LTS9500 uses a line-laser sensor with a per-channel sampling frequency of 5 kHz (Ames Engineering, 2024). Because the scanner operates in a stationary laboratory setup, the scan movement is relatively slow. As a result, the system achieves a very fine spatial resolution of approximately 0.0496 mm in the scan direction (x) and 0.0415 mm across the laser line (y) (Ames Engineering, 2024). These spacing values are significantly smaller than the 1 mm sampling interval required by ASTM E1845 for macrotexture measurement, ensuring that the surface profile is captured with sufficient accuracy (Ames Engineering, 2024). Previous research by Li et al. (2010) showed that very high sampling frequencies (54–90 kHz) are necessary only for vehicle-mounted systems operating at highway speeds (Li et al., 2010). In contrast, for stationary laboratory measurements such as the LTS9500, a sampling frequency of 1 to 5 kHz is sufficient, as the scanning speed is much slower (Li et al., 2010). Therefore, the 5 kHz laser frequency used in this study provides adequate resolution for accurate macrotexture characterization.

The Ames Engineering LTS9500 operates on a non-contact laser triangulation principle (Ames Engineering, 2024). A line laser is projected onto the specimen surface, and the reflected laser light is captured by an optical sensor positioned at a fixed angle from the laser source. When the laser passes over surface peaks and valleys, the position of the reflected light changes on the sensor. Because the geometry between the laser source, the specimen surface, and the sensor is known, the system converts the change in reflected-light position into vertical (z direction) elevation values.

During scanning, the line laser moves across a selected area of the sample surface and records a dense set of elevation points. These elevation data are used to develop a three-dimensional surface map of the asphalt specimen as shown in Figure 3.11 in Chapter 3 later. The software then extracts surface profile elevations and calculates the Mean Profile Depth (MPD) in accordance with the principles of ASTM E1845/ISO 13473-1. In this process, each profile segment is divided into two halves, the highest peak in each half is identified, and the average peak height relative to the mean profile level is used to determine MPD. .

Figure 2.7: Sample setup in Laser Texture Scanner (LTS) for surface macrotexture measurement.

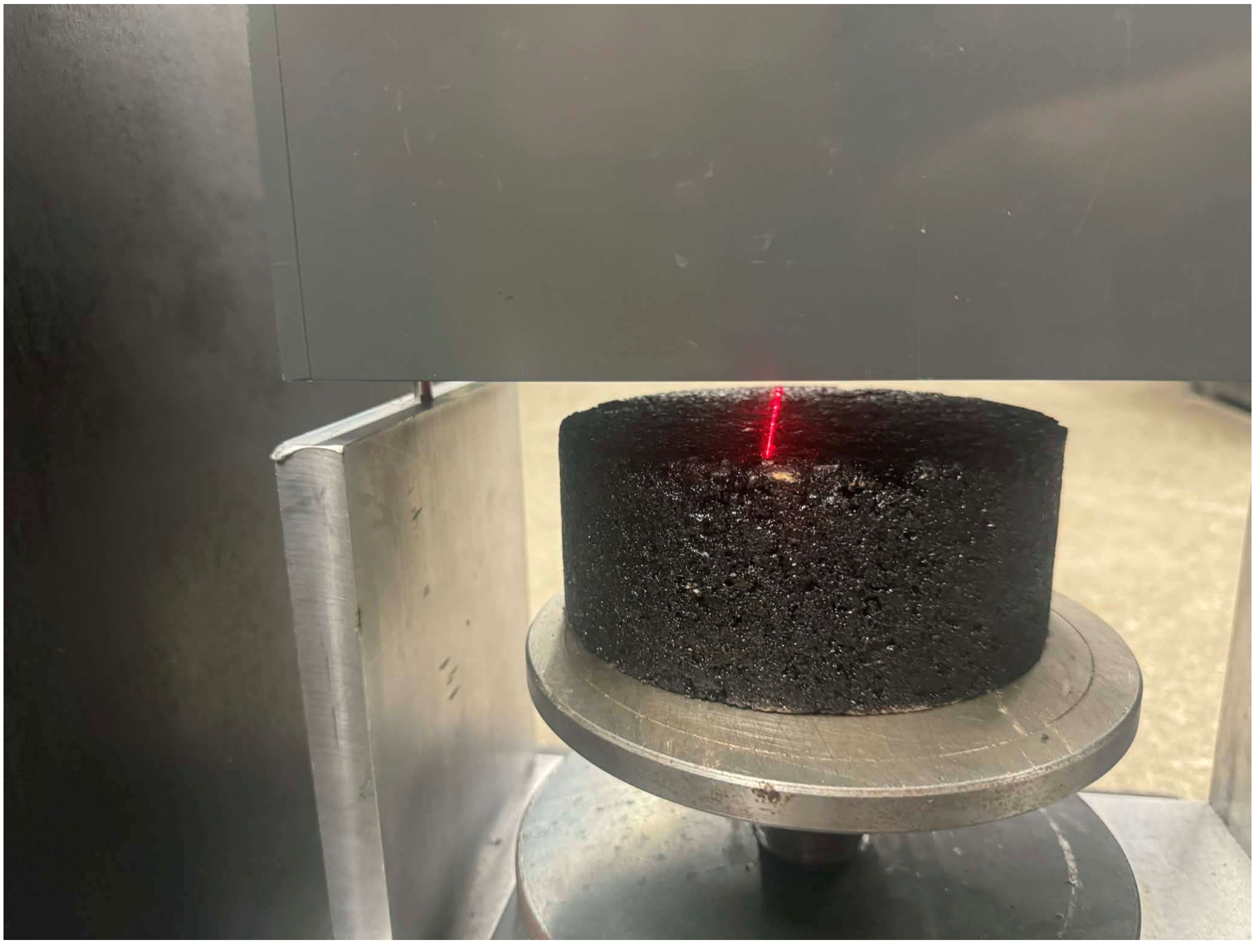

Figure 2.8: Sample setup in Laser Texture Scanner (LTS) showing the laser line scanning across the top surface of the asphalt specimen for macrotexture measurement.

Many state DOTs use different MPD values depending on surface type, speed, and weather. Therefore, FHWA suggested a lower threshold value for MPD. An FHWA study found that when the MPD is less than 0.016 in. (0.4 mm), the crash probability increases by 200%. Consequently, FHWA suggested that when the MPD is 0.016 to 0.020 in. (0.4-0.5 mm), the section should be investigated (FHWA, 2019). Another study from Louisiana reported that a minimum MPD of 0.020 in. (0.5 mm) is required for the surface texture to support drainage of water beneath the tires (Pulugurtha, 2008). International and UK practice often classifies texture into condition bands using thresholds around 0.016, 0.031, and 0.043 in. (0.4, 0.8, and 1.1 mm), where values below 0.016 in. (0.4 mm) trigger concern and investigation, and values approximately 0.031 to 0.043 in. (0.8 to 1.1 mm) are considered progressively better for wet-skid management on high-speed networks (Federal Highway Administration, 2022). A VDOT/VTRC study measured macrotexture using MPD and reported that the initial MPD value range for the high-friction surface treatment

(HFST) was 0.051 to 0.063 in. (1.3 to 1.6 mm). The study indicated that HFST-type treatments could provide substantially higher macrotexture than many dense-graded asphalt surfaces (Virginia Transportation Research Council, 2022). The North Carolina DOT reported in its crash macrotexture report that crashes generally decreased as macrotexture increased and suggested macrotexture greater than 0.059 in. (1.5 mm) (Pulugurtha, 2008).

Table 2.2 Surface Texture Requirements (MPD - Mean Profile Depth) for Pavement

Source	Requirement	Application
FHWA Tech Brief (Federal Highway Administration, 2019)	0.016 to 0.020 in. (0.4 to 0.5 mm)	Low macrotexture/investigation range for pavement friction screening
Virginia DOT (Virginia Transportation Research Council, 2022)	≥ 0.051 to 0.063 in. (1.3-1.6 mm)	Reported initial MPD range for HFST surfaces
FHWA (Federal Highway Administration, 2022)	> 0.039 in. (>1.00 mm)	HFST/friction-improvement for pavement

2.7.2 Permeability

Permeability is the hydraulic conductivity, which describes how easily water can flow through a pavement or bridge's interconnected voids (FDOT, 2015). For asphalt overlays on bridge decks, permeability is critical because water that passes through the asphalt overlay joints or voids can carry chlorides from deicing salts. These chloride ions cause corrosion of reinforcement and subsequent rapid deterioration of bridge decks. The Oregon bridge-deck overlay study explicitly noted that water can pass through asphalt overlays and penetrate the concrete deck, reaching the steel reinforcement. Thus, an HMA overlay needs to be impermeable to prevent the bridge deck deterioration (FDOT, 2015; Oregon Department of Transportation, 2018).

The permeability of asphalt specimens is measured using two primary laboratory methods. These are the falling-head and constant-head methods. In the constant-head method, a constant hydraulic head is maintained throughout the test, resulting in a steady flow rate. This method is suitable for highly permeable materials that can sustain continuous flow under a stable hydraulic gradient, such as coarse-grained soils/aggregates or open-graded asphalt mixtures. However, dense-graded asphalt mixtures typically have low permeability and limited interconnected air voids. Therefore, the falling-head method is more appropriate for measuring their permeability. Moreover, forcing water through the specimen at a rate that is not representative of field behavior. Therefore, the constant head method can overestimate permeability for a dense-graded asphalt mixture used in a bridge deck. The falling-head method is frequently used to assess permeability for asphalt surfaces on bridge decks (FDOT, 2015). This method uses a specific volume of water on the specimen's upper surface and allows the water level to rise over time as infiltration occurs. As a result, the driving hydraulic gradient is not constant. Rather, the gradient progressively decreases as the water head dissipates due to gravity flow, creating a temporary flow condition. This approach is particularly suitable for low-permeability materials, where flow rates are low and extremely sensitive to changes in hydraulic head. Additionally, the interconnection of air voids significantly affects the permeability of dense-graded asphalt mixtures. Initially, water penetrates larger connected voids when the water head is high. Narrower, less connected paths control water movement as the head falls and flow becomes more constrained. The falling head test captures this gradual decrease in flow rate. This water movement represents the real-world infiltration situation. Researchers also use rainfall-based infiltration methods (e.g., sensors at the asphalt–concrete interface) when infiltration is near zero for an extended period, because traditional coefficient of permeability (k) values can become extremely small and difficult to distinguish (Cooley & Brown, 2000).

Florida Test Method FM 5-565 is one of the most widely used lab procedures for asphalt mixture water permeability. The permeability of the asphalt mixtures is measured using the falling-head permeability test. In this test, a cylindrical, compacted asphalt specimen (6 in. x 3.15 in. or 250 mm x 80 mm) is placed inside a sealed chamber, as shown in Figure 2.9. Florida Test Method FM 5-565 does not specify a required target air-void content for the test specimen. In this study, permeability specimens were prepared at the selected target air-void content of 5.0 ± 0.5% to evaluate water flow through compacted asphalt specimens under controlled laboratory conditions. The specimen is positioned on the pedestal and covered with a flexible membrane to prevent water from running along its sides. The top cap and bottom pedestal are sealed using O-rings so that water can flow only through the interconnected air voids of the asphalt specimen. A graduated cylinder is provided at the top of the specimen to provide the hydraulic head. Before testing, the specimen is saturated for 1 to 2 hours to remove trapped air from the connected void spaces by applying a vacuum pressure. During testing, the latex membrane was pressurized to 10 ± 0.5 psi (68.9 ± 3.4 kPa) to prevent side leakage around the specimen. This membrane pressure was not used to drive water through the specimen. Water flow occurred under the falling hydraulic head in the graduated cylinder.

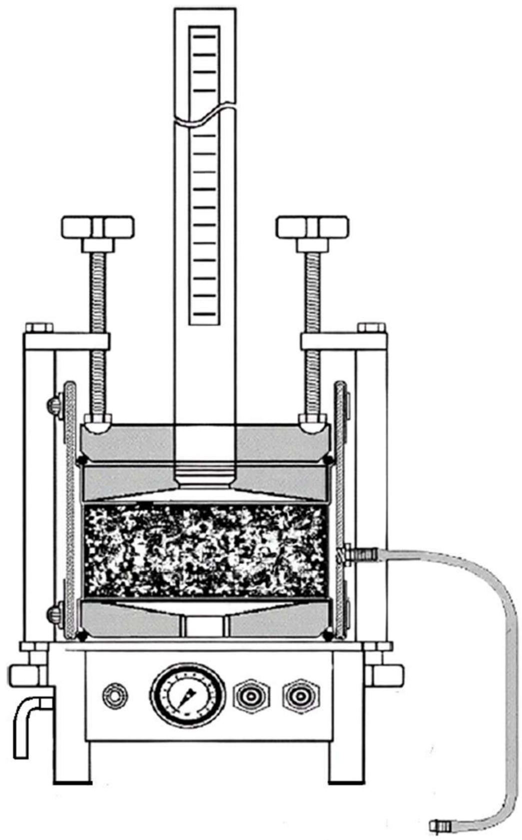

Figure 2.9: Schematic diagram of water permeability testing apparatus (Florida Method FM 5-565)

After the specimen is properly sealed and saturated, water is introduced into the graduated cylinder. The initial water level is recorded as h_1, corresponding to the upper timing mark. Water is then allowed to flow vertically through the asphalt specimen under gravity. As water passes through the specimen, the water level in the graduated cylinder gradually decreases. The time required for the water level to fall from the upper timing mark h_1 to the lower timing mark h_2 is recorded. This elapsed time represents the time required for water to pass through the internal void structure of the mixture. A faster drop in water level indicates higher permeability, while a slower drop indicates lower permeability. The coefficient of permeability, k is then computed using Darcy's law. The coefficient of permeability,

$$k = \frac{aL}{At} * ln\left(\frac{h_1}{h_2}\right) * t_C \quad (2.2)$$

where k = coefficient of permeability (cm/s), a = graduated cylinder area (cm^2), A = specimen area (cm^2), L = specimen thickness (cm), t = elapsed time (s), h_1, h_2 = initial/final heads (cm), and t_c = temperature correction. The temperature correction for water viscosity, standardized to 68°F (20°C), which helps make results more comparable across testing conditions (FDOT, 2015). In general, test is conducted at room temperature, and the measured permeability is corrected for water viscosity using the temperature correction factor.

There is no universal bridge-deck permeability limit, but according to NCAT, pavements can become "excessively permeable" when permeability is around 3.94×10^{-5} in./s (100×10^{-5} cm/s) for 3/8 to 1/2-in. (9.5 to 12.5 mm) NMAS mixtures and about 4.72×10^{-5} in./s (120×10^{-5} cm/s) for 3/4-in. (19 mm) NMAS (Cooley et al., 2001). FDOT reported that an average permeability criterion for surface course mix should be less than 4.92×10^{-5} in./s (125×10^{-5} cm/s) (FDOT, 2003). The Wisconsin DOT investigated the water permeability (k) of a fine-graded HMA mixture, which ranged from 0 to 1.97×10^{-5} in./s (0 to 5×10^{-5} cm/s), and considered it nearly impermeable (Williams et al., 2010). Virginia research reports that at Virginia DOT, the maximum allowable permeability is about 4.92×10^{-5} in./s (125×10^{-5} cm/s) for new mix designs (Maupin, 2003). According to NYSDOT, the permeability of bridge deck HMA overlays mixture should be approximately 3.94×10^{-8} in./s (1×10^{-7} cm/s) or less when tested at 4.0% ± 1.0% air voids (NYSDOT, 2015).

2.7.3 Rutting

Rutting resistance is the ability of an asphalt surface to withstand permanent deformation in the wheel paths caused by heavy traffic loads, high temperatures, and inadequate structural stability within the mix. Depression develops in pavement in two ways. One is when air voids collapse, and the mix is further compacted under loading, a process called densification. Another one is shear flow, in which the asphalt–aggregate skeleton is more compacted under high tire shear stresses at warm temperatures (Rahman et al., 2014). The bridge deck overlay is much thinner than the pavement. Therefore, it will have to withstand higher stress. Consequently, rutting is more critical for a bridge deck than the pavement. The Hamburg wheel-tracking test is the most widely used method for analyzing rutting (FHWA, 2017; TxDOT, 2009).

2.7.3.1 Hamburg Wheel-Track Test (HWTD)

The Hamburg wheel Tracking test (TxDOT, 2019) is widely used by DOTs to evaluate an asphalt mixture's susceptibility to rutting and moisture-related damage (stripping) under repeated wheel loading. The HWTD will also be useful for bridge-deck overlay mixture evaluations, especially for thin, high-binder, low-permeability surface courses, because it directly simulates a concentrated wheel load repeatedly moving over the surface. This test loading procedure is somewhat correlated with field temperatures and field loading conditions.

In the typical HWTD test procedure, laboratory-compacted specimens (typically gyratory-compacted cylinders or saw-cut slabs) are placed in a hot-water bath at 122°F (50°C). A steel wheel load of approximately 158 lb (705 N) is applied to the specimen during testing. The rut depth is recorded repeatedly as a function of wheel passes (Rahman et al., 2014). According to the Texas Department of Transportation (TxDOT) Tex-242-F specification, the HWTD requires asphalt samples to withstand 20,000 passes with a maximum rut depth of 0.5 in. (12.5 mm) (Rahman et al., 2014; TxDOT, 2019). HWTD output is typically a rut depth versus wheel passes curve that can be interpreted in phases. Many agencies divide the curve into three phases. The first part of the curve, called the early post-compaction phase or consolidation, is mainly caused by the first few wheel passes. With these wheel passes, the sample continues to compact further. The second phase is a creep phase, characterized by continuous deformation. And the final phase is the one in which deformation accelerates due to moisture damage. The final phase is indicated by a stripping inflection point (SIP) and a subsequent "stripping slope." In practice, agencies may use the total rut depth at a specified number of passes to confirm rutting resistance. At the same time, some agencies use SIP/stripping-related slope as indicators to evaluate moisture susceptibility when a stripping response is present (Rahman et al., 2014).

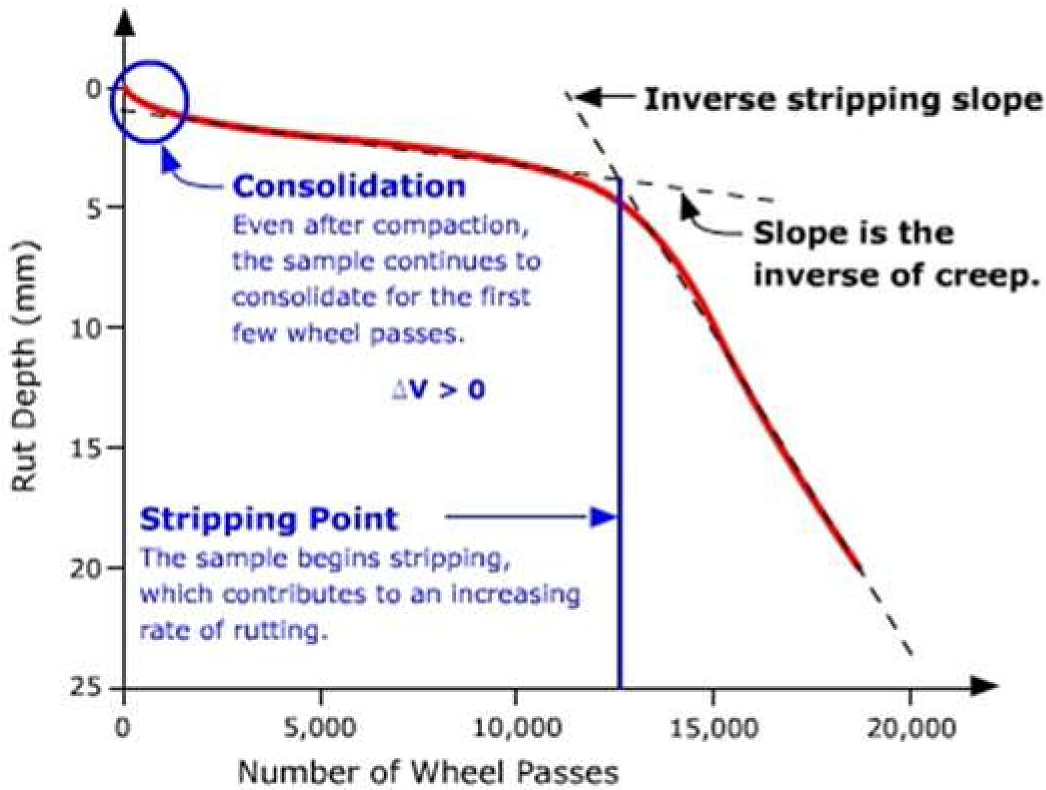

Figure 2.10: Typical Hamburg Wheel Tracking Test (HWTT) curve showing rut depth versus number of wheel passes and the stripping point (TxDOT Tex-242-F)

Different agencies follow different criteria based on PG binder grade and their region's climate. Table 2.3 shows the criteria for selected states that use HWTD test results. Early European practice used very strict limits (e.g., <4 mm at 20,000 passes), while U.S. agencies often adopted less restrictive thresholds better aligned with local materials and climate. Kansas follows Tex-242-F, and for PG binder 64-xx, at 0.5 in (12.5 mm) rut depth, the minimum wheel passes should be 20,000 (Rahman et al., 2014; TxDOT, 2019).

Table 2.3 Summary of State DOT Hamburg Wheel Tracking Device (HWTD) Test Rutting Criteria for Asphalt Mixtures (Yin et al., 2020)

State	Binder/Mixture type	Temperature	Criteria
California	PG 58-xx	122°F (50°C)	Min. 10,000 passes at 0.5 in. (12.5 mm) rut depth
	PG 64-xx		Min. 15,000 passes at 0.5 in. (12.5 mm) rut depth.
	PG 70-xx		Min. 20,000 passes at 0.5 in. (12.5 mm) rut depth.
	PG 76-xx		Min. 25,000 passes at 0.5 in. (12.5 mm) rut depth.
Colorado	PG 58-xx	113°F (45°C)	Max. 0.16 in. (4.0 mm) rut depth at 10,000 passes
	PG 64-xx	122°F (50°C)	
	PG 70-xx, 76-xx	131°F (55°C)	
Texas	PG 64-xx	122°F (50°C)	Min. 10,000 passes at 12.5 mm rut depth
	PG 70-xx		Min. 15,000 passes at 0.5 in. (12.5 mm) rut depth.
	PG 76-xx		Min. 20,000 passes at 0.5 in. (12.5 mm) rut depth
Oklahoma	PG 64-xx	122°F (50°C)	Min. 10,000 passes at 0.5 in. (12.5 mm) rut depth
	PG 70-xx		Min. 15,000 passes at 0.5 in. (12.5 mm) rut depth
	PG 76-xx		Min. 20,000 passes at 0.5 in. (12.5 mm) rut depth
Illinois	PG 58-xx (or lower)	122°F (50°C)	Max. 0.5 in. (12.5 mm) rut depth at 5,000 passes
	PG 64-xx		Max. 0.5 in. (12.5 mm) rut depth at 7,500 passes
	PG 70-xx		Max. 0.5 in. (12.5 mm) rut depth at 15,000 passes
	PG 76-xx (or higher)		Max. 0.5 in. (12.5 mm) rut depth at 20,000 passes
Utah	PG 58-xx	114.8°F (46°C)	Max. 0.39 in. (10.0 mm) rut depth at 20,000 passes
	PG 64-xx	122°F (50°C)	
	PG 70-xx	129.2°F (54°C)	

Oregon DOT's SPR-815 report ("Bridge Deck Asphalt Concrete Pavement Armoring") evaluated four bridge deck waterproofing strategies. The strategies were: (1) sprayed liquid membrane, (2) poured liquid membrane, (3) roll-on sheet membrane, and (4) roll-on sheet membrane with a mastic asphalt layer. For the mastic asphalt layer, they designed a low-void, pourable layer using 11.0% binder, PG 70-22ER, and very fine-grained aggregate with NMAS 0.094 in. (2.38 mm) (placed in a 10 mm layer). A plant-produced asphalt overlay was compacted over each system. All mixtures were made as a composite block with 2 in. (50 mm) concrete and a waterproofing system, and a 2 in. (50 mm) asphalt overlay. To avoid puddling, a tack coat application rate of 0.071 gal/yd² (0.32 L/m²) was used for higher-texture sprayed or poured membranes, whereas 0.051 gal/yd² (0.23 L/m²) was used for low-texture roll-on or mastic systems. For HWTD testing, the composite asphalt blocks were submerged in a hot-water bath at 122°F (50°C) and subjected to 20,000 wheel passes. The study compared the samples with and without freeze-thaw conditioning. The results showed that for the first three strategies, the rut depth was higher in freeze-thaw conditioning samples. The results explained that when samples undergo freeze-thaw, the molecular bond between the membrane and deck weakens. Moreover, they found that among all membranes, mastic asphalt layers were less susceptible to freeze-thaw, whereas sprayed membranes were more susceptible. However, the study also noted that mastic asphalt showed greater rut depth than the other membranes due to its 11% binder content (Haynes et al., 2020). Table 2.4 shows HWTD results for bridge decks.

Table 2.4 Rutting Resistance Standards (HWTD) (Tex-242-F)

Study	Binder Type	Temperature	Wheel Passes	Key Bridge Deck Finding
"Bridge Deck Asphalt Concrete Pavement" (SPR-815)-ODOT (Haynes et al., 2020)	Waterproofing strategy block samples + mastic layer (mastic reported 11% binder, PG70-22ER, very fine NMAS)	122°F (50°C)	20,000	Poured membranes were less affected by freeze–thaw than sprayed membranes; the mastic layer deformed more due to its low stiffness and high binder content.
"Comparison of Asphalt Binder and Mixture Performance-Related Tests" -TxDOT (Yildirim et al.,2006)	PG 76-xx (bridge decks) PG 64-xx PG 70-xx	122°F (50°C)	20,000 10,000 15,000	PG grade and additives dominate Hamburg test results; aggregates have a less significant influence; TxDOT requires more passes for higher PG grades.
"Development and Field Experience of Performance-Based Low-Permeability Asphalt Mixture Used to Overlay Bridge Decks"-MTO (Ontario) (Varamini et al., 2019).	Low permeability mix reported as 70-28J LP Polymer Modified Asphalt (with 7% binder)	122°F (50°C)	20,000	Higher binder + finer gradation did not significantly worsen rutting.

2.7.3.2 IDEAL-RT (Rapid Shear Rutting Test)

State transportation agencies frequently use HWTD to assess an asphalt mixture's susceptibility to rutting/stripping. The test can also be used to evaluate moisture resistance by submerging the specimens in water. Including time for temperature conditioning and testing, an average HWTD test can take up to eight hours to complete. This extended duration is a challenge for production testing, where rapid test results are required for reactive Quality Control and Quality Assurance (QC/QA) program. The Indirect Tensile Asphalt Rutting Test is an alternative to the HWTD test for evaluating rutting resistance during HMA production (TxDOT, 2019). Many studies have shown a correlation between these two tests, despite differences observed in some asphalt mixtures.

The IDEAL-RT (Indirect Tensile Asphalt Rutting/Rapid Shear Rutting Test) is a rapid, monotonic loading test used to screen asphalt mixtures for high-temperature rutting susceptibility. It is now standardized as ASTM D8360 for determining the Rutting Tolerance Index (RTIndex) from a load–displacement curve. Higher RTIndex indicates better rutting resistance (Zhou et al., 2020).

Most IDEAL-RT procedures use gyratory, or core, specimens prepared as 6.0 in. (150 mm) diameter samples. The thickness of the specimen depends on NMAS. For 3/4 in. (19 mm) or smaller, the thickness is 2.44 ± 0.04 in. (62 ± 1 mm); for mixes with an NMAS of 1 in. (25 mm) or larger, the thickness is 3.74 ± 0.04 in. (95 ± 1 mm). They are compacted to 7.0 ± 0.5% air voids (no notching or cutting is required beyond thickness trimming). Specimens are then commonly conditioned at an elevated test temperature of 122 ± 2°F (50°C ± 15 °C) for a short period (typically 1–2 hours) before testing to simulate warm rutting field conditions (ASTM, 2021). The target test temperature is generally selected within the range of 50 ± 15°C, depending on local climate and agency practice.

In IDEAL-RT, a vertical compressive load is applied along the diametral plane of the cylindrical specimen. The specimen has been applying load under load-line displacement control at a constant rate of 1.97 ± 0.08 in./min (50 ± 2 mm/min), and the test is typically terminated shortly after the peak load is reached. During loading, the system records time, load, and displacement. The primary measurement extracted from the load–displacement curve is the maximum load, which represents the mixture's peak shear resistance under the imposed high-temperature condition (ASTM, 2021; Zhou et al., 2020).

The curved lower cradle is important because it spreads the support reaction over a larger area at the bottom of the specimen. This prevents the bottom of the specimen from failing locally under a concentrated support load. If narrow loading strips were used at both the top and bottom, as in a conventional IDT test setup, shear zones could develop on both sides of the specimen. This would create competing failure mechanisms and make the load–displacement response harder to interpret. Therefore, the curved cradle helps promote a more controlled shear failure and allows the peak load to better represent the mixture's rutting-related shear resistance.

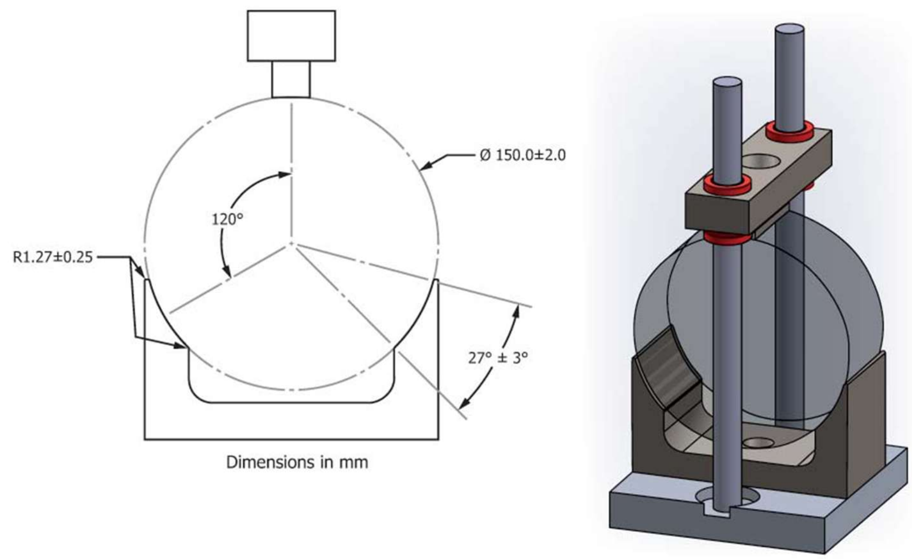

Figure 2.11: Schematic and 3D view of the IDEAL Rutting Test (IDEAL-RT) fixture (Option A), illustrating the cylindrical specimen placed on a curved support cradle and loaded vertically along the diametral plane using a top loading strip (ASTM D8360-22).

The test setup corresponds to the indirect tensile (IDT) splitting test. However, the failure mechanisms of the two tests differ due to the binder-aggregate reaction bond. In the conventional IDT test, conducted at lower and normal temperatures, the binder is stiff enough to behave elastically and tensile stress develops across the vertical diametral plane, causing the specimen to split. In the IDEAL-RT, the test is conducted at high temperature, where the asphalt binder becomes softer and has limited tensile strength. As a result, the specimen response is governed mainly by shear deformation rather than tensile splitting. These inclined shear planes show the probable locations where shear deformation and failure begin (Zhou et al., 2020). As loading continues, the aggregate skeleton begins to rearrange, and the softened asphalt binder allows aggregate particles to slide and rotate relative to one another. This internal particle movement is called shear flow. The shear flow represents the same fundamental mechanism that contributes to rutting in asphalt pavements under repeated traffic loading.

Figure 2.12 illustrates the conceptual stress distribution and failure mechanism in the IDEAL-RT test. The asphalt specimen is idealized as a circular disk subjected to a vertical compressive load P applied through a loading strip at the top. The load is distributed over a finite contact width, defined by the angle 2α. At the bottom, the specimen is supported at two locations, which provide reaction forces and are separated by an angle 2β. Each support has a contact arc defined by the angle 2δ.

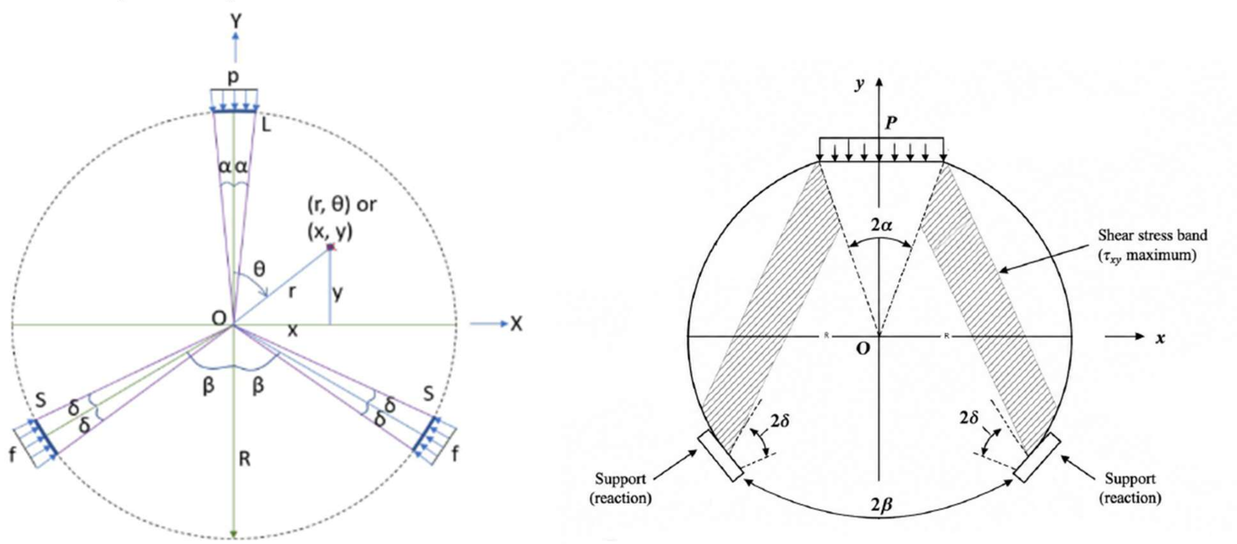

Figure 2.12: (a) Idealized IDEAL-RT loading configuration and coordinate system (Luo et al., 2022); (b) conceptual stress distribution showing inclined shear stress bands and shear-dominated failure mechanism.

Although the load is applied vertically, the internal stress condition within the specimen is not purely compressive. Due to the presence of two discrete supports, the load is redistributed, resulting in a complex stress field with compressive, tensile, and shear components. The most important feature shown in the figure is the formation of two inclined shear stress bands, indicated by the shaded regions. These bands originate near the edges of the loading strip and extend downward toward the support locations. The shaded regions in Figure 2.12 represent locations where the shear stress (τ_{xy}) reaches its maximum value. These zones define the probable paths of shear deformation and failure (Zhou et al., 2020). Unlike the conventional indirect tensile (IDT) test, where tensile stress dominates along the vertical diametral plane and causes splitting, the IDEAL-RT configuration suppresses tensile failure and promotes shear-dominated behavior. As a result, no continuous vertical tensile crack forms through the center of the specimen. Instead, the specimen fails through shear flow along the inclined bands. The angle between the supports (2β) and the contact lengths (2α and 2δ) control the location and intensity of the shear stress bands, thereby influencing the failure mode. Luo et al. (2022) showed that changing the conventional IDT support condition from a single bottom support to two bottom supports shifts the internal stress field from tensile-dominated splitting to shear-dominated failure. Their stress analysis using finite element method (FEA) showed that two inclined shear stress bands form within the specimen, supporting the use of this configuration for evaluating rutting resistance in asphalt mixtures (Luo et al., 2022).This shear-dominated failure mechanism is representative of rutting behavior in asphalt pavements, where permanent deformation occurs due to repeated shear loading under traffic.

In this test, the peak load on the load–displacement curve is the maximum load the mixture can withstand before shear failure occurs. ASTM D8360 converts this peak load into shear strength and then into the RT Index. Therefore, the RT Index provides a simple performance indicator of the mixture’s resistance to rutting. The test uses this peak load to measure the mixture's resistance to rutting.

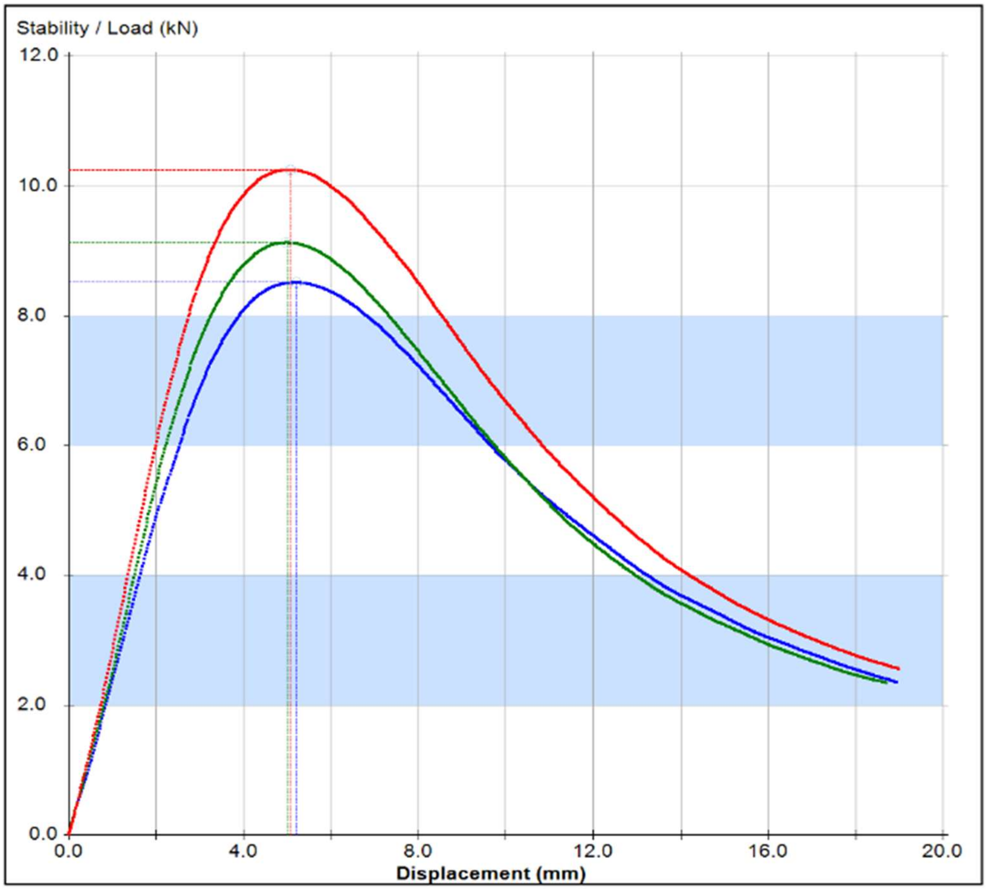

In order of peak load (High to Low):

RCI RCI-1A-11
RCI RCI-1A-10
RCI RCI-1A-7

Figure 2.13: Load–displacement curves from the IDEAL-RT test for RCI mixtures showing peak load and rutting resistance comparison

As mentioned earlier, the peak load measured during the IDEAL-RT must be converted into shear strength on the failure plane. This conversion is based on the contact area between the upper loading strip and the specimen. First, the peak load, P_{max}, is divided by the product of specimen thickness, t, and loading strip width, w, to estimate the average contact stress beneath the loading strip:

$$\frac{P_{max}}{t \times w} \tag{2.3}$$

This is just the load divided by the area where it is applied. However, the actual shear stress on the inclined failure plane is not the same as this contact stress. The load is redistributed within the specimen as it travels from the top strip to the failure surface. Zhou et al. (2020) studied this stress redistribution using finite element analysis and found that the shear stress on the failure plane is about 0.356 times the contact stress under the strip. This factor depends only on the shape and size of the test fixture, so it is the same for every mixture tested. Adding this factor gives the shear strength equation used in ASTM D8360 (ASTM, 2021).

$$\tau_f = 0.356 * \left(\frac{p_{max}}{t * w}\right) \tag{2.4}$$

where τ_f is the shear strength (Pa), P_{max} is the maximum load (N), t is the specimen thickness (m), and w is the width of the upper loading strip, defined in the standard as w= 0.0191 (m). For a typical specimen 62 mm thick, the equation simplifies to $\tau_f = 301 \times Pmax$ (in Pa, with P_{max} in N).

Once the shear strength is known, the RTIndex is calculated from a simple linear scaling:

$$\text{RTIndex} = 6.618 \times 10^{-5} \, (\tau_f / 1\,\text{Pa}) \tag{2.5}$$

The number 6.618×10^{-5} is just a scale factor. Shear strength values for asphalt at 50°C are usually around 1,000,000 Pa (1 MPa), and multiplying by this scale factor gives RTIndex values between about 60 and 200. This range is easier to use for comparing mixtures. Because the equation is a simple multiplication, the RTIndex and the shear strength always rank the mixtures the same way.

As many DOTs are familiar with HWTD, a study at Washington State University (WSU) tried to establish a correlation between IDEAL-RT and the Hamburg Wheel-Tracking Test (HWTD) results (WSU, 2022). The study developed a relationship between IDEAL-RT's RTIndex and Hamburg rutting performance using 23 dense-graded mixtures (11 are lab mixed-lab compacted and the rest are aged plant mixed-plant compacted). Both HWTD and IDEAL-RT tests were performed at 122°F (50°C). The test results showed that, for the HWTD tests, almost half of the mixtures met the criteria. Thus, rut depth cannot be determined alone or compared across all mixtures. Therefore, the study introduced the Rutting Resistance Index (RRI). Wheel passes and rut depth can determine the index, so this equation better captures the nonlinear increase.

$$RRI = N^{0.3}(1 - RD/25.4) \tag{2.6}$$

where RRI = Rutting resistance index, N = 20,000 or number of passes reaching 0.5 in. (12.5 mm) rut depth, and RD = Rut depth at 20,000 passes, or 0.5 in. (12.5 mm) rut depth, whichever comes first (WSU, 2022).

The target maximum RRI values for mixtures with PG64-XX, PG70-XX, and PG76-XX are 8, 9, and 10, respectively. The statistical analysis showed that mixtures with larger RTIndex consistently had higher RRI and better rutting resistance. The study calculated IDEAL-RT thresholds using HWTD criteria. Minimum RTIndex values of ≥60 for PG64-XX (95% confidence), ≥65 for PG70-XX (95% confidence), and ≥75 for PG76-XX or higher (98% confidence) were recommended (WSU, 2022).

Table 2.5 IDEAL RT Index for Highways for Different States

Source	RTIndex
Zhou et al. (2021), NCAT (2012)	Plants produced mixture: 75
VDOT/VTRC (2023)	Coarse graded: ≥ 72 Fine graded: ≥ 59
FDOT research report (2023)	≥ 65 (screen)
Texas (TxAPA, 2023)	PG 64 > 60 PG 70 > 65 PG 76 > 75

2.8 Summary

Bridge deck deterioration caused by deicing salts, freeze-thaw cycles, and fatigue cracking needs an alternative solution. This chapter reviewed the main causes of bridge deck deterioration and explained why overlays are widely used as an effective rehabilitation method. Bridge decks are constantly exposed to traffic, moisture, deicing chemicals, and temperature changes, which can lead to problems such as corrosion, freeze–thaw damage, cracking, spalling, and loss of durability over time. Thus, overlays are used to resolve these issues.

This chapter also reviewed the bridge deck overlay systems commonly used in practice, including polymer-based overlays, cementitious overlays, HMA overlays, waterproofing membranes, and the BDWSC concept developed by NJDOT. It further discussed the key performance properties required for bridge deck overlays, particularly friction, permeability, and rutting resistance, as well as the test methods commonly used to evaluate these. The literature review indicates that although several low-permeability asphalt systems have been developed for bridge deck applications, limited research has focused on the use of an RCI-based layer as the primary bridge deck overlay. Therefore, further investigation is needed to determine whether an RCI-based overlay can provide the combination of waterproofing, surface texture, and rutting resistance needed for bridge deck applications.

Chapter 3: Research Methodology

3.1 Introduction

This study was based on the concept of modifying an existing RCI-based mixture for potential application as a bridge deck surface overlay. Conventional RCI mixtures are primarily used as interlayers. RCI is effective in reducing reflective cracking. However, they are not suitable as a surface overlay due to their limited frictional performance and susceptibility to rutting. Nevertheless, bridge deck overlays must provide a highly impermeable layer to protect the deck from moisture and chloride infiltration. The conventional practice is to use an RCI layer and, on top of that, use a surface overlay to provide a riding surface. These two layers increase the overlay thickness and the additional dead load, potentially resulting in height constraints. This study investigated whether the RCI concept could be modified into a single mixture that could serve several purposes to solve these issues. The research mainly focuses on increasing friction, reducing permeability, and improving acceptable rutting resistance by modifying an RCI-based mix design. Therefore, the new modified RCI mix can serve as both a protective and functional surface layer for bridge deck applications.

This chapter provides an overview of the laboratory testing program for designing RCI-based asphalt mixtures for bridge deck overlays. Figure 3.1 presents the flowchart of the laboratory testing program adopted in this study. The laboratory tests included evaluation of volumetric properties, resistance to water infiltration (permeability), adequate friction (surface texture), and capacity to resist permanent deformation under repeated wheel loads (rutting resistance). The test results were used to compare the performance of the selected mixtures and to identify the binder content and the aggregate structure that can achieve the required impermeability, durability, and surface texture characteristics for bridge deck overlay use.

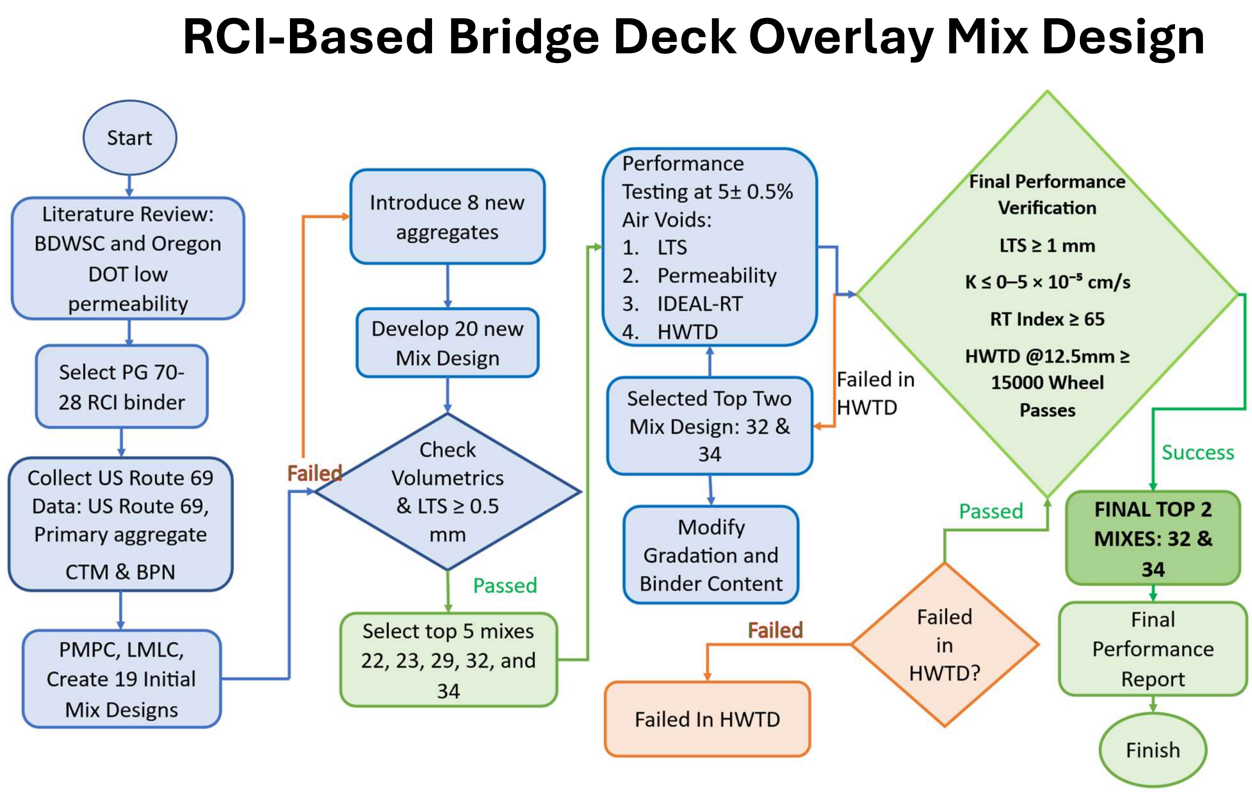

Figure 3.1: Laboratory test program flowchart

3.2 Material Properties

3.2.1 Asphalt Binder

The asphalt binder used in this study was PG 70-28 RCI, supplied by Flint Hills Resources (FHR), Omaha, Nebraska. This binder, used exclusively for the reflective crack interlayer (RCI) mixture, provides a balance between high-temperature rutting resistance and low-temperature cracking resistance. The PG 70-28 RCI binder is a polymer-modified asphalt binder. The binder components are primarily petroleum asphalt, with smaller amounts of oil distillates and a proprietary polymer modifier. The polymer content is at least 12%, which is comparatively high. The binder contains minor additives, including antistrip agents, other proprietary additives, and a vulcanizing agent. The binder is a dark brown to black, viscous liquid with an asphalt odor, a flash point greater than 450°F (232.2°C), a relative density of 0.9 to 1.1, and a viscosity of 250 to 24,000 Pa·s at 140°F (60°C). In this study, the target binder content was 8.3% by total mix weight. The recommended mixing temperature range was 311 to 319°F (155 to 159°C), while the compaction temperature range was 290 to 295°F (143 to 146°C).

3.2.2 Aggregates

The aggregate blend used in this study consisted of approved aggregate stockpiles selected for the RCI asphalt mixture. The blend included CH-1A, SSG-1, CS-2A, CS-2B, and SSG-2 aggregates, which were collected from various sources (Table 3.1). These materials were selected to produce a dense, predominantly fine-graded aggregate structure suitable for reflective-cracking interlayer applications, where low permeability, uniform texture, and adequate volumetric properties are important. The percentage retained on the US No. 4 (4.75 mm) sieve ranged from 0 to 11%, while the percentage passing the US No. 4 (4.75 mm) sieve ranged from 89 to 100%. These values indicate that the selected aggregate materials were primarily composed of fine materials, which is consistent with the intended purpose of the RCI mixture. The bulk specific gravity values of the aggregates ranged from about 2.56 to 2.61.

In addition to the primary aggregate blend, calcined bauxite manufactured by Great Lakes Minerals (GLM) was also studied. The calcined bauxite, also called Grip Grain Chinese calcined bauxite. This aggregate has high hardness, durability, and high resistance to polishing. These properties are desirable characteristics for improving surface friction in bridge deck overlay applications. The reported chemical and physical properties of the calcined bauxite included a bulk density of 204 lb/ft^3 (3.27 g/cc), soundness value of 1.3 (AASHTO T 104), polished stone value (PSV) of 71 (AASHTO T 279), and resistance to L.A. Abrasion Loss of 9.3% (AASHTO T 96). The chemical composition of the material consisted primarily of Al_2O_3 (88.10%), along with smaller amounts of Fe_2O_3 (1.45%), SiO_2 (5.10%), and TiO_2 (3.70%).

Table 3.1 Primary Aggregates Source

Aggregate	Producer / Source	County	Bulk Dry Specific Gravity
CH-1A	Williams Diversified Fine Drag Sand	Ottawa, OK	2.526
SSG-1	Cornejo Materials Mason Sand	Sedgewick, KS	2.554
CS-2A	Nelson Fort Scott Man. Sand	Bourbon, KS	2.572
CS-2B	Nelson Fort Scott Screenings	Bourbon, KS	2.572
SSG-2	Cornejo Materials FAA Sand	Sedgewick, KS	2.554

Table 3.2 Primary Aggregates Gradation

Aggregate	% Retained										
	1 in.	3/4 in.	1/2 in.	3/8 in.	#4	#8	#16	#30	#50	#100	#200
CH-1A	0	0	0	0	5	29	55	75	88	93	96
SSG-1	0	0	0	0	0	0	2	6	43	93	99.5
CS-2A	0	0	0	0	11	49	80	93	94	95	96
CS-2B	0	0	0	0	9	37	61	77	84	88	91
SSG-2	0	0	0	0	0	5	29	56	85	98	99
Calcined Bauxite	0	0	0	0	0	38	97	97	97	97	97

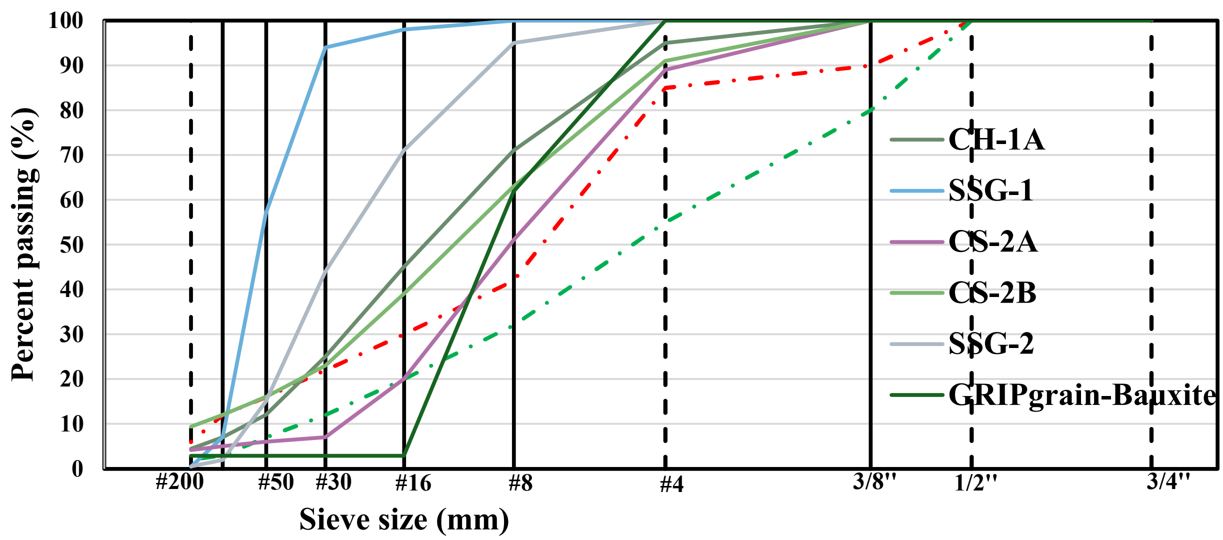

Figure 3.2: Gradation curves for primary aggregate

Figures 3.3 and 3.4 show the other aggregates and sources used in this study in addition to those identified in Table 3.1 The Dolese aggregate used in this study was obtained from Dolese Bros. Co. The source was identified as Richards Spur Quarry, located in Elgin, Oklahoma. The aggregate had an absorption of 0.50% and a specific gravity (SSD) of 2.69. CS-1 was a limestone aggregate, sourced from Johnson County, Kansas. CS-2 was identified as a non-carbonated trap rock aggregate from Iron Mountain (St. Francois County, Missouri). The CME aggregate used in this study was supplied by Williams Diversified Materials**,** which was identified as Picher, Oklahoma, “St. Joe” Pile Run Chat Wear Grading C. The aggregate had a bulk dry specific gravity of 2.525**,** a bulk specific gravity (SSD) of 2.575, an apparent specific gravity of 2.658, and an absorption of 2.0%. Additional physical test results showed a Los Angeles abrasion loss of 23%, a Micro-Deval value of 6.6, and a soundness value of 0.92. CG-1 and CG-1A were coarse aggregates supplied by Venture Lakin from Kearny County, Kansas. The CG-1 and CG-2 sources were located in Hamilton County, Kansas. The aggregate sources represented eastern, southeastern, south-central, and western Kansas, and several aggregates were obtained from out-of-state sources in Oklahoma and Missouri that are known to provide nonpolishing, hard aggregates. No RAP has been used in this study.

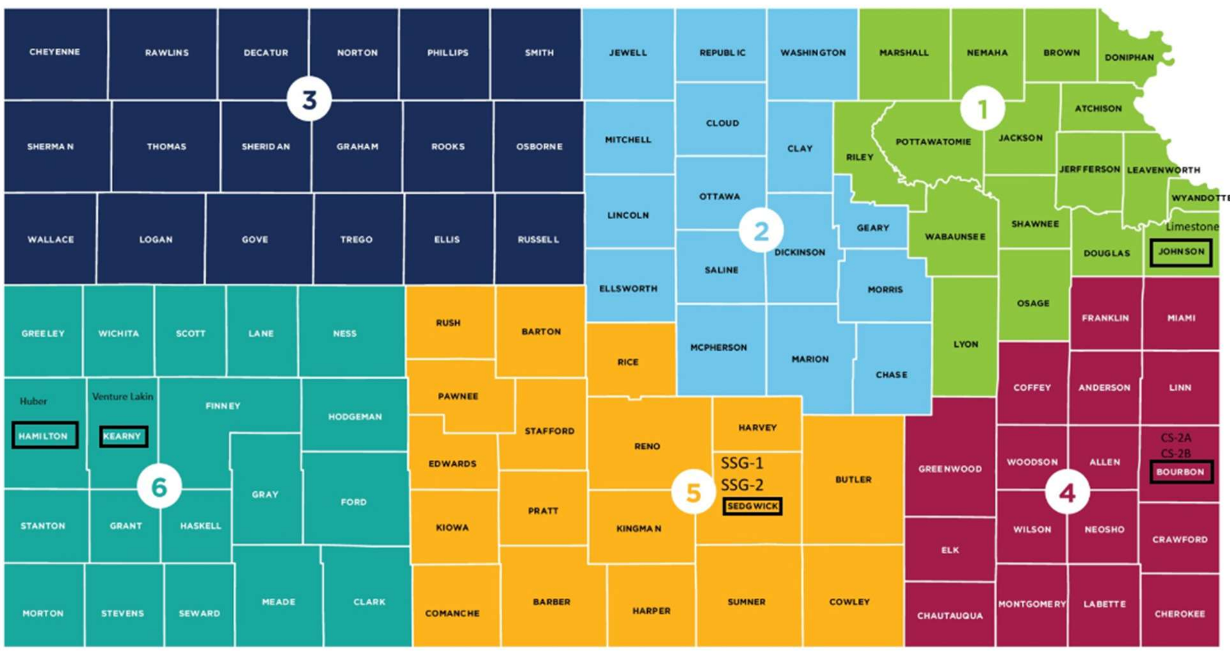

Figure 3.3: Locations of study aggregates in Kansas

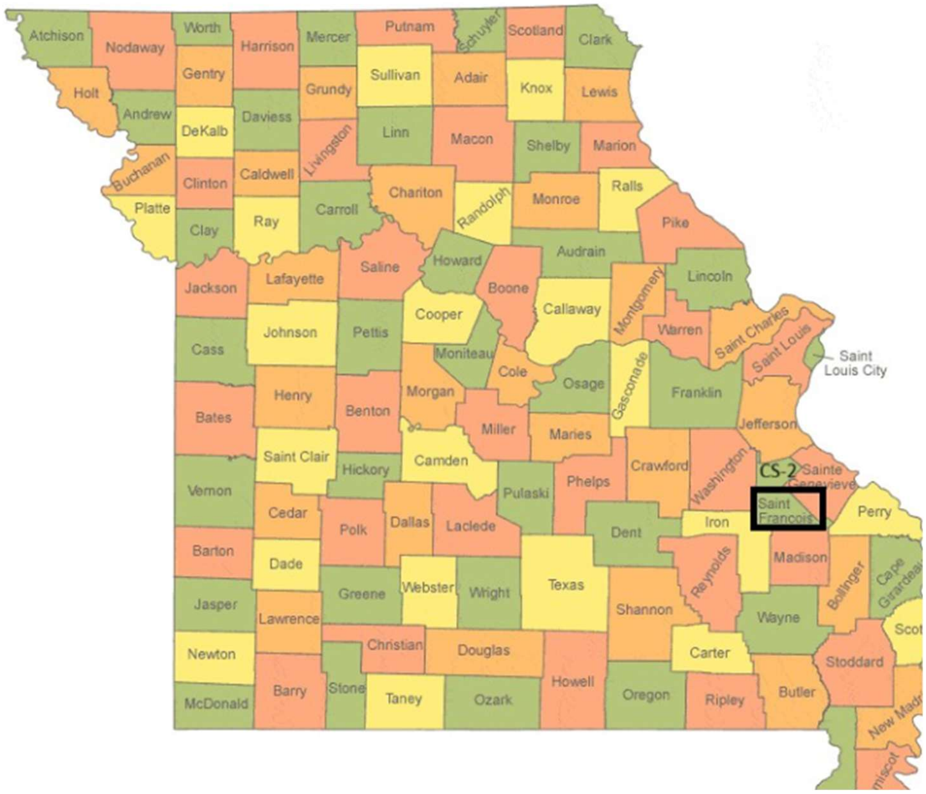

Figure 3.4: Location of the CS-2 aggregate source in Saint Francois County, Missouri.

Table 3.3 Secondary Aggregates Source

Aggregate ID	Aggregate / Material	Source / Producer	Quarry / Location	Specific Gravity
Dolese	Dolese	Dolese Bros. Co.	Richards Spur Quarry, Elgin, Oklahoma	2.69
Trap Rock	Trap Rock	Ideker, Inc		
CS-1	Limestone 1/2"	Hamm Olathe	Johnson County, KS	2.578
CS-2	Non-carbonated Trap Rock 1/2"	Iron Mountain	St. Francois County, Missouri	2.569
CME	Williams Diversified Materials	Williams Diversified Materials	Picher, Oklahoma	2.575
CG-1	Venture Lakin 5/8" Rock	Venture Lakin	Kearny County, Kansas	2.568
CG-1A	Venture Lakin 1/2" Rock	Venture Lakin	Kearny County, Kansas	2.568
CG-1	Huber 3/4" Rock	Huber	Hamilton County, Kansas	2.560
CG-2	Huber 1/2" Rock	Huber	Hamilton County, Kansas	2.568

Note: CS- Crushed Stone; CME = project-specific designation for St. Joe Chat aggregate supplied by Williams Diversified Materials, Picher, Oklahoma; CG-Crushed Gravel

Table 3.4 Secondary Aggregates Gradation

Aggregate	1 in.	3/4 in.	1/2 in.	3/8 in.	#4	#8	#16	#30	#50	#100	#200
Dolese	0	0	0	4	80	97	98	98	98	98	99.9
Trap Rock	0	0	13	67	99	99.9	99.9	99.9	99.9	99.9	99.9
CS-1 Limestone 1/2"	0	0	26	51	90	97	97	97	98	98	98
CS-2 Non-carbonated Trap Rock 1/2"	0	0	6	54	95	97	98	99	99	99	99
CME	0	0	0	2	63	89	96	99	99	99	99
CG-1 Venture Lakin 5/8" Rock	0	0	8	47	96	97	98	98	98	98	99
CG-1A Venture Lakin 1/2" Rock	0	0	0	15	95	96	97	98	98	98	98
CG-1 Huber 3/4" Rock	0	0	38	69	97	97	98	99	99	99	99
CG-2 Huber 1/2" Rock	0	0	0	13	81	94	96	97	97	98	98

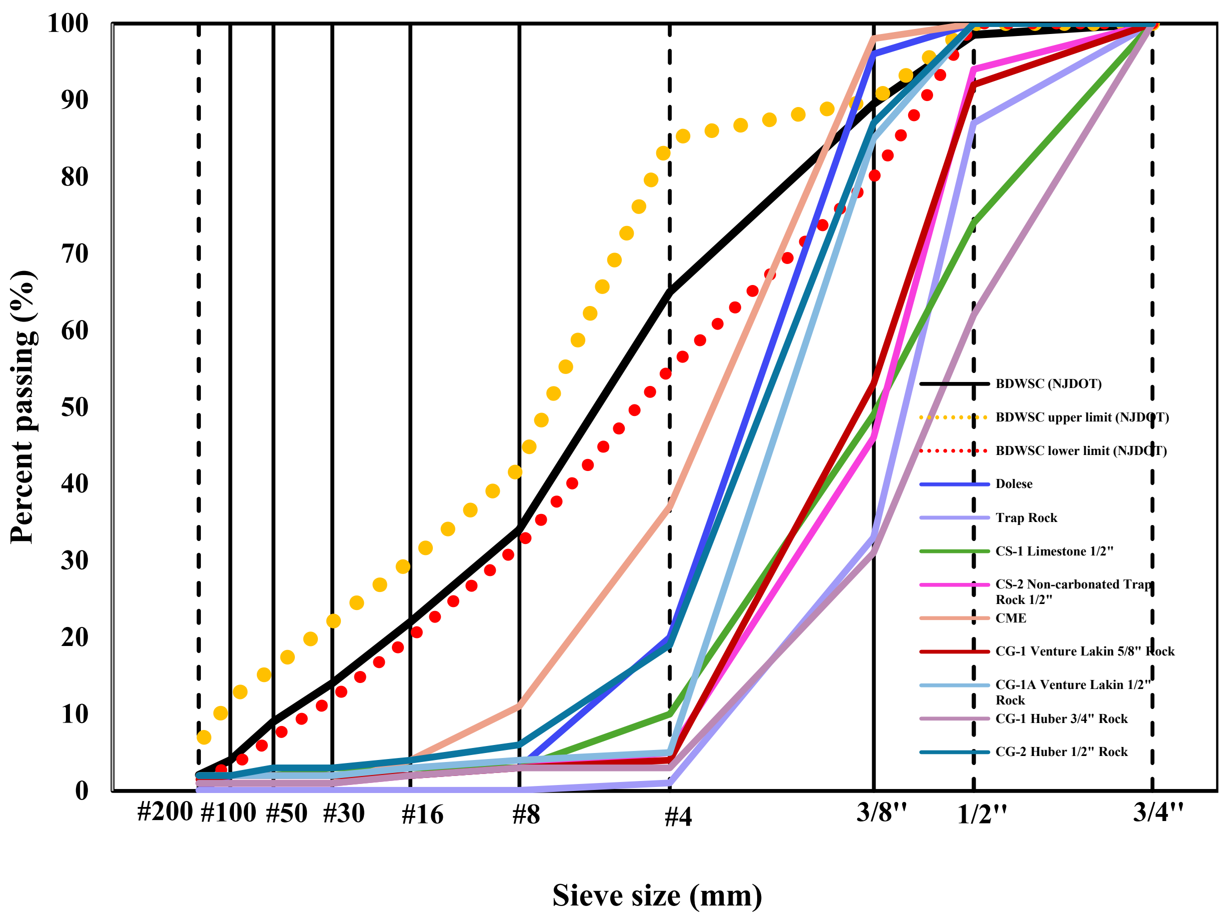

Figure 3.5: Gradation curves for secondary aggregates

3.3 Field Visit of US Route 69

An RCI pavement layer construction site on US Route 69 in Fort Scott, Kansas, was visited to collect primary aggregates and friction-related field data from the newly paved RCI surface. The British Pendulum test and the Circular Texture Meter (CTM) were used during the visit to evaluate the new pavement's surface texture and friction characteristics at eight different locations. The British Pendulum test showed a mean wet British Pendulum Number (BPN) of roughly 82, while the CTM results indicated a mean Profile Depth (MPD) with an average of 0.021 in. (0.54 mm), with values ranging from 0.011 to 0.024 in. (0.27 to 0.62 mm). These results show that the initial average surface texture and wet friction performance of the plant-produced RCI mix applied on US 69 were somewhat satisfactory. However, the MPD values were inconsistent across all locations, and several measurements were below the FHWA minimum limit. The inconsistent results indicated that friction needed improvement if this mixture were to be used as a riding surface. Therefore, a plant-produced mixture was collected and compacted in the lab as a reference mix.

3.3.1 British Pendulum Test

The British Pendulum Test (BPT) is a widely used method for evaluating the skid resistance (friction) of pavement surfaces. It measures the frictional resistance between a standardized rubber slider and the pavement surface, and reports the result as the British Pendulum Number (BPN). The test primarily captures the effect of microtexture, which governs friction at low speeds and under wet conditions. The test is conducted using a pendulum device in which a rubber slider attached to the arm swings over the pavement surface, as shown in Figure 3.6(a). Before testing, the specimen or pavement surface is typically wetted to simulate wet-weather conditions. As the pendulum swings, the rubber slider contacts the surface over a fixed length, and energy is lost to friction. This loss of energy is measured on a calibrated scale and reported as the BPN. Higher BPN values indicate greater frictional resistance, while lower values suggest smoother or polished surfaces with reduced skid resistance. The test is standardized under procedures such as ASTM E303 (ASTM, 2018).

The BPT provides rapid, repeatable results and is commonly used for both laboratory specimens and field pavement evaluations. Typical BPN values vary depending on surface condition and material. Studies have shown that newly constructed or high-friction surfaces may exhibit BPN values greater than 70–80, while polished or worn surfaces may fall below 40–50, indicating reduced friction (Hall et al., 2009; Henry, 2000).

(a) (b)

Figure 3.6: Field friction data collection (a) British Pendulum Test, (b) Circular Texture Meter (CTM)

3.3.2 Circular Texture Meter (CTM) Test

The Circular Texture Meter (CTM) was used to evaluate the surface macrotexture of the asphalt specimens. CTM is a laser-based device that measures the surface profile by scanning along a predefined circular track and recording elevation data. The collected profile is divided into multiple segments (typically eight), and the Mean Profile Depth (MPD) is calculated as the average of these segment values, as shown in Figure 3.6(b). ASTM E2157 specifies that CTMeter software reports MPD and Root Mean Square (RMS) values of macrotexture profiles, while FHWA describes CTM as a laser-based device for measuring MPD at a fixed pavement location. In this study, CTM measurements were taken at multiple positions (8 positions) of US 69 on the same surface to account for spatial variability, and the reported MPD value represents the average of these measurements, as shown in Figure 3.4 (b). Zahir et al. (2017) reported that CTM results showed a strong correlation with other texture parameters, such as Mean Texture Depth (MTD). The study found that HFST sections typically exhibited MTD values greater than 1.0 mm and that a strong relationship existed between skid number and MTD within the range of 0.5 to 1.5 mm, indicating that higher macrotexture improves friction performance (Zahir et al., 2017). Keeney (2017) reported $R^2 = 0.943$, indicating strong correlation between CT Meter and sand patch texture measurements. The results indicate that CTM-derived MPD can be reliably related to sand patch texture depth. However, this correlation does not by itself define a universal friction requirement (Keeney, 2017). According to FHWA, an average texture depth of approximately 0.7 mm is needed to reduce hydroplaning, while a minimum texture depth of approximately 0.015–0.020 in. (0.4–0.5 mm) has been suggested for pavement surface texture evaluation (FHWA, 2014a; FHWA, 2019).

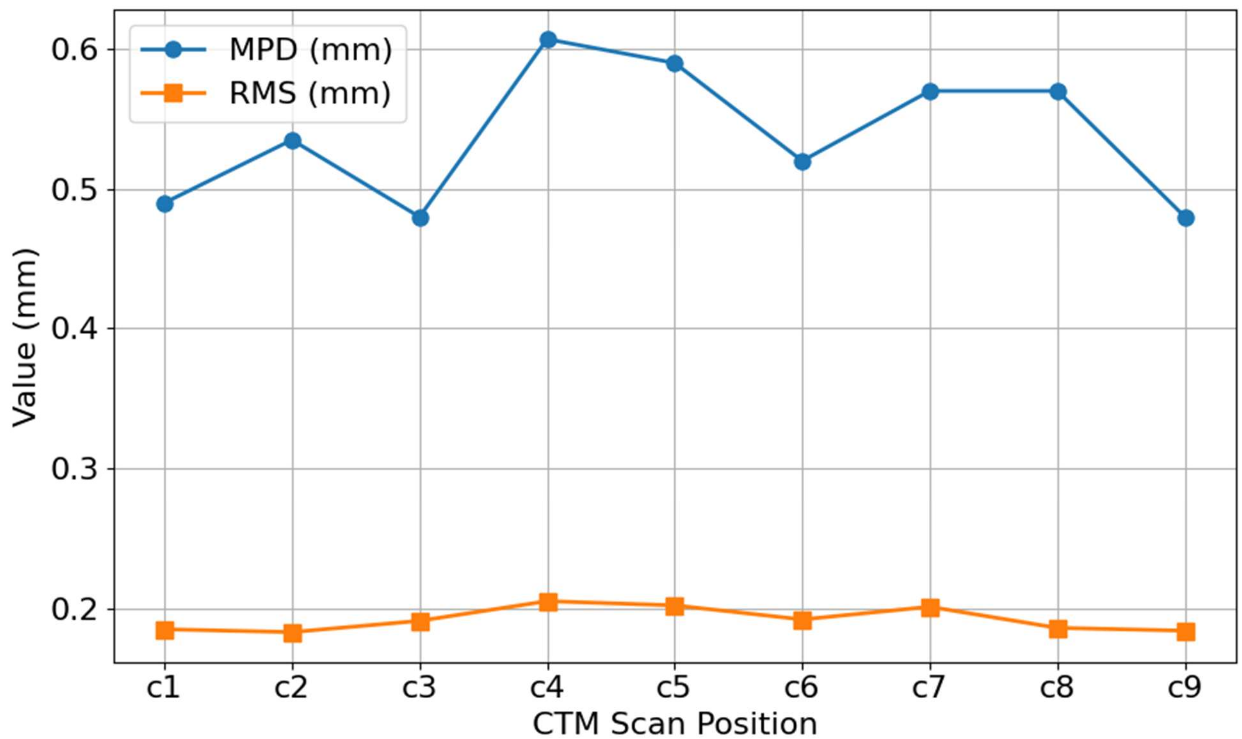

Figure 3.7: CTM test results collected from US-69

The figure 3.7 presents the variation in Mean Profile Depth (MPD) and Root Mean Square (RMS) values measured at different CTM scan positions (c1–c9) at the same pavement location. The MPD values range approximately from 0.48 mm to 0.61 mm, indicating moderate surface macrotexture across the location. The RMS values remain relatively consistent across all scan positions, ranging from approximately 0.18 mm to 0.21 mm, with only minor fluctuations. This indicates that the overall surface roughness is fairly uniform despite slight variations in macrotexture.

3.4 Mix design

The mix design process was developed based on the NJDOT BDWSC gradation range while using aggregate types in RCI mixes. This gradation was selected because it provides a dense aggregate structure suitable for bridge deck mixtures requiring low permeability. The total binder content of 8.3% was selected based on the plant-produced RCI mixture collected from US-69. First, the mixture collected from US-69 was compacted in the lab. The plant mixture-lab compacted (PMLC), Lab mixed-lab compacted (LMLC), and the approved mixture from US-69 have been tested for volumetrics. The design air-void limits have been set to achieve 2.5±0.5% air voids based on BDWSC at 50 gyrations. The approved mixture achieved 2.2% air voids, whereas PMLC yielded 3.9% air voids, exceeding the upper limit of the design air voids range. With the five primary aggregates mixed in various quantities to make 10 trial mix designs to shift the plant and approved gradation curve of US-69 to within the BDWSC limits. Surface texture was measured using the Laser Texture Scanner (LTS) on design gyratory compactor-compacted plugs. Although some mixes showed good volumetric characteristics, the LTS values remained close to 0.016 in. (0.4 mm), indicating that the surface texture still needed to be investigated for friction loss. Calcined bauxite was added to the mixes to further improve the texture. Ten additional mixtures were prepared with calcined bauxite at about 5%, 8%, and 10%. The gradations of these mixtures and the MPDs on design plugs are shown in Table 3.6. However, adding calcine bauxite did not make a major difference in the MPD results. The results indicate that calcined bauxite alone did not provide improved texture. Therefore, the primary aggregate structure also needed to be modified to achieve a desired MPD of 0.039 in. (1.0 mm) or higher.

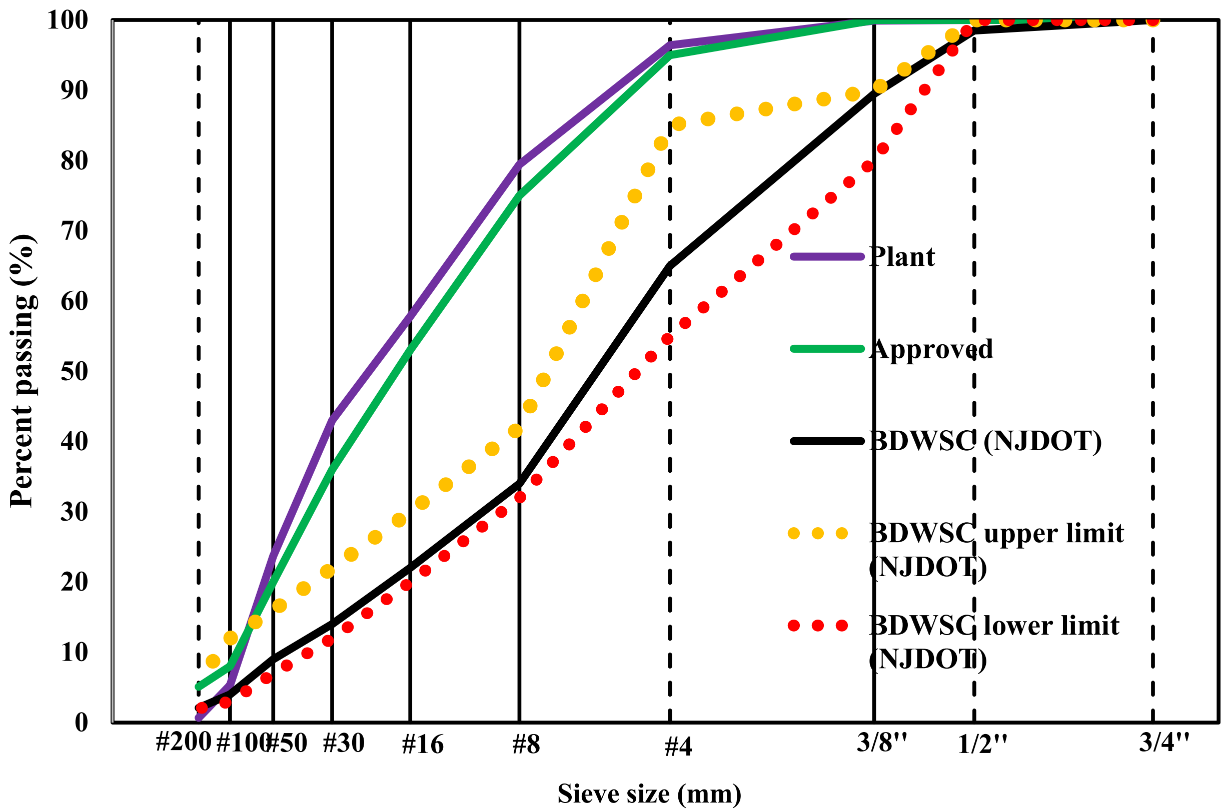

Figure 3.8: Aggregate gradation curves for plant and approved mixtures of US-69

Table 3.5: Mix Design with Primary Aggregates

Aggregate	App	Plant	1	2	3	4	5	6	7	8	20	21
CH-1A	37	34	42	37	37	32	34	40	36	37	37	28
SSG-1	15	26	15	15	15	11	15	15	17	13	11	0
CS-2A	4	16	9	33	19	5	19	5	3	4	42	42
CS-2B	33	8	23	4	18	40	21	29	33	35	0	30
SSG-2	11	16	11	11	11	12	11	11	11	11	10	0
AV (%)	2.2	3.9	2.7	4.2	4.3	3.9	4.9	5.4	4.2	4.6	4.1	6.9

Table 3.6 Mix Design with Primary Aggregates and Calcined Bauxite

Aggre-gate	App	Plant	9	10	11	12	13	14	15	16	17	18	19
CH-1A	37	34	37	37	37	36	32	35	37	35	30	40	42
SSG-1	15	26	8	6	11	9	10	18	13	24	20	8	8
CS-2A	4	16	26	29	26	26	24	26	25	20	25	26	30
CS-2B	33	8	13	10	10	11	10	0	7	0	0	0	5
SSG-2	11	16	11	10	11	13	14	11	12	11	13	11	5
AV (%)	2.2	3.9	5	8	5	5	10	10	6	10	12	15	10
MPD, in. (mm)	0.020 (0.51)	0.011 (0.29)	0.020 (0.52)	0.016 (0.40)	0.018 (0.45)	0.019 (0.48)	0.015 (0.39)	0.019 (0.48)	0.017 (0.42)	0.017 (0.42)	0.019 (0.49)	0.017 (0.42)	0.024 (0.60)

Since the calcined bauxite-modified mixtures could not achieve MPD close to 0.039 in. (1 mm), new aggregate sources were used in the next investigation of an RCI-based mix design for bridge deck overlays. In this stage, several alternative coarse aggregates, including Dolese trap rock, TP trap rock, CME, CS-1 limestone, CS-2 non-carbonated trap rock, Venture Lakin 5/8 in. rock, Venture Lakin 1/2 in. rock, Huber 3/4 in. rock, and Huber 1/2 in. rock, were incorporated into the mixture blends. These new trial mixtures were developed by replacing portions of the original aggregate structure while maintaining the overall mix gradation within the BDWSC-based gradation range. Fifteen new trial mixtures were prepared and evaluated to determine whether the new aggregate combinations could improve surface texture performance. The measured design air voids with secondary aggregate trial mixes ranged from 0.1% to 6.1%. The targeted design air voids were 2.5 ± 0.5%. For example, mix designs 26, 28, and 30 had air-void contents of 0.1%, 0.5%, and 0.1%, respectively. This indicates that some new aggregate mixtures have become either too dense or volumetrically unbalanced. Therefore, five aggregates for which air voids are close to the target range were selected.

The LTS results showed that introducing secondary aggregates to the mix design significantly improved the MPD compared to the approved and PMLC. The approved mixture's MPD was 0.020 in. (0.512 mm), while the PMLC's MPD was 0.011 in. (0.286 mm). The secondary aggregate mixture's MPD values ranged from 0.029 to 0.071 in. (0.741 mm to 1.806 mm). The secondary aggregates improved the macrotexture while shifting the curve closer to the BDWSC gradation limit. Mix Design 29 showed the highest MPD of 0.071 in. (1.806 mm), followed by Mix Design 27, 0.067 in. (1.693 mm), Mix Design 30, 0.059 in. (1.508 mm), and Mix Design 34, 0.058 in. (1.462 mm). These results suggest that incorporating one coarse aggregate was more effective than adding calcined bauxite. Based on MPD values and volumetric characteristics, we selected the top five mix designs for permeability and durability analysis. The top five mixes are numbers 22, 23, 29, 32, and 34. The samples were compacted at 5±0.5% air voids.

Table 3.7 Mix Design with Secondary Aggregates

Aggregate	App*	Plant	22	23	24	25	26	27	28	29	30	31	32	33	34	35
CH-1A	37	34	20	20	15	25	15	20	15	25	11	20	10	14	20	11
SSG-1	15	26	9	10	9	9	15	5	15	5	13	5	15	15	5	13
CS-2A	4	16	15	15	15	15	15	20	15	20	20	25	20	25	35	15
CS-2B	33	8	0	0	0	0	0	0	0	0	0	0	0	0	0	0
SSG-2	11	16	11	10	11	11	10	10	10	10	11	10	11	11	10	11
Dolese	0	0	45	25	0	0	0	0	0	0	0	0	0	0	0	0
TP	0	0	0	20	0	0	0	0	0	0	0	0	0	0	0	0
CME	0	0	0	0	50	40	0	0	0	0	0	0	0	0	0	0
CS-1	0	0	0	0	0	0	0	0	45	40	0	0	0	0	0	0
CS-2	0	0	0	0	0	0	45	45	0	0	0	0	0	0	0	0
CG-1	0	0	0	0	0	0	0	0	0	0	0	0	44	0	0	0
CG-1A	0	0	0	0	0	0	0	0	0	0	45	40	0	0	0	0
CG-1-H	0	0	0	0	0	0	0	0	0	0	0	0	0	35	30	0
CG-2	0	0	0	0	0	0	0	0	0	0	0	0	0	0	0	50
AV (%)	2.2	3.9	1.9	1.1	6.1	5.7	0.1	1.7	0.5	0.9	0.1	3.1	1.6	0.9	2.6	0.6
MPD (mm)	0.51	0.29	0.90	1.02	1.24	0.93	0.81	1.69	0.74	1.81	1.51	0.91	1.09	1.25	1.46	1.02

App*=approved

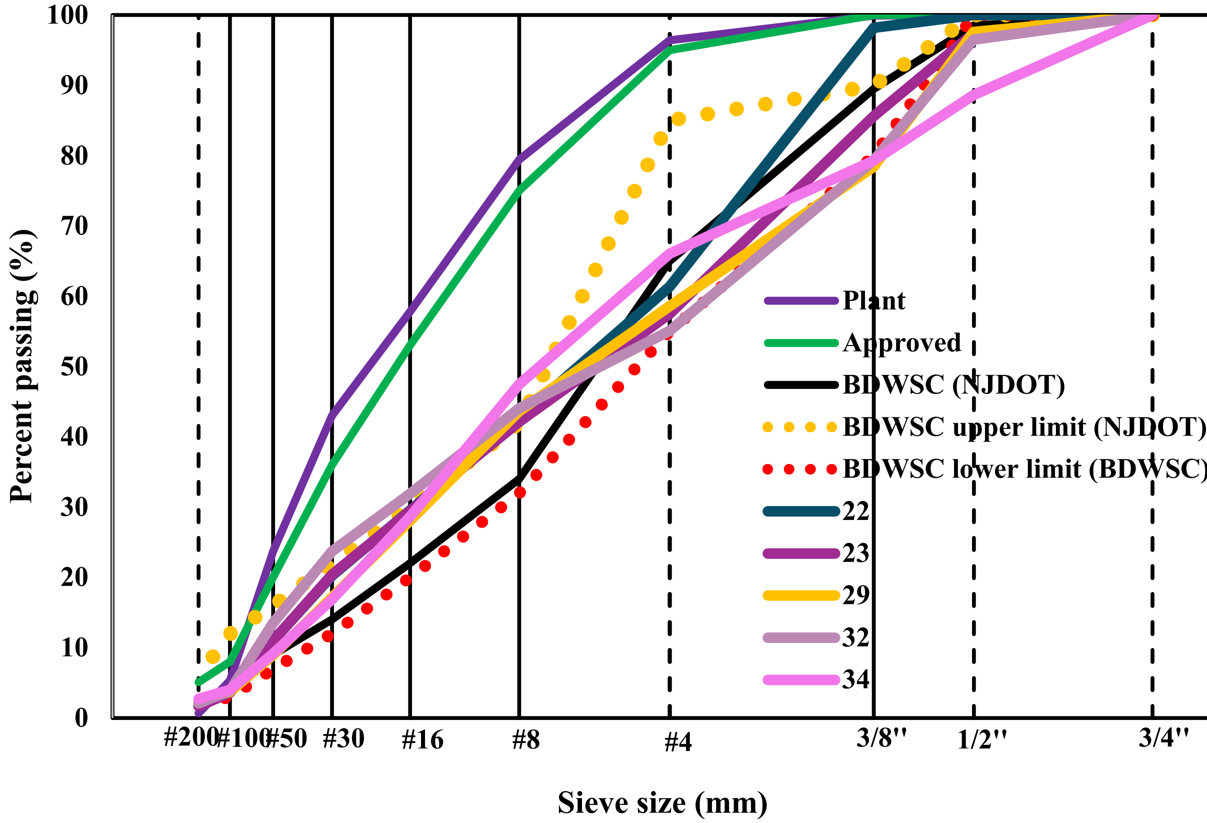

Figure 3.9: Aggregate gradation curves for the top five mix designs

Table 3.8 Top Five Mix Design's Volumetric Properties (@ 50 Gyrations)

Mix Design	Air Voids (%)	G_{mm}	G_{mb}	VMA (%)	VFA (%)	Absorbed Asphalt Content (%)	Effective Asphalt Content (%)	Passing #200 (%)	D/B
Plant	3.85	2.333	2.221	21.0	82	0.31	7.92	3.2	0.4
Approved	4.59	2.3	2.223	20.8	78	0.82	7.55	5.7	0.8
Lab	4.58	2.336	2.221	21.0	78	0.31	7.92	3.2	0.4
22	1.88	2.358	2.314	17.7	89	0.31	7.92	1.7	0.2
23	1.07	2.321	2.296	18.3	94	0.31	7.92	1.7	0.2
29	0.89	2.326	2.305	18.0	95	0.31	7.92	2.5	0.3
32	1.55	2.321	2.285	18.7	92	0.31	7.92	2.1	0.3
34	2.61	2.341	2.280	18.9	86	0.31	7.92	2.8	0.4

3.5 Specimen Preparation

Proper specimen preparation was an important part of this study because the consistency of mixing, aging, and compaction highly influences the laboratory performance of asphalt mixtures. Preparation of the test specimens for the permeability and IDEAL-RT tests required sample compaction, determination of the specimen's air voids, and preconditioning. The LTS measurement was taken on each plug before the permeability and IDEAL-RT tests.

3.5.1 Sample Mixing

Before mixing each mixture, aggregates were arranged according to the designated blend amounts and heated in the oven to the mixing temperature of 305 to 325°F (152 to 163°C). The asphalt binder was heated separately to the same mixing temperature, 305 to 325°F (152 to 163°C), to maintain the workability. These equi-viscous temperatures were based on the RCI binder grade (PG 70-28) used in this study. Once the materials were heated, half the aggregate was placed in a bucket, and the correct amount of binder was added. The aggregate and binder are mixed in the heated bucket with a mixing machine. The remaining aggregate was then added to the mixing. The materials were then mixed thoroughly until the aggregate particles were uniformly coated with the asphalt binder, resulting in a consistent mixture.

3.5.2 HMA Material Aging

After mixing, the loose asphalt mixture was aged, then compacted and subjected to performance testing. For short-term aging, the mix was uniformly spread on a flat pan and heated for 2 hours ±5 min at a compaction temperature of 290–315°F (143–157°C). To ensure uniform aging throughout the mix, the mixture was stirred every 60 ± 5 minutes during this time (Thomas et al., 2013). This short-term aging was done to simulate aging during field compaction, transportation, and plant mixing. The mixture was removed from the oven and used to prepare specimens after aging.

3.5.3 Sample Compaction

In this study, samples were compacted using a Superpave gyratory compactor (SGC). During compaction, a vertical pressure of 87 ± 3 psi (600 ± 18 kPa) was applied, along with an angle of gyration of 1.16° ± 0.02°. The compactor operated at a rotation speed of 30 ± 0.5 gyrations per minute. Before compaction, the molds and mixtures were preheated to reach the compaction temperature at 290 to 315°F (143 to 157°C). The approximate weight of each compacted specimen was estimated to meet the targeted air-void requirements of 5 ± 0.5% (test specimen preparation). After ensuring the correct compaction temperature, the pre-weighed loose mixture was charged into the mold using a pouring pan, and then the mold was transferred into the SGC. The compactor was set to the "fixed height" mode at 2.44 ± 0.08 in. (62 ± 2 mm) for 5.9-in. (150 mm) diameter samples. Both the permeability and IDEAL-RT test methods required this sample height. Compaction stopped automatically when the SCG reached the specified height. The compacted sample was then removed from the mold and cooled for a few minutes. For each mix, six replicates were compacted: three for permeability testing and the other three for IDEAL-RT testing.

3.5.4 Air Void Content Determination

The Kansas test method KT-39 was used to determine the theoretical maximum specific gravity (G_{mm}) of the loose mixture. The KT-15 test procedure was used to determine the bulk specific gravity (G_{mb}) of the compacted specimens.

3.5.4.1 Theoretical Maximum Specific Gravity (G_{mm}) Test Procedure

Based on NMAS, the sample size for the G_{mm} test is determined. For 3/8-in. (9.5-mm) NMAS mixtures, a minimum of 2.20 lb (1,000 g of sample) is typically used, whereas 0.5 in. (12.5 mm) NMAS mixtures require a minimum of 3.31 lb (1,500 g). Since all mixtures used in this study had a nominal maximum aggregate size (NMAS) of 1/2-in. (12.5 mm), A minimum of 3.31 lb (1,500 g) of loose mixture was used for the maximum theoretical specific gravity (G_{mm}) test. The sample was weighed and placed in a calibrated flask. Then, water at 77 ± 2°F (25 ± 1°C) was added to the flask until the sample was fully submerged. The flask was then placed on a mechanical agitator, and a vacuum was applied for 14 minutes to remove entrapped air from the mixture. After vacuuming, the flask was immersed in a water bath maintained at 77 ± 2°F (25 ± 1°C) for 10 ± 1 minutes, and the final submerged mass was recorded. The G_{mm} value was then determined using Equation 3.1.

$$G_{mm} = \frac{Dry\ Sample\ Weight,\ \ gms}{Dry\ Sample\ Weight{-}Weig\quad of\ Water\ displaced\ by\ Sample} \tag{3.1}$$

3.5.4.2 Bulk Specific Gravity (G_{mb}) Test Procedure

The bulk specific gravity (G_{mb}) of the compacted specimens was determined in accordance with the KT-15 method. After compaction, the specimens were allowed to cool to room temperature, and their dry masses were recorded. The compacted specimens were then immersed in a water bath maintained at 77 ± 2°F (25 ± 1°C) for 4 ± 1 minutes. After that, the submerged masses were measured. Following immersion, the specimens were removed from the water and rolled on a damp towel to remove excess surface moisture. The saturated surface-dry (SSD) mass was then recorded. The G_{mb} value of each specimen was calculated using Equation 3.2.

$$G_{mb} = \frac{Dry\ \text{mass of specimen in air},\ \ gms}{Sample\ SSD\ weight{-}\text{submerge}\quad \text{mass in wat}er} \tag{3.2}$$

The air void content (V_a) of each compacted specimen was calculated using the measured values of maximum theoretical specific gravity (G_{mm}) and bulk specific gravity (G_{mb}). The air void content was determined using Equation 3.3.

$$V_a = \left(1 - \frac{G_{mb}}{Gmm}\right) \times 100 \tag{3.3}$$

After determining the air voids of all specimens, any specimen that did not meet the air void requirements was discarded. For the permeability and IDEAL RT tests, the target air void was 5 ± 0.5%. For highway mixtures, the IDEAL-RT and permeability tests are commonly conducted at an air void level of 7.0 ± 0.5%. However, in this study, the mixtures were intended for bridge deck applications, where a lower air void content is desirable to reduce moisture infiltration and improve waterproofing performance. Therefore, the specimens used for the IDEAL-RT and permeability tests were prepared and tested at 5.0 ± 0.5% air voids.

3.6 Laser Texture Scanner (LTS) Test

Before IDEAL-RT and permeability tests, all specimens used in those tests were scanned by the LTS scanner. The Ames Engineering LTS9500 scanner was used to measure the surface texture of the compacted specimens and generate MPD. The specimen surface was cleaned and dried to prevent dust, loose particles, or surface moisture from affecting the laser reading. Before scanning, the Ames Texture Scanner software was opened, and the scanner was connected through the USB

Scanner tab. The scanner and the operating tablet were powered on, and the system was checked to confirm that the device was properly connected and ready for scanning. The scanner was then positioned directly above the specimen, with the selected test area centered within the scanning window as shown in Figure 3.8. The compacted specimen was placed flat and firmly under the scanner, with the test surface facing upward to ensure the laser traversed the surface uniformly during data collection. When the Scan button was pressed, the scanner first returned to its home position and then performed the surface scan. The scanner uses a 4 in. (100.0 mm) laser line width, has a vertical sample resolution of 0.00039 in. (0.01 mm), a length sample spacing of about 0.00195 in. (0.0496 mm), and a width resolution of about 0.00163 in. (0.0415 mm). A full scan takes about 90 seconds and produces 2,448 scan lines across the scan width. After completion, the scanner returned to the home position, and the scan file was stored for analysis. The collected scan files were then opened in the software's File Viewer for analysis. The LTS software displayed the scanned surface as a three-dimensional graph and calculated the selected texture indices in the Results tab. In this study, the primary texture parameters used were MPD and ETD, although other indices such as RMS, Ra, Rq, Rsk, and Rku were also available in the software output. Optional outputs, such as surface area, surface area-to-base area ratio, STL export, PSD plots, and cropped files, are also available in the software.

Although ASTM E1845 and ISO 13473-1 do not specify any required number of scans or replicate measurements. Previous studies (e.g., Hanson & Prowell, 2004; Praticò & Vaiana, 2012) have shown that multiple measurements and averaging improve the reliability of MPD results and reduce the effects of local surface variations. Moreover, the use of three repeated scans was based on the past research practice for laser-based MPD measurement. Hanson and Prowell (2004) used three replicate CTM measurements to evaluate the repeatability of MPD results (Hanson & Prowell, 2004). Similar repeat-measurement approaches have also been used in later CTM and laser-based texture studies. Therefore, in this study, three scans were taken on each specimen face and averaged to reduce measurement variation and obtain a more reliable MPD value.

In this study, the established practice was extended by scanning both the top and bottom faces of each specimen (compacted by the Superpave Gyratory compactor (SGC)), providing a more representative measurement of the overall surface texture than using only one face. For statistical analysis and comparison among mixtures, we kept the sample size constant across tests. The IDEAL-RT test (ASTM D8360-22, Section 8.4) requires a minimum of three specimens per mix, and the falling-head permeability test was conducted on a separate set of three specimens per mix. Therefore, following previous practice in laser-based MPD measurements, three repeat scans were performed for each surface (top and bottom) on each specimen to enable a statistically comparable comparison.

Figure 3.10: Laser Texture Scanner (LTS) test setup

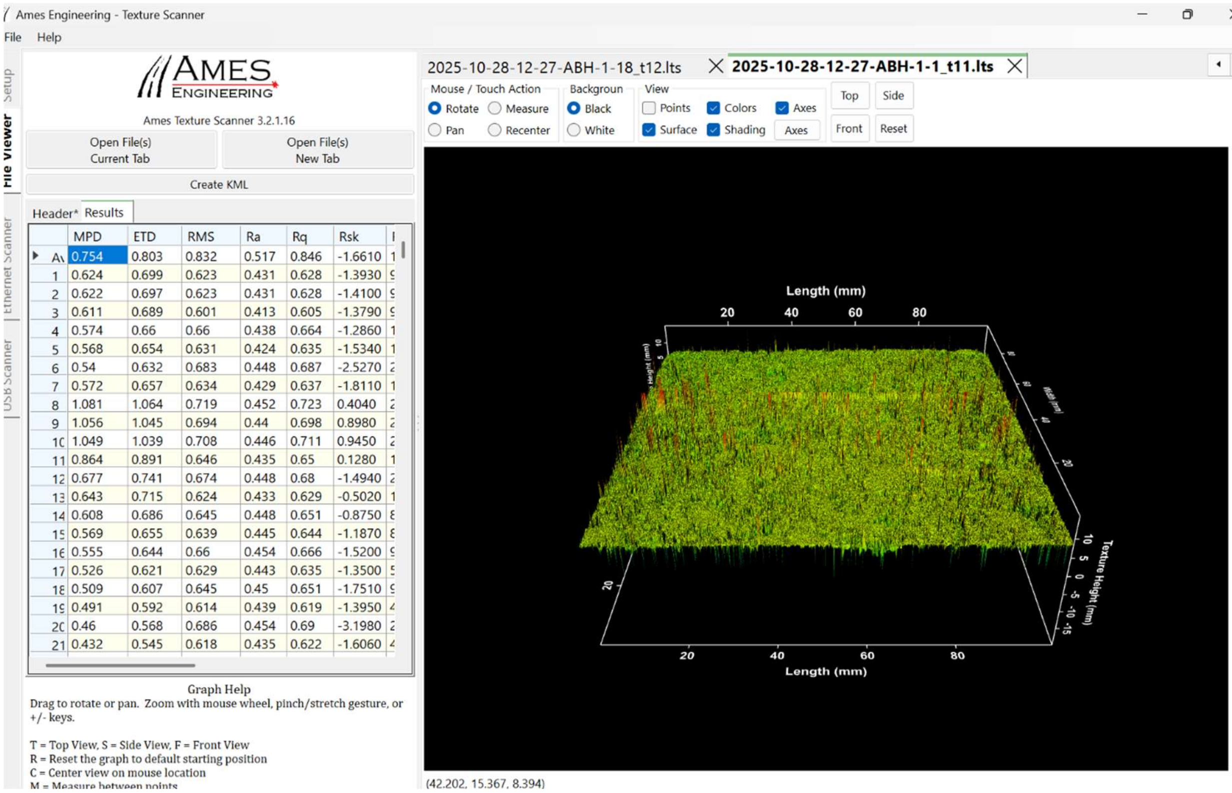

Figure 3.11: Laser Texture Scanner test result output

Table 3.9 Typical MPD and ETD Replicate Results

Mix Design	Replicate	MPD, in. (mm)	ETD, in. (mm)
32	1	0.0572 (1.452)	0.0134 (0.340)
	2	0.0482 (1.224)	0.0116 (0.295)
	3	0.0489 (1.243)	0.0118 (0.299)
	Mean	0.0514 (1.306)	0.0122 (0.311)
	Std. Dev.	0.0050 (0.127)	0.0010 (0.025)
	CV (%)	9.7	8.0

Table 3.9 provides a representative example of replicate measurements and the resulting mean, standard deviation, and coefficient of variation for one selected mix design and one SGC-compacted sample. These typical results are included to demonstrate how repeated measurements were summarized for LTS texture measurements. Overall, these statistics provided a useful means for assessing repeatability of the LTS test. 3.7 Preconditioning

After completing LTS, the IDEAL-RT specimens were placed in a 122 ± 2°F (50 ± 1°C) water bath for at least 45 minutes to achieve uniform temperature throughout the specimens (ASTM D 8360). Immediately after preconditioning, the specimens were removed from the bath and tested according to the IDEAL-RT procedure to minimize the effect of temperature changes during handling. For the FM 5-565 permeability test, the compacted specimens were soaked in water at room temperature for about 1 to 2 hours to aid saturation.

3.7 IDEAL-RT Test

The IDEAL-RT test was conducted in accordance with ASTM D8360, which determines the rutting tolerance of asphalt mixtures at high temperatures. The specimens are placed in the fixture of the testing machine and positioned at the load center before the test begins. Then, the machine reached the test position and started loading. load was applied at a constant deformation rate of 1.97 in./min (50 mm/min) until the specimen response was fully captured. During the test, load and displacement were continuously recorded and used to calculate the rutting tolerance index. The test continued until the peak load was reached and the specimen response was fully captured. Based on recorded data, a software called SmartLoader was used to determine the RTIndex. In the software, the specimen diameter, height, air void, binder content, and G_{mm} must be entered as inputs, and the software then calculates the RT index. Table 3.10 shows replicate measurements on a sample from Mix 32. The coefficient of variability is higher in this test.

Figure 3.12: IDEAL-RT test setup

Table 3.10 Typical RTIndex Replicate Results

Mix Design	Replicate	RT Index
32	1	56.0
	2	63.0
	3	92.0
	Mean	70.3
	Std. Dev.	19.1
	CV (%)	27.2

3.8 Permeability Test

The permeability test was conducted in accordance with the Florida Department of Transportation Test Method FM 5-565 (Figure 3.13). Before the permeability test, a thin layer of Vaseline was applied to the sides of the lab-compacted specimens (at 2.44 ± 0.08 in. height) to fill the large pores. The specimen was then enclosed in a latex membrane and confined in the permeability device. According to FM 5-565, the membrane pressure is maintained at 10 ± 0.5 psi (68.9 ± 3.4 kPa) during testing. Water was introduced into the graduated cylinder, and the elapsed time was measured as the water level dropped between the specified marks. The permeability test was then conducted three times on each specimen, and the results were accepted when the variation among the measured values was within 10%. Table 3.11 shows the typical results.

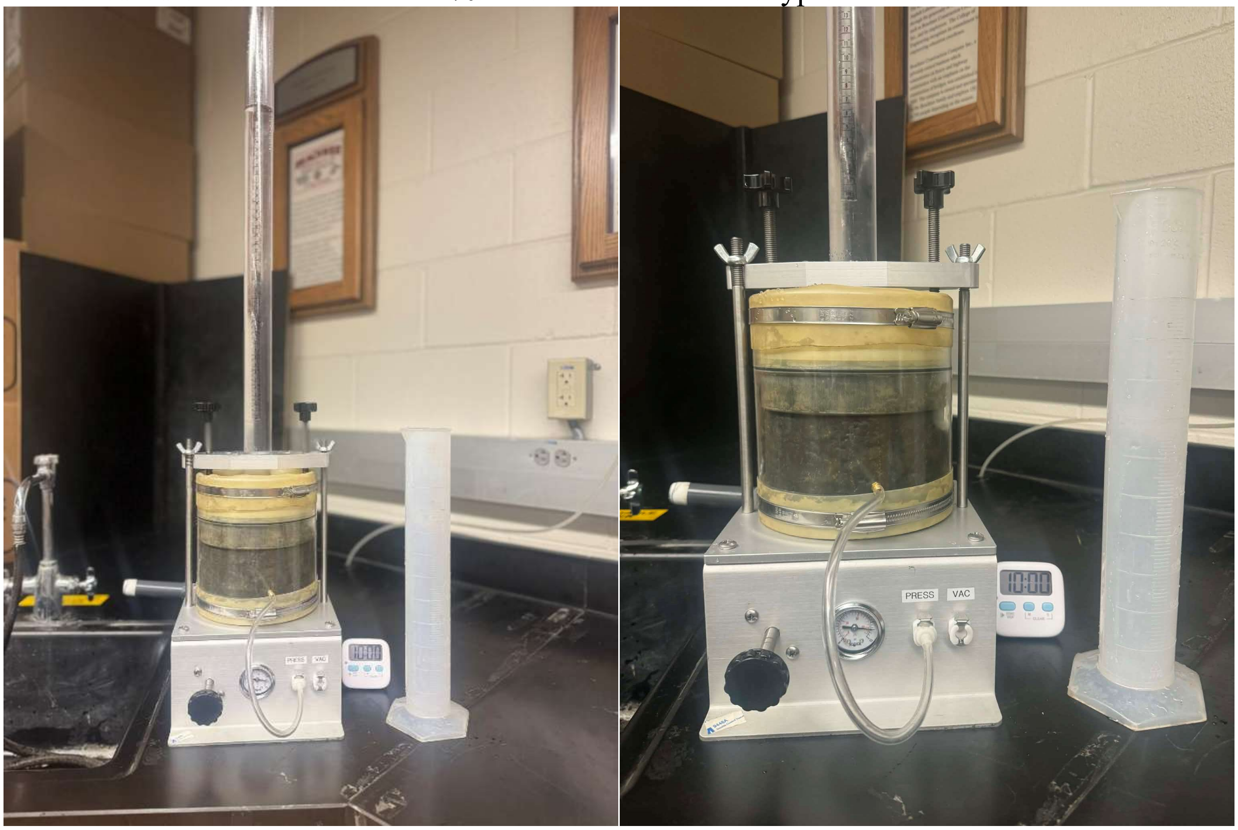

Figure 3.13: Permeability test setup

Table 3.11 Typical Coefficient of Permeability Replicate Results

Mix Design	Replicate	k, in./s (cm/s)
32	1	1.46×10^{-5} (3.70×10^{-5})
	2	1.50×10^{-5} (3.80×10^{-5})
	3	1.46×10^{-5} (3.70×10^{-5})
	Mean	1.47×10^{-5} (3.73×10^{-5})
	Std. Dev.	2.27×10^{-7} (5.77×10^{-7})
	CV (%)	1.5

3.9 Hamburg Wheel Tracking Device Test

Following TxDOT Tex-242-F, the Hamburg Wheel-Tracking Device (HWTD) specimens were prepared by trimming each to fit the HWTD test mold. After trimming, two specimens were placed side by side in an abutting position inside the mold, as shown in Figure 3.14. The molds were securely fastened to the machine so that no specimen movement occurred during wheel tracking. After mounting, the molds were set up in the HWTD water bath, which was maintained at 122 ± 2°F (50 ± 1°C). During the test, a steel wheel repeatedly moved back and forth across the top of the paired specimens under a load of 158 ± 5 lb (705 ± 22 N) at approximately 50 ± 2 passes per minute. Rut depth was automatically monitored during the test, and the results were used to evaluate the mixtures' susceptibility to rutting and moisture damage.

Figure 3.14: Hamburg wheel tracking device test setup

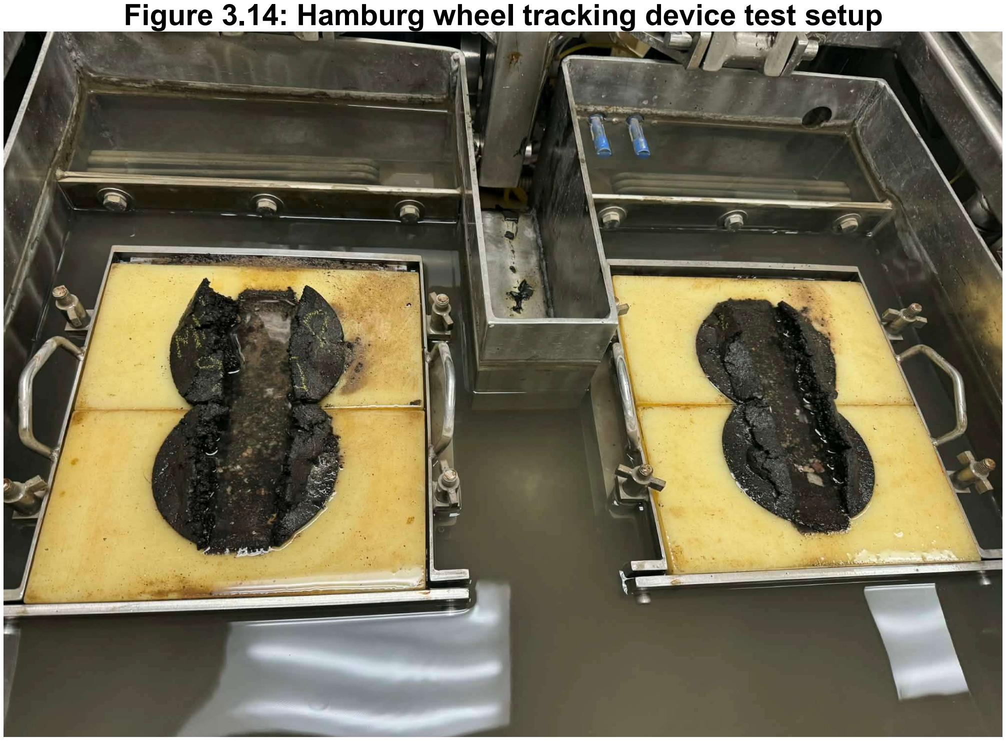

Figure 3.15: Specimens after completed HWTD test

Chapter 4. Results and Discussion

4.1 Laser Texture Scanner Test Results

Figure 4.1 shows that air voids significantly affected MPD. In Figure 4.1, the PMLC and the approved mixture MPD of 0.013 in. (0.32 mm) and 0.015 in. (0.38 mm), respectively, at 7.0 ± 0.5% air voids. The approved mixture exhibited comparatively low variability with an average MPD of 0.017 in. (0.44 mm) at 7±0.5% air voids. However, when compacted to 2.5 ± 0.5% air voids, the MPD decreased to 0.013 in. (0.33 mm), and the coefficient of variation increased from 4.70% at 7 ± 0.5% air voids to 26.41% at 2.5 ± 0.5% air voids. The trial mix 1 with 2.5 ± 0.5% air voids had the lowest MPD of 0.011 in. (0.28 mm). The MPD for all five primary mixtures was less than 0.016 in. (0.4 mm). Consequently, these mixtures fail to meet the FHWA minimum friction requirement and require redesign. Overall, the results indicate that lower air-void mixes produce smooth surfaces with reduced macrotexture. Therefore, it is necessary to modify the aggregate structure to improve texture while maintaining the low air voids for the bridge deck overlay. As air voids affect MPD, they are fixed at 5±0.5%.

Table 4.1 summarizes the LTS MPD measurements using mean, standard deviation, and coefficient of variation. The Plant, Lab, and Approved mixtures at 7.0 ± 0.5% target air voids showed relatively consistent MPD values, with CV values below 10%. In contrast, the approved mixture at 2.5 ± 0.5% target air voids and mix design 1 showed higher CV values, indicating greater local variability in surface texture across the specimen surface.

Table 4.1 Summary of MPD on Primary Mix Designs

Mix Design	Target Air Voids (%)	Mean MPD, in. (mm)	Std. Dev., in. (mm)	CV (%)
Plant	7.0 ± 0.5	0.017 (0.442)	0.001 (0.034)	7.78
Lab	7.0 ± 0.5	0.015 (0.391)	0.001 (0.023)	5.83
Approved	7.0 ± 0.5	0.017 (0.441)	0.001 (0.021)	4.76
Approved	2.5 ± 0.5	0.014 (0.349)	0.004 (0.092)	26.33
1	2.5 ± 0.5	0.011 (0.290)	0.002 (0.058)	20.17

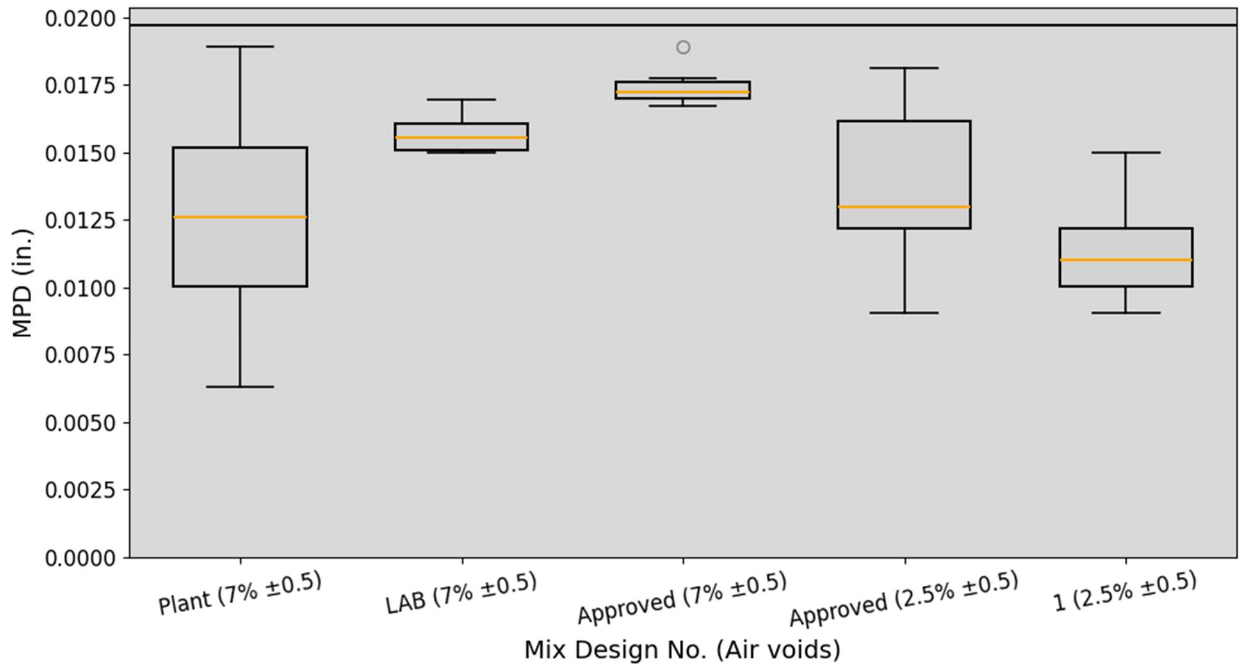

Figure 4.1: LTS test results on primary aggregate mixes

Similarly, LTS has been performed on the design plugs, and Figure 4.2 shows that the bottom part of the plugs exhibits a higher MPD value than the top part. The LTS results on the design plugs showed that adding Calcined Bauxite did not increase the MPD value as expected. Four Bauxite-modified mixes were evaluated as their air voids are close to the range (2.5±0.5% Air Voids). Mixture 9 with 5% Calcined Bauxite and 3.2% air voids, 14 with 10% Calcined Bauxite and 3.4% air voids, 16 with 10% Calcined Bauxite and 3.8% air voids, and 17 with 12% Calcined Bauxite and 3.5% air voids. The target air void for this study was 2.5 ± 0.5%, but none of these mixtures could achieve this range of air voids. In terms of texture, the measured MPD was 0.020 in. (0.5 mm) or lower, showing only limited improvement. Although some mixtures, especially mix designs 9 and 17, produced MPD close to 0.020 in. (0.5 mm). Increasing the calcined bauxite content from 5% to 12% did not produce a statistically significant improvement in surface macrotexture. These results indicate that calcined bauxite, when added to a fine-graded primary aggregate matrix, cannot overcome the texture limitation. At the mixture level, MPD is controlled primarily by the aggregate skeleton and particle arrangement, rather than by surface mineralogy alone. In this case, the fine-grained primary aggregate matrix likely surrounded the Calcined Bauxite particles, preventing them from forming the desired surface asperities. Overall, the results showed that adding Calcined Bauxite to the original fine-graded mixture was not sufficient to achieve both the desired low-air-void mixture and improved macrotexture. For this reason, the next phase of the study focused on introducing new coarse aggregate sources rather than increasing the Calcined Bauxite content further.

Table 4.2: Summary Statistics of Top and Bottom MPD Measurements

Mix Design	Surface	Bauxite (%)	Mean MPD, in. (mm)	Std. Dev., in. (mm)	CV (%)
Plant	Bottom	0	0.013 (0.320)	0.006 (0.160)	50.0
Plant	Top	0	0.010 (0.254)	0.000 (0.000)	0.0
Approved	Bottom	0	0.024 (0.600)	0.002 (0.050)	8.3
Approved	Top	0	0.017 (0.427)	0.001 (0.025)	6.0
1	Bottom	0	0.015 (0.391)	0.000 (0.010)	2.6
1	Top	0	0.015 (0.391)	0.000 (0.010)	2.6
9	Bottom	5	0.021 (0.520)	0.003 (0.080)	15.4
9	Top	5	0.002 (0.500)	0.001 (0.048)	9.7
14	Bottom	10	0.018 (0.450)	0.001 (0.031)	6.8
14	Top	10	0.020 (0.511)	0.001 (0.028)	5.5
16	Bottom	10	0.016 (0.411)	0.001 (0.029)	7.1
16	Top	10	0.017 (0.425)	0.003 (0.070)	16.4
17	Bottom	12	0.020 (0.511)	0.003 (0.071)	13.9
17	Top	12	0.019 (0.477)	0.002 (0.060)	12.5

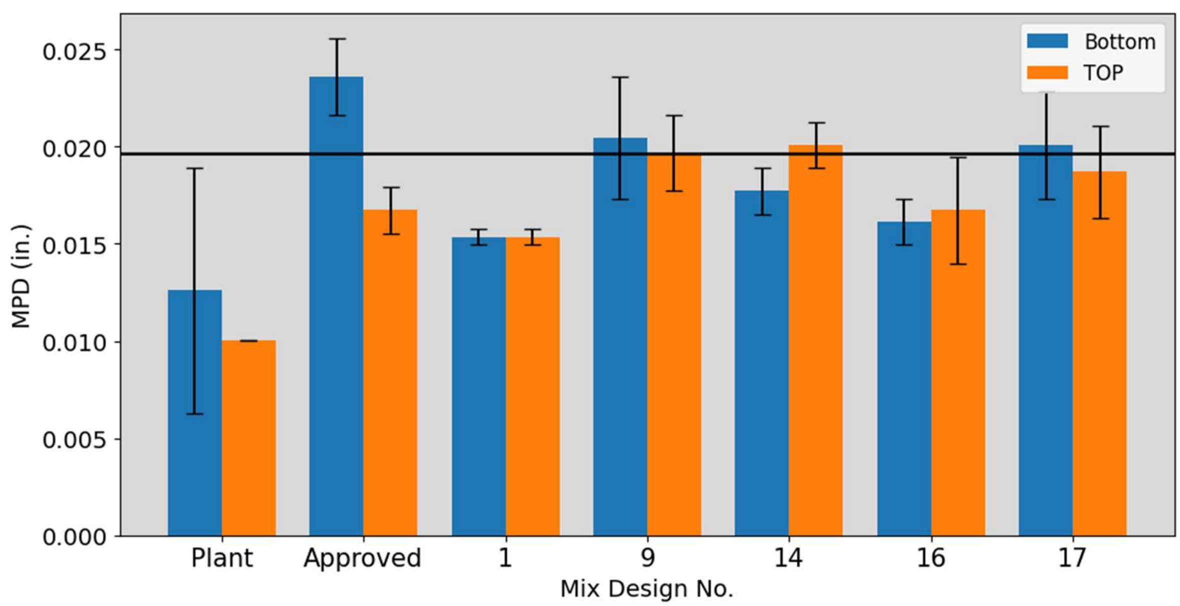

Figure 4.2: LTS on design plugs

Compared with the PMLC mixtures, LTS mixtures produced with secondary aggregates showed a significant improvement in surface texture. As illustrated in Figure 4.3, the corresponding ETD values ranged from roughly 0.038 to 0.052 in. (0.96 mm to 1.32 mm), and the measured MPD values ranged from 0.037 to 0.056 in. (0.94 mm to 1.41 mm) when they were all compacted at 5± 0.5% air voids. With texture values among the mixtures. With MPD values of roughly 0.050 in. (1.26 mm) and 0.047 in. (1.19 mm, respectively, mix designs 23 and 29 also had comparatively high texture values. The MPD for mix designs 22 and 34 was significantly larger than that for the approved and PMLC mix designs. The research's first objective was to increase the MPD of PMLC mixtures from 0.012 in. (0.3 mm) to close to 0.039 in. (1 mm). The five mixtures can achieve the targeted MPD.

Table 4.3: Summary Statistics of MPD Measurements on Secondary Mix Design

Mix Design	Mean MPD, in. (mm)	MPD Std. Dev., in. (mm)	MPD CV (%)	Mean ETD, in. (mm)	ETD Std. Dev., in. (mm)	ETD CV (%)
22	0.038 (0.956)	0.002 (0.042)	4.4	0.038 (0.968)	0.001 (0.034)	3.5
23	0.054 (1.370)	0.004 (0.110)	8.0	0.051 (1.299)	0.004 (0.088)	6.8
29	0.049 (1.245)	0.008 (0.210)	16.8	0.047 (1.199)	0.007 (0.168)	14.0
32	0.051 (1.306)	0.005 (0.127)	9.7	0.049 (1.248)	0.004 (0.101)	8.1
34	0.038 (0.973)	0.002 (0.049)	5.1	0.039 (0.981)	0.002 (0.039)	4.0

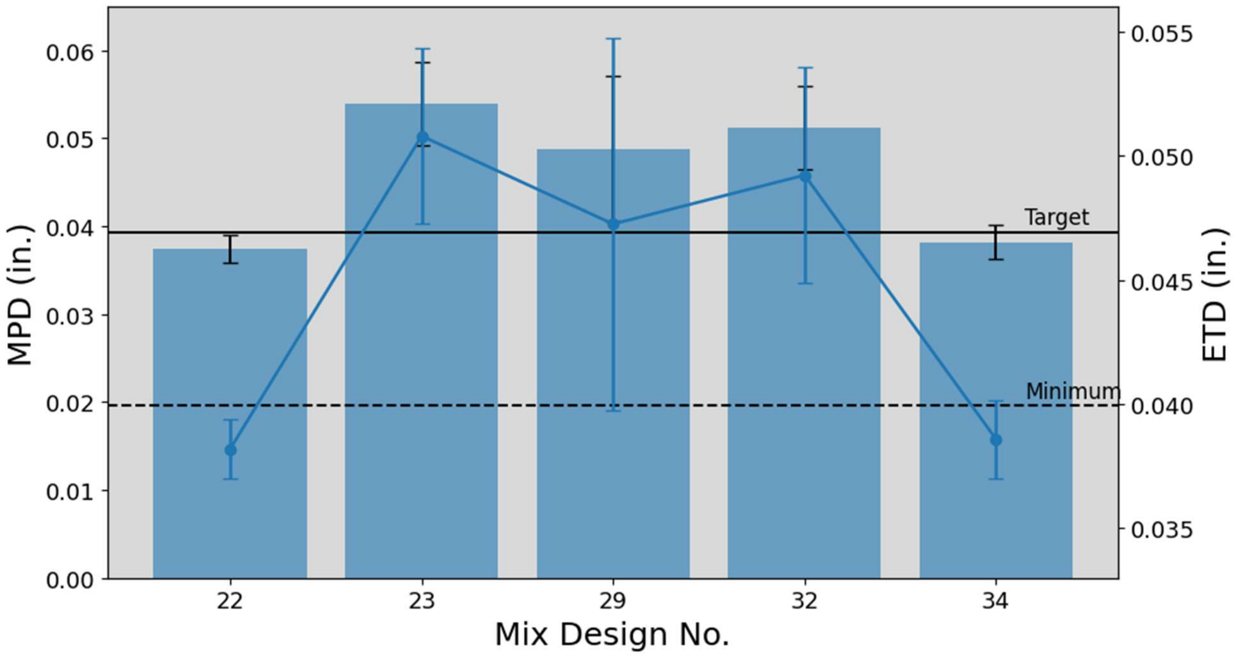

Figure 4.3: LTS test results on the top five selected mix designs

Changes in aggregate gradation and angularity directly affect the macrotexture morphology, particularly the wavelength (peak spacing) and amplitude (peak height). During the LTS, MPD measures the peak spacing and peak height. The microtexture (wave length ≤ 0.5 mm; Amplitude ≤ 0.2 mm) generally cannot be directly observed. The pavement microtexture depends on the aggregate surface texture, shape, and angularity. In addition, the microtexture is affected by binder type (Chen et al., 2022). Macrotexture (0.5–50 mm wavelength) is primarily controlled by aggregate size, gradation, and particle shape.

In this study, the increase in MPD with the use of secondary coarse aggregates was due to changes in the aggregate skeleton and surface texture. When the primary fine-graded mixture was used, the surface remained smooth because the smaller particles filled the voids between aggregates. As illustrated in Figure 3.6, the aggregate gradation for the plant and the approved mixture shows higher percentages passing through No. 4 (4.75 mm) and No. 8 (2.36 mm) sieves. These fine particles fill the voids, create a smoother surface, and reduce MPD. Moreover, the smaller particles reduce the exposure of larger surface asperities.

In contrast, the introduction of secondary coarse aggregates changed the mixture structure by creating a stronger coarse aggregate skeleton and exposing larger particles at the surface. This increased both the texture height and the effective voids of surface protrusions, which improved the MPD. The macrotexture increased texture depth, optimized voids, facilitated rapid water drainage, reduced hydrodynamic pressure, and restored tire–pavement contact. Even though the top five mixtures had similar NMAS, their MPD varied because their gradations differed. According to past research, coarser gradations and better aggregate skeleton structure improve macrotexture by increasing surface roughness and aggregate exposure to the surface (Chen et al., 2022). These results support previous research by showing that the percentage passing the US No.4 (4.75 mm) and No. 8 (2.36 mm) sieves controls MPD.

4.2 Permeability Results

Figure 4.4 shows that the PMLC and LMLC mixtures compacted at 7±0.5% air voids exhibited the highest permeabilities, 9.84×10^{-7} in./s (2.5×10^{-6} cm/s) and 1.10×10^{-6} in./s (2.8×10^{-6} cm/s), respectively. In contrast, the approved mix at 7% ± 0.5 air voids had 72.9% lower PMLC and 75.6% lower LMLC than PMLC and LMLC, respectively. When this approved mix was compacted to 2.5% ± 0.5 air voids, the permeability decreased even further, by about 37.0% compared with the same mix at 7% ± 0.5 air voids. The RCI-1A mixture had the lowest permeability at 2.5% ± 0.5 air voids. Overall, these results indicate that fine-graded primary aggregates achieved an impermeable mixture. All the mixtures are near-impermeable, as their permeability values are less than 0 to 1.97×10^{-5} in./s (0 to 5×10^{-5} cm/s).

Table 4.4: Summary Statistics of Permeability Results

Mix Design	No. of Measurements	Mean k, in./s (cm/s)	Std. Dev., in./s (cm/s)	CV (%)
Plant (7% ± 0.5)	3	9.95×10^{-7} (2.53×10^{-6})	9.34×10^{-8} (2.37×10^{-7})	9.4
Lab (7% ± 0.5)	3	1.11×10^{-6} (2.82×10^{-6})	7.33×10^{-8} (1.86×10^{-7})	6.6
Approved (7% ± 0.5)	3	2.72×10^{-7} (6.91×10^{-7})	1.70×10^{-8} (4.31×10^{-8})	6.2
Approved (2.5% ± 0.5)	3	1.80×10^{-7} (4.58×10^{-7})	5.88×10^{-9} (1.49×10^{-8})	3.3
1 (2.5% ± 0.5)	3	1.19×10^{-7} (3.02×10^{-7})	1.00×10^{-8} (2.54×10^{-8})	8.4

Table 4.4 summarizes the permeability results shown in Figure 4.4. The Plant and Lab mixtures showed higher permeability values than the Approved and Mix 1 specimens. The approved mixture with 2.5 ± 0.5% air voids and Mix 1 showed the lowest permeability values,

indicating a denser, less connected void structure. The CV values were generally below 10%, suggesting good repeatability among the three replicate permeability measurements.

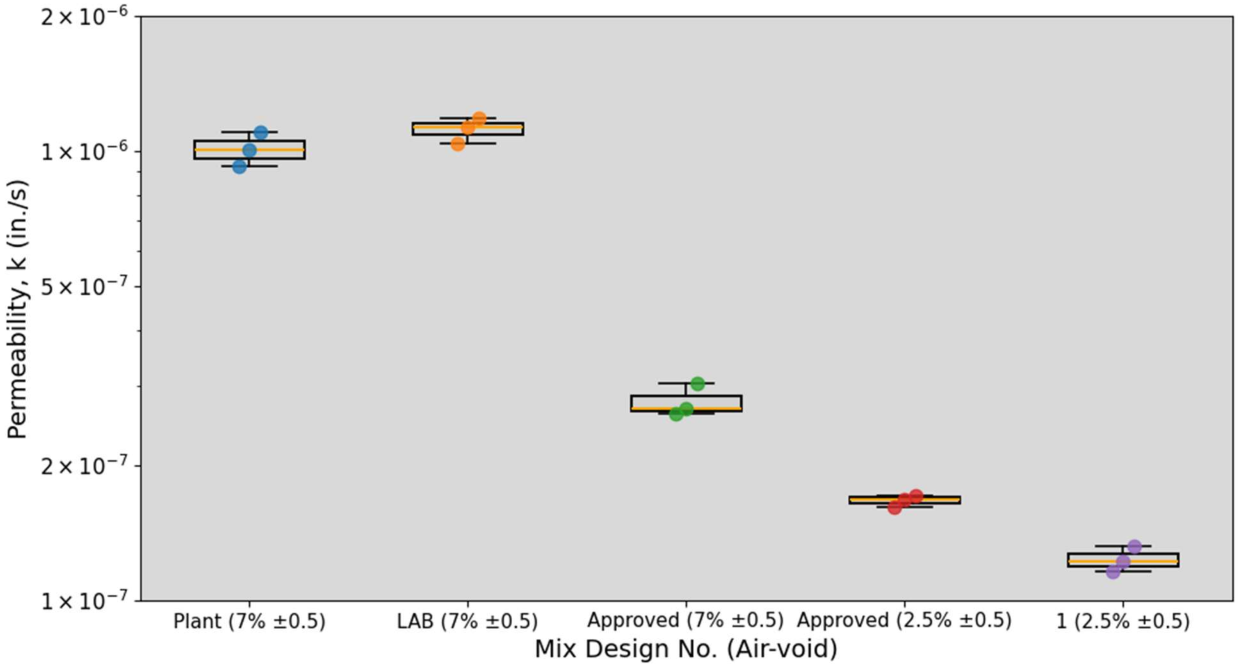

Figure 4.4: Permeability results for primary mix designs

The top five selected mix designs' permeability results are shown in Figure 4.5. Each boxplot shows the distributions of the test results for mix designs No. 22, 23, 29, 32, and 34, while the individual points show the average permeability coefficient for each specimen. Figure 4.5 shows that mix designs 22 and 23 had the lowest permeability values among all mixtures. Their values were very close to 3.94×10^{-7} in./s (1×10^{-6} cm/s). According to the literature (Williams et al., 2010), a mixture is classified as impermeable if its permeability coefficient is less than or equal to 1.97×10^{-5} in./s (5×10^{-5} cm/s). Based on the literature review, this value is consistent with the threshold used by Cooley et al. (2001, NCAT Report 01-03) and is referenced in Florida DOT practice (FM 5-565). However, the mix design 29 mixture permeability coefficient is 6.57×10^{-5} in./s (1.67×10^{-4} cm/s), the highest among the five mixtures. This indicates that limestone was the most permeable material and the only mixture that exceeded the range. The mix designs No. 32 and 34 showed intermediate behavior. Their permeability coefficients were noticeably higher than those of mix designs 22 and 23. However, mix designs 22 and 32 show 77% and 76% lower permeability, respectively, compared to mix design 29. The permeability coefficients of mix designs 32 and 34 were 1.57×10^{-5} in./s (4.0×10^{-5} cm/s) and 1.50×10^{-5} in./s (3.8×10^{-5} cm/s), respectively. Both mixtures remained within the impermeable range of 0 to 1.97×10^{-5} in./s (0 to 5×10^{-5} cm/s).

Table 4.5: Summary Statistics of Permeability Results for Top Five Mix Designs

Mix Design	No. of Measurements	Mean k, in./s (cm/s)	Std. Dev., in./s (cm/s)	CV (%)
22	3	1.05×10^{-6} (2.67×10^{-6})	4.55×10^{-8} (1.15×10^{-7})	4.3
23	3	7.61×10^{-7} (1.93×10^{-6})	1.64×10^{-7} (4.16×10^{-7})	21.5
29	3	6.72×10^{-5} (1.71×10^{-4})	7.73×10^{-6} (1.96×10^{-5})	11.5
32	3	1.47×10^{-5} (3.73×10^{-5})	2.27×10^{-7} (5.77×10^{-7})	1.5
34	3	1.59×10^{-5} (4.03×10^{-5})	2.41×10^{-6} (6.11×10^{-6})	15.1

Table 4.5 summarizes the permeability results for the top five selected mix designs shown in Figure 4.5. Mixes 22 and 23 showed the lowest permeability values, indicating very low water flow through the compacted specimens. Mixes 32 and 34 also remained below the target permeability limit of 1.97×10^{-5} in./s (5.0×10^{-5} cm/s), suggesting acceptable impermeability for bridge deck overlay application. In contrast, Mix 29 exceeded the target limit, indicating a more connected void structure and greater potential for water infiltration. The CV values were generally low to moderate, except for Mix 23, which showed higher variability due to the small magnitude of the measured permeability values.

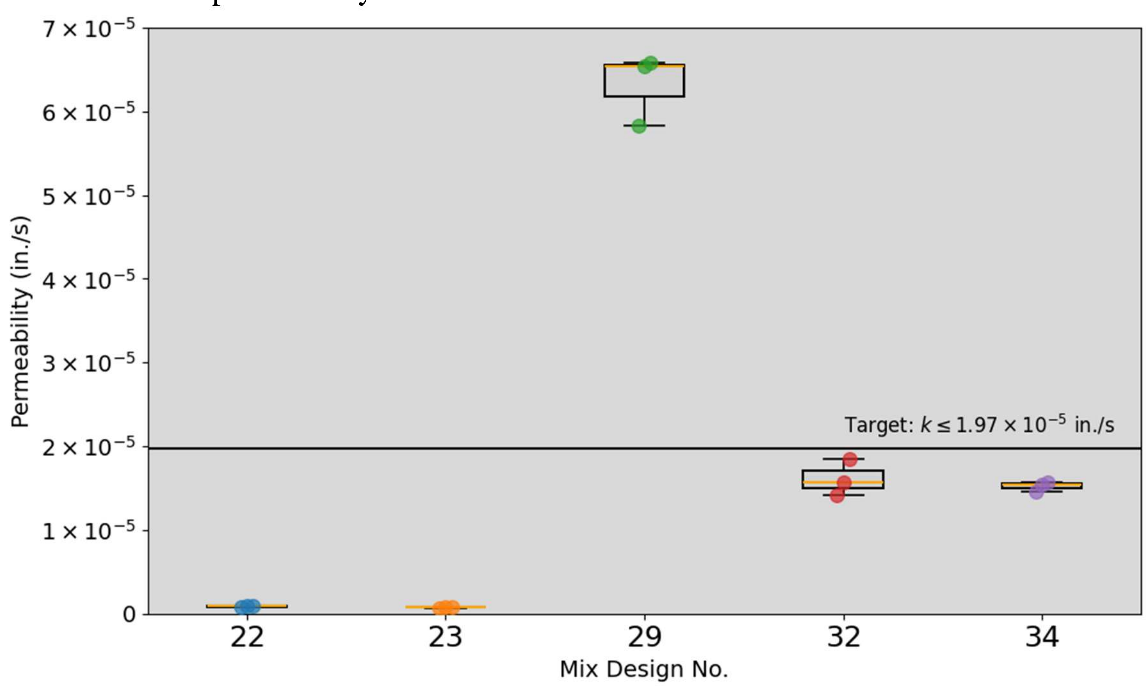

Figure 4.5: Permeability test results of the top five mix designs

Mix designs 22, 23, 32, and 34 were within the acceptable range, whereas the limestone mix design exceeded this limit and was therefore not considered impermeable.

Previous research indicates that permeability in asphalt mixtures is strongly influenced by NMAS, interconnected air voids, and aggregate gradation (Cooley et al., 2002). Permeability is proportional to the square of pore size diameter ($k \propto d^2$) for porous materials (Bear, 1972; Carman, 1937). According to the permeability results, this research also indicates that aggregate gradation significantly affects the permeability coefficient (k). Gradation affects connection and void sizes. Due to the filling of air voids by fine aggregates, mixtures with higher fine aggregate content (Plant, approved, and mix 1) showed reduced permeability. Conversely, the top five mix designs with coarser gradation showed a noticeable increase in permeability. Although Mix 29 contained limestone, the gradation is more open-graded in the US. No. 4 (4.75 mm) to US No. 8 (2.36 mm) sieve size range (Figure 3.6). Compared with the lower-permeability mixtures, mix 29's coarser gradation likely resulted in larger, interconnected internal void channels, facilitating rapid water flow. Therefore, the mix 29's permeability coefficient was much higher. However, the mixtures have a high binder content, which also helps reduce interconnected voids.

4.3 IDEAL-RT Results

Figure 4.6 shows the IDEAL-RT Index of the PMLC, LMLC, approved, and RCI-1 mixtures at different air-void levels. The approved mix at 7±0.5% air voids showed the highest IDEAL-RT Index of 182, indicating the best rutting resistance among the evaluated mixtures. The approved mix at 2.5±0.5% air voids showed an RT index of 162. Compared with the approved mix at 7±0.5% air voids, the RT index of the approved mix at 2.5±0.5% decreased by 9%. The RCI-1A mixture at 2.5±0.5% air voids showed intermediate performance, with an IDEAL-RT Index of 120, which was higher than those of both the PLMC and LMLC. Based on Figure 4.6, the IDEAL-RT index for the LMLC was approximately 109, whereas the PMLC had an index of 78, approximately 40% higher than the LMLC. Results in Figure 4.6 indicate that all mixtures met the IDEAL-RT minimum criteria of 65.

Table 4.6 summarizes the IDEAL-RT Index results shown in Figure 4.6. The approved mixture at 7.0 ± 0.5% air voids showed the highest mean RT Index, followed by the approved mixture at 2.5 ± 0.5% air voids and Mix 1. The Plant mixture showed the lowest RT Index, indicating comparatively lower rutting resistance. The CV values were low for Plant, Lab, and Mix 1, indicating good repeatability, while the approved mixtures showed higher variability, especially at 2.5 ± 0.5% air voids. This suggests that rutting resistance may be more sensitive to specimen-to-specimen differences and internal aggregate-binder structure.

Table 4.6: Summary Statistics of IDEAL-RT Index Results

Mix Design	Air Voids (%)	No. of Measurements	RT Index Mean	RT Index Std. Dev.	RT Index CV (%)
Plant	7.0 ± 0.5	3	77.9	2.9	3.7
Lab	7.0 ± 0.5	3	109.8	7.7	7.0
Approved	7.0 ± 0.5	3	172.2	30.1	17.5
Approved	2.5 ± 0.5	3	147.2	37.4	25.4
1	2.5 ± 0.5	3	122.9	10.5	8.6

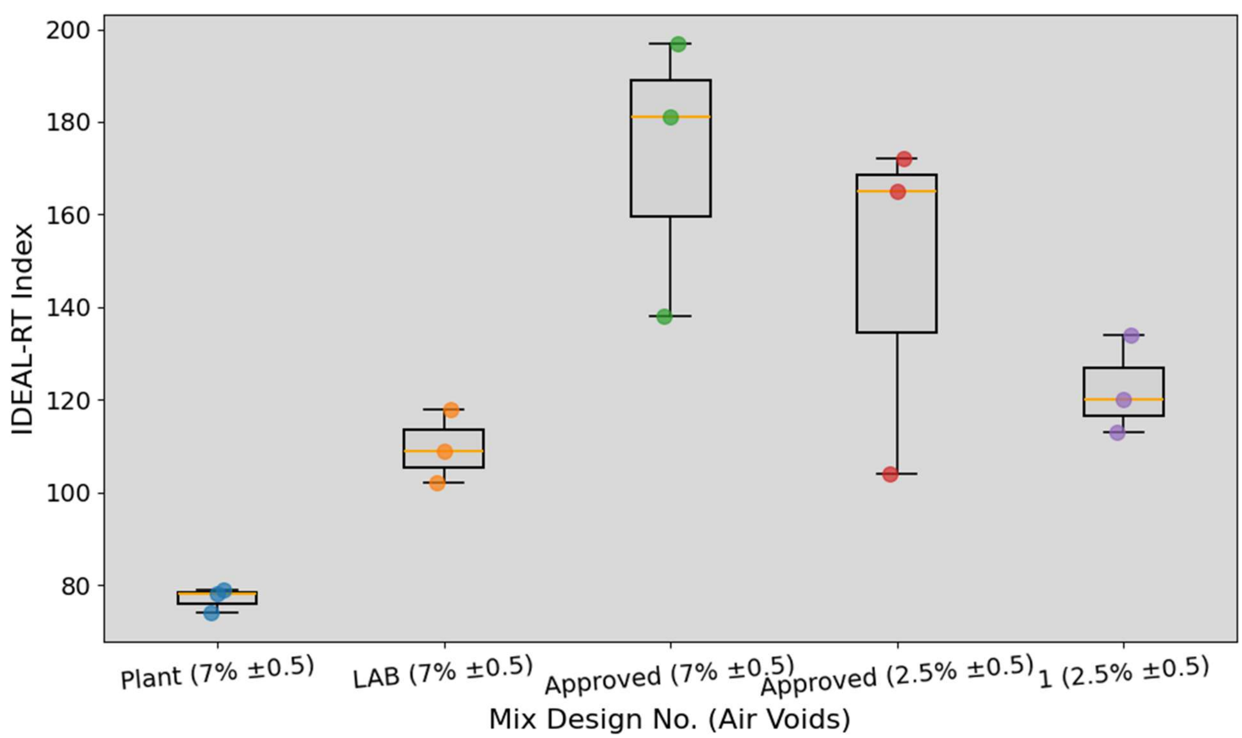

Figure 4.6: IDEAL-RT Index of primary mixes

Table 4.7 summarizes the IDEAL-RT Index results for five selected mix designs shown in Figure 4.7. Mix 34 showed the highest mean RT Index, followed by Mix 22 and Mix 32. These mixtures exceeded the target RT Index of 65, indicating acceptable rutting resistance under the selected criterion. In contrast, Mix 23 and Mix 29 had mean RT Index values below the target, indicating lower resistance to shear-induced rutting. The CV values show that Mix 23 had the most consistent RT Index results, while Mix 32 and Mix 34 showed higher variability.

Results in Figure 4.7 demonstrated the IDEAL-RT index of the selected five promising mix designs compacted at 5 ± 0.5% air voids. Among these five mixtures, mix 34 had the highest IDEAL-RT index of 90. Mix 22 showed the second-highest IDEAL-RT Index of 75, which was about 16.7% lower than mix design 34. Mix 32 had a moderate IDEAL-RT index of 63. Mix 32 mix RT Index is 3.1% lower than the minimum IDEAL-RT requirement. On the other hand, the mix designs 29 and 23 had RT Index values of 44 and 37, respectively. Based on the minimum IDEAL-RT requirement of 65 for PG 70-XX mixtures, only mix designs 22 and 34 achieved the minimum rutting resistance, while mix designs 23, 29, and 32 had RT Index values that were below the required threshold.

Table 4.7: Summary Statistics of IDEAL-RT Index Results for Top Five Mix Designs

Mix Design	No. of Measurements	RT Index Mean	RT Index Std. Dev.	RT Index CV (%)
22	3	79.0	9.9	12.5
23	3	36.6	1.7	4.7
29	3	45.7	7.7	16.8
32	3	70.3	19.1	27.2
34	3	98.1	29.6	30.2

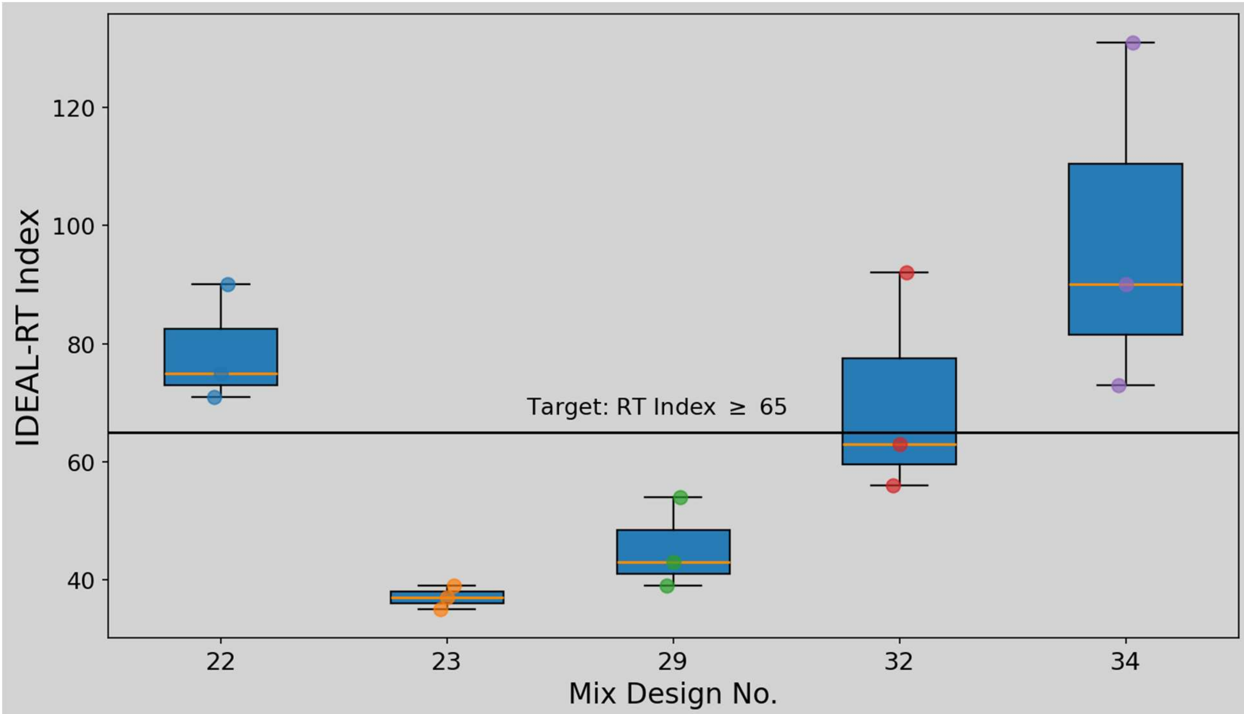

Figure 4.7: IDEAL-RT Index of the top five selected mix designs

4.4 Hamburg Wheel Tracking Test Results

The HWTD test was performed to validate the IDEAL-RT results. Table 4.8 summarizes the HWTD results for the top five selected mix designs shown in Figures 4.8 and 4.9. Mix 32 showed the lowest CV, indicating more consistent HWTD performance among the replicate specimens, while Mix 34 showed higher variability due to the wider spread in wheel-pass results.

Table 4.8: Summary Statistics of HWTD Results for Top Five Mix Designs compacted at 5±0.5% Air Voids and 7±0.5% Air Voids

Mix Design	5.0% Air Voids			7% Air Voids		
	Mean Wheel Passes	Std. Dev.	CV (%)	Mean Wheel Passes	Std. Dev.	CV (%)
22	9,818	1,831	18.6	7,853	367	4.7
23	9,210	926	10.1	6,164	492	8.0
29	9,600	1,550	16.1	7,880	293	3.7
32	12,967	947	7.3	N/A	N/A	N/A
34	12,287	2,522	20.5	6,079	690	11.3

Figure 4.8 shows that none of the five mixtures achieved the target of 15,000 wheel passes at a 0.5 in. (12.5 mm) rut depth. Among the mixtures, mix design 32 showed 12,000 wheel passes at a 0.5 in. (12.5 mm) rut depth, the highest number among all mixtures. Next, mix design 34 with 10,600 wheel passes at 0.5 in. (12.5 mm) rut depth. Mix designs 22 and 29 exhibited similar performance, 9,000–9,200 wheel passes at 0.5 in. (12.5 mm) rut depth, whereas mix design 23 showed the lowest rutting resistance. The number of wheels passing for mix designs 22, 23, 29, and 34 was lower than for mix design 32 by 24.2%, 32.5%, 23.3%, and 11.7%, respectively. Although none of the mixtures met the 15,000-pass criteria, the mixture ranking is similar to the IDEAL-RT results. Mix design 32 and 34 showed better rutting resistance, while mix 23 showed the worst.

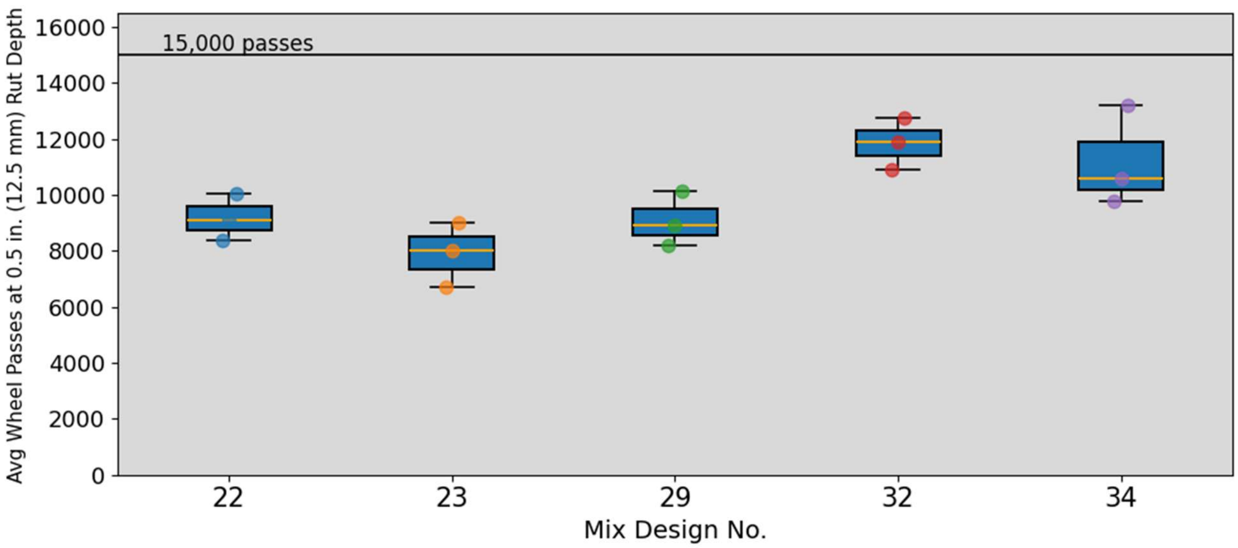

Figure 4.8: HWTD test results on the top five mix designs

As shown in Figure 4.8, the HWTD specimens were compacted to 5±0.5% air voids to represent bridge deck overlay performance better, because low air voids are the target design condition for this type of bridge mixture. However, according to Tex 242 F, 15,000 wheel passes at a 0.5 in. (12.5 mm) rut depth apply to specimens that are compacted at 7±0.5% air voids. The 7 ± 0.5% air-void HWTD test was included only for comparison with the highway standard and is not directly applicable to bridge deck overlay mixtures. A bridge-specific rutting criterion has not yet been established, and this remains an important gap for future research. Therefore, additional HWTD specimens were compacted at 7±0.5% air voids, and the results are presented in Figure 4.9. The results showed that for all mixtures, the number of wheel passes decreased as air voids increased from 5±0.5% to 7±0.5%. For mix design 22, the average wheel passes decreased from 9,203 at 5±0.5% air voids to 7,853 at 7±0.5% air voids, which is a decrease of 14.7%. The highest

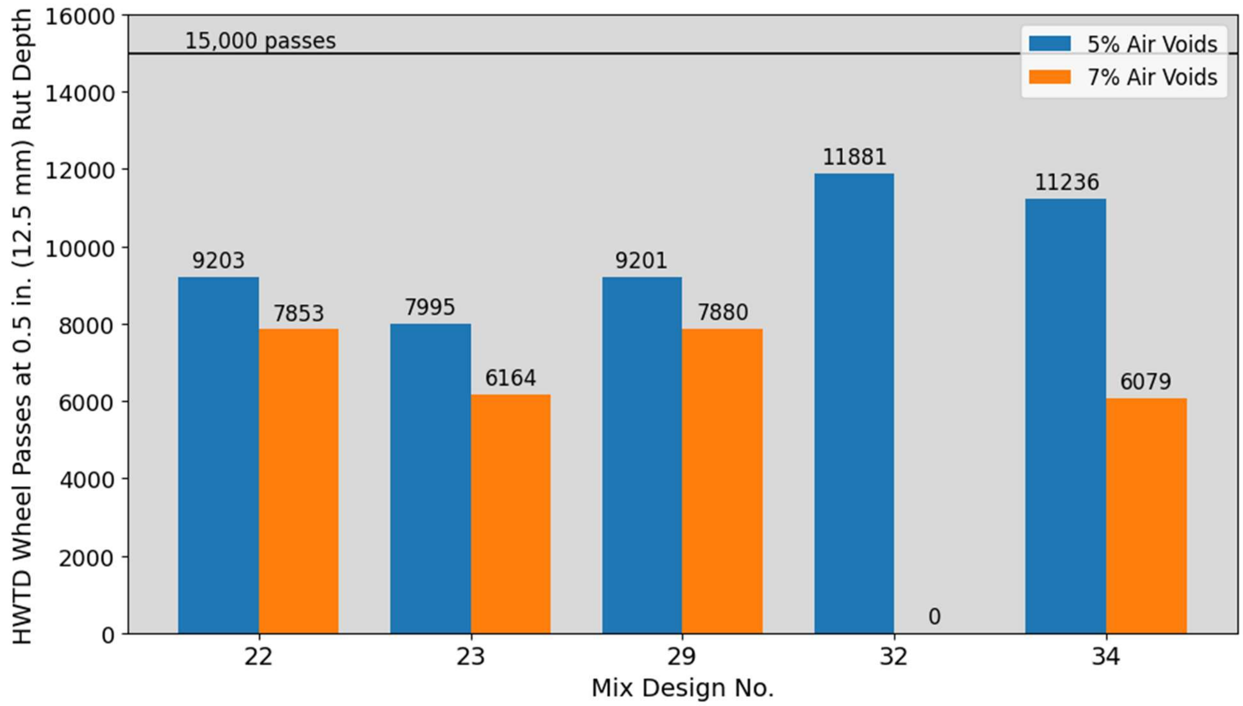

Figure 4.9: HWTD test results of the top five selected mix designs (compacted at 5±0.5% air voids)

was observed for mix design 34. For mix design 34, the average wheel passes decreased from 11,236 to 6,079, representing a decrease of about 45.9%. The results showed that as the mixture's air voids increased, their rutting resistance decreased. None of the mixtures compacted at 7±0.5% air voids achieved the target of 15,000 wheel passes. For mix design 32, no HWTD result was obtained at 7% air voids. The mix design of 32 specimens reached approximately 5±0.5% air voids after only three gyrations. The specimen was obtained from the gyratory mold with no gyration during compaction, resulting in a 7% air void. For the mix design 32, compaction to 7±0.5% air voids could not be achieved with this gradation and binder content.

Aggregate gradation not only influences macrostructure and permeability, but also aggregate skeleton and rutting behavior. The mixture can resist rutting deformation when aggregate interlocking and interparticle friction are adequate. Fine-graded mixtures typically exhibit reduced aggregate interlock, thereby increasing susceptibility to rutting. Furthermore, excessive binder content can exacerbate this issue by increasing the film thickness between aggregate particles, effectively lubricating the matrix and reducing internal friction. Mix 32 with Venture 5/8” aggregate reached the target air voids of 5±0.5 % after only two gyrations, indicating extreme workability and potential instability. This rapid compaction, combined with high binder content, suggests a lack of aggregate interlock, which directly contributed to its poor rutting resistance. Therefore, in the next phase of the study, the binder content was reduced to examine the binder effect on rutting.

Table 4.9 and Figure 4.10 and compare the average MPD, permeability coefficient, IDEAL-RT index, and HWTD wheel passes for the top five promising mix designs. Among these five mixtures, mix designs 23 and 32 showed the highest MPD, while mix designs 22 and 34 had relatively lower macrotexture. However, the MPD of the mix designs 22 and 34 is close to 0.039 in. (1 mm). Mix design 29 had the highest permeability coefficient, whereas mix designs 22 and 23 had the lowest. In terms of rutting resistance, mix design 34 exhibited the highest IDEAL-RT index, while mix design 32 illustrated the highest number of HWTD wheel passes. Overall, mix designs 22 and 34 have more balanced performance across all four indicators. Mix design 32 also performed well in texture and showed favorable HWTD results. In contrast, mix design 29 was the least feasible mixture because of its high permeability and lower IDEAL-RT Index. Finally, these results suggest that mix designs 32 and 34 were the most consistent performers among the mixtures evaluated.

Table 4.9: Summary Statistics of Texture, Permeability, IDEAL-RT, and HWTD Results

Mix Design	Mean MPD, in. (mm)	MPD Std. Dev., in. (mm)	MPD CV (%)	Mean k, in./s (cm/s)	k Std. Dev., in./s (cm/s)	k CV (%)	RT Mean	RT Std. Dev.	RT CV (%)	HWTD Mean	HWTD Std. Dev.	HWTD CV (%)
22	0.0376 (0.956)	0.0017 (0.042)	4.4	1.05×10^{-6} (2.67×10^{-6})	4.55×10^{-8} (1.15×10^{-7})	4.3	79.0	9.9	12.5	9,818	1,831	18.6
23	0.0539 (1.370)	0.0043 (0.110)	8.0	7.61×10^{-7} (1.93×10^{-6})	1.64×10^{-7} (4.16×10^{-7})	21.5	36.6	1.7	4.7	9,210	926	10.1
29	0.0490 (1.245)	0.0083 (0.210)	16.8	6.72×10^{-5} (1.71×10^{-4})	7.72×10^{-6} (1.96×10^{-5})	11.5	45.7	7.7	16.8	9,600	1,550	16.1
32	0.0514 (1.306)	0.0050 (0.127)	9.7	1.47×10^{-5} (3.73×10^{-5})	2.27×10^{-7} (5.77×10^{-7})	1.5	70.3	19.1	27.2	12,967	947	7.3
34	0.0383 (0.973)	0.0019 (0.049)	5.1	1.59×10^{-5} (4.03×10^{-5})	2.41×10^{-6} (6.11×10^{-6})	15.1	98.1	29.6	30.2	12,287	2,522	20.5

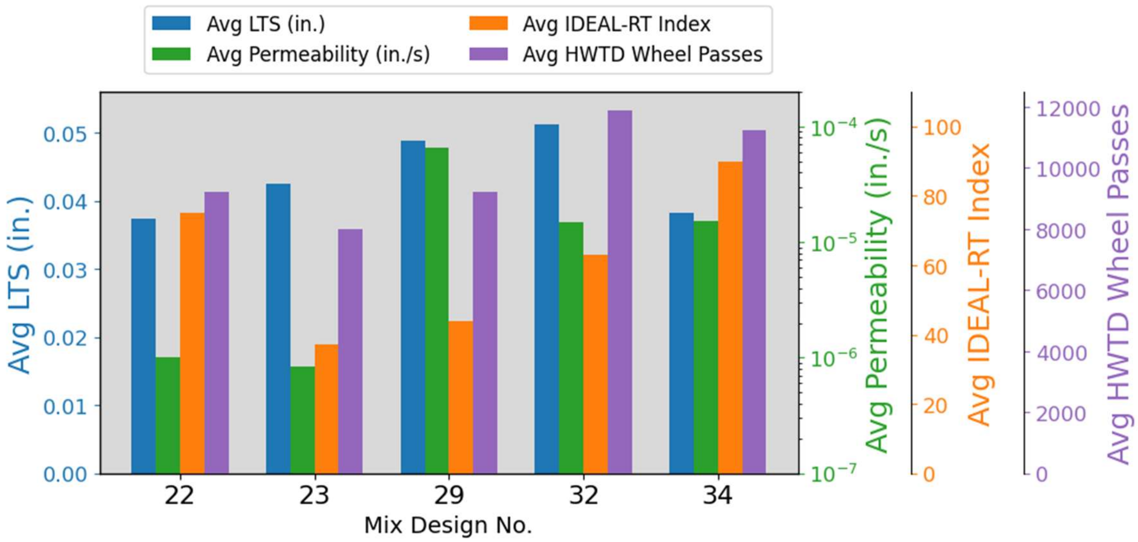

Figure 4.10: Comparison of test results of the top five selected mix designs (compacted at 5±0.5% air voids)

Across all trial mixtures, mix designs 32 and 34 performed best, but their HWTD wheel passes at 0.5 in. (12.5 mm) rut depth did not reach 15,000. To improve these mixtures' rutting resistance while remaining within the BDWSC gradation limits, additional trial mix designs were done for the two best-performing aggregate blends (mix designs 32 and 34). The goal of these trials was to adjust the mix proportions and binder content in a controlled way so that the design air voids increased from 2.5±0.5 % at design 50 gyrations to 3.5±0.5 %. As shown in the trial matrix, binder content was varied in Table 4.1 (7.0–8.3%), and coarse aggregate proportion was increased while keeping the overall gradation within the BDWSC limits.

Table 4.10: Huber 3/4 Aggregates Trial Blends

Trial	Air voids @50 gyrations (%)	VMA (%)	VFA (%)	AC (%)	G_{mm}	G_{mb}	CH-1A	SSG-1	CS-2A	CS-2B	SSG-2	CG-H-3/4
T1	2.6	18.7	86	8.3	2.341	2.28	20	5	35	0	10	30
T2	0.9	17.9	95	8.0	2.318	2.296	20	5	35	0	10	30
T3	1.7	19.6	91	7.5	2.275	2.237	20	5	35	0	10	30
T4	5.9	19.2	69	7.8	2.411	2.268	20	5	35	0	10	30
T5	4.5	19.7	79	7.0	2.326	2.221	18	0	35	0	8	39
T6	4.1	20.4	80	7.5	2.329	2.233	20	0	35	0	10	35
T7	6.7	20.7	68	7.0	2.351	2.194	20	0	35	0	13	32

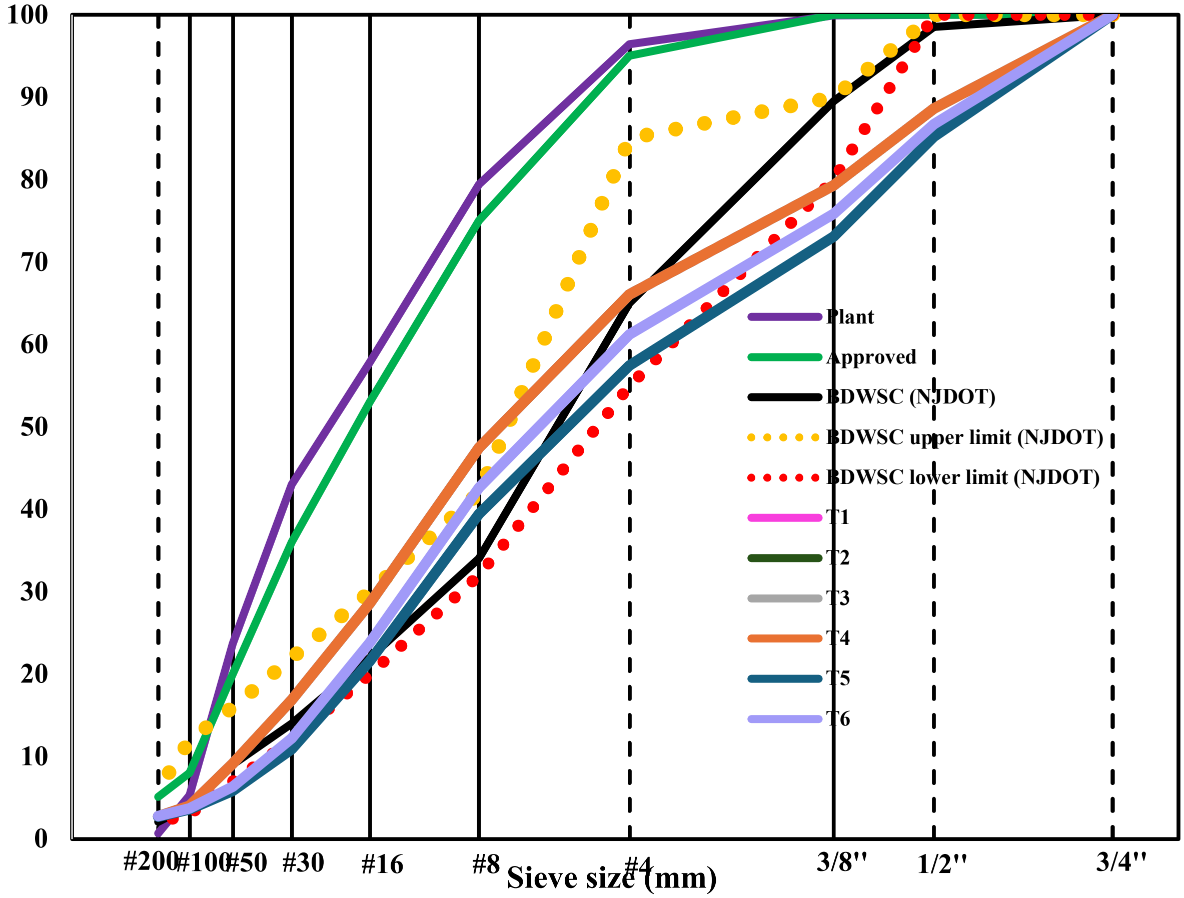

Figure 4.11: Trial Mixes with Huber ¾ aggregate blends

Table 4.11: Venture-5/8 Aggregates Trial Blends

Trial	Air voids @50 gyrations (%)	VMA (%)	VFA (%)	AC (%)	G_{mm}	G_{mb}	CH-1A	SSG-1	CS-2A	CS-2B	SSG-2	CG-V-5/8
T8	1.6	18.6	92	8.3	2.321	2.285	10	15	20	0	11	44
T9	2.1	18.7	89	8.0	2.324	2.275	14	0	25	0	11	50
T10	1.7	17.5	90	7.5	2.321	2.296	5	10	24	0	11	50
T11	2.2	16.9	87	7.5	2.364	2.312	15	5	20	0	10	50
T12	2.3	10.3	78	7.5	2.555	2.496	15	0	30	0	5	50
T13	2.3	16.8	86	7.5	2.368	2.314	10	15	20	0	11	44
T14	3.3*	16.3	80	7.0	2.393	2.315	10	15	20	0	11	44

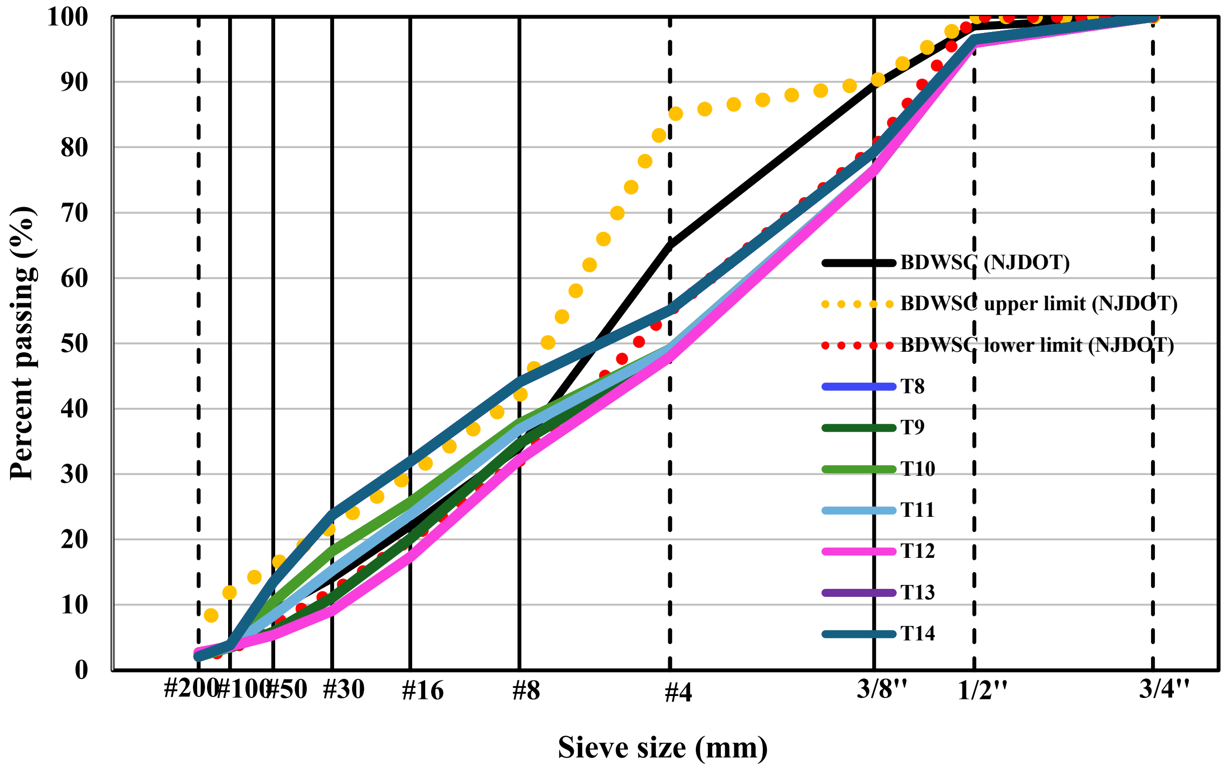

Figure 4.12: Trial mix gradations with Venture 5/8 aggregate blends

For Huber aggregate blends, one trial (T6) achieved 4.1% air voids at 50 gyrations, which was slightly above the target range of 3.5 ± 0.5%. On the other hand, for venture 5/8" aggregate blends, none of the trials fell within the 3.5 ± 0.5% air-void range. For venture 5/8 aggregate blends, the six trial mix designs had air voids below 3%, except for one trial (T14). The T14 had an air-void content of 3.3%, but it exhibited excessive binder bleeding. Therefore, venture 5/8" aggregate trial mixes did not meet the target range based on these trials. For the Huber 3/4 trial mix, T6 was compacted to 5±0.5% air voids, and HWTD (T6) was performed. The mixture improved the HWTD wheel passes at a 0.5 in. (12.5 mm) rut depth. T6 exhibited approximately 10% higher wheel passes than mix design 34 using the same five aggregates by reducing the binder content from 8.3% to 7.5%.

Table 4.12: Summary Statistics of HWTD Results Including T6

Mix Design	No. of Measurements	Mean Wheel Passes	Std. Dev.	CV (%)
22	3	9,818	1,831	18.6
23	3	9,210	926	10.1
29	3	9,600	1,550	16.1
32	3	12,967	947	7.3
34	3	12,287	2,522	20.5
T6	3	12,000	500	4.2

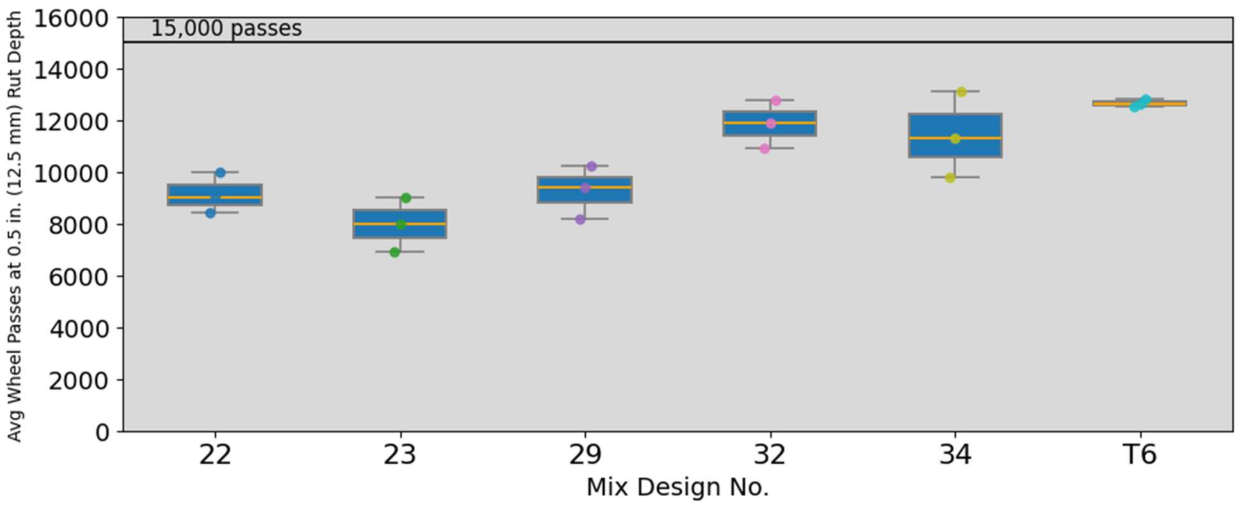

Figure 4.13: HWTD test results of the top five selected mix designs with trial of Huber ¾ (T6) blend

4.5 Statistical Analysis

This study performed a statistical analysis to further interpret the laboratory results. The statistical analysis was performed to evaluate the relationships between the mixture gradation and volumetric properties with the measured performance. Response Surface Methodology (RSM) was used to quantify the relationships among mix design variables and three bridge deck overlay performance measures studied in this project: friction, permeability, and rutting resistance. RSM is a regression-based statistical technique that can quantify not only the individual effects of input variables but also their interactions and curvilinear effects on the response (Myers et al., 2016). Therefore, RSM was selected for this study. Friction surrogate surface macrotexture (MPD), permeability, and rutting resistance may depend not only on coarse aggregate (CA) size, fine aggregate, and coarse aggregate quantities, but also on their interactions. However, size is not a variable in this study, as explained later. A second-order RSM model can be written as

$$Y = \beta_0 + \sum_{i=1}^{k} \beta_i x_i + \sum_{i=1}^{k} \beta_{ii} x_i^2 + \sum_{i<j} \sum \beta_{ij} x_i\, x_j + \varepsilon \tag{4.1}$$

where β_0, β_i, β_{ii}, and β_{ij} are regression coefficients.

A total of nine mix designs, with three replicates each, were included in the analysis. Among the predictors, aggregates retained on 3/8 in. (9.5 mm) and US No. 30 (0.6 mm) sieves, percent passing No. 200 (0.075 mm) passing, and air voids at 50 gyrations (AV) were selected as the top four variables. The sieve sizes (#4, #8, #16, #30, #50, #100, and #200) are related to each other because material retained on one sieve cannot be on another finer sieve. The volumetric properties (AV, VMA, VFA, G_{mb}, G_{mm}) are also autocorrelated through Superpave mix design equations. Thus, using all of them together would cause multicollinearity. To avoid this, one variable was selected from each group based on the Pearson correlation presented in Figure 4.14. MPD tended to increase with coarser aggregate structure, but this same structural change also tended to increase permeability, because coarser mixtures created larger and more connected voids. In contrast, rutting resistance did not vary in the same direction as MPD, indicating that mixtures with high texture did not always provide high rutting resistance. These cross-response relationships help explain why the feasible optimization region was narrow: improving one performance measure, particularly macrotexture, could reduce impermeability or rutting resistance unless the gradation and volumetric properties were carefully balanced. The percent retained on 3/8 in. sieve ($r = +0.87$) was chosen to represent the coarse aggregate. The 1/2 in. (12.5 mm) fraction was not used because its correlation was weak. The percentage retained on the US No. 30 (0.6mm) sieve ($r = -0.94$) was chosen to represent the intermediate-to-fine aggregate fraction. It had the strongest correlation with MPD among all variables. To represent dust, the percentage passing the US No. 200 (0.075 mm) sieve was chosen ($r = -0.81$). Air voids (AV) ($r = -0.72$) were selected to represent the volumetric properties of the mix. AV at 50 gyrations was preferred over VMA because air-void design is the primary acceptance criterion in the Superpave mix design and defines rutting behavior.

Pearson Correlations with MPD, k, and RT Index

3 With Variables:	MPD k RT_Index
15 Variables:	1/2 in 3/8 in #4 R #8 R #16 R #30 R #50 R #100 R #200 R AV Gmm Gmb VMA VFA #200 P

Pearson Correlation Coefficients, N = 27
Prob > |r| under H0: Rho=0

	1/2 in	3/8 in	#4 R	#8 R	#16 R	#30 R	#50 R	#100 R	#200 R	AV	Gmm	Gmb	VMA	VFA	#200 P
MPD	0.44620 0.0197	0.86951 <.0001	0.79226 <.0001	-0.72665 <.0001	-0.89107 <.0001	-0.93915 <.0001	-0.84235 <.0001	-0.74262 <.0001	-0.83963 <.0001	-0.71594 <.0001	0.24923 0.2100	0.80521 <.0001	-0.78992 <.0001	0.72301 <.0001	-0.80670 <.0001
k	0.25961 0.1910	0.73735 <.0001	0.17410 0.3851	-0.40354 0.0369	-0.24463 0.2188	-0.31555 0.1089	-0.49728 0.0083	-0.52373 0.0051	-0.64649 0.0003	-0.46872 0.0137	0.01069 0.9578	0.45133 0.0181	-0.43553 0.0232	0.49305 0.0090	-0.26232 0.1862
RT_Index	-0.15249 0.4476	-0.61203 0.0007	-0.56697 0.0020	0.64317 0.0003	0.70874 <.0001	0.68633 <.0001	0.45010 0.0185	0.34587 0.0772	0.49266 0.0090	0.29321 0.1377	-0.41207 0.0327	-0.47487 0.0123	0.44924 0.0187	-0.30907 0.1167	0.85631 <.0001

Spearman Correlations with MPD, k, and RT Index

3 With Variables:	MPD k RT_Index
15 Variables:	1/2 in 3/8 in #4 R #8 R #16 R #30 R #50 R #100 R #200 R AV Gmm Gmb VMA VFA #200 P

Spearman Correlation Coefficients, N = 27
Prob > |r| under H0: Rho=0

	1/2 in	3/8 in	#4 R	#8 R	#16 R	#30 R	#50 R	#100 R	#200 R	AV	Gmm	Gmb	VMA	VFA	#200 P
MPD	0.73288 <.0001	0.89513 <.0001	0.68201 <.0001	-0.78196 <.0001	-0.88930 <.0001	-0.88930 <.0001	-0.60962 0.0007	-0.60983 0.0007	-0.69127 <.0001	-0.72551 <.0001	0.23326 0.2416	0.67276 0.0001	-0.67276 0.0001	0.66449 0.0002	-0.84288 <.0001
k	0.58330 0.0014	0.68221 <.0001	0.22573 0.2576	-0.66793 0.0001	-0.54026 0.0036	-0.54026 0.0036	-0.51932 0.0055	-0.50881 0.0067	-0.59022 0.0012	-0.33674 0.0859	0.51654 0.0058	0.33489 0.0877	-0.33489 0.0877	0.25937 0.1914	-0.42921 0.0255
RT_Index	-0.44787 0.0191	-0.71459 <.0001	-0.53077 0.0044	0.72310 <.0001	0.74160 <.0001	0.74160 <.0001	0.39837 0.0396	0.40686 0.0352	0.42166 0.0285	0.60105 0.0009	-0.25165 0.2054	-0.56776 0.0020	0.56776 0.0020	-0.55207 0.0028	0.77909 <.0001

Figure 4.14: Correlation Analysis of MPD, Permeability, and IDEAL-RT Index with 16 variables

In RSM, variables are coded (Myers et al., 2016). All input variables were coded to a [−1, +1] scale using the formula. $x_{\_coded} = (x - \text{center}) / \text{half-range}$, where center = (min + max) / 2 and half-range = (max − min) / 2. This normalization ensures that coefficients across variables are directly comparable regardless of their original units and numerical ranges—Table 4.13 summarizes the coding parameters for each input variable.

Table 4.13: Input Variable Coding Parameters

Variable	Min	Max	Center / Half-range
AV (X_1)	0.89	4.58	X_1_coded=(AV-2.735) / 1.845
R#3/8 (X_2)	0.0	19.2	X_2_coded=(R#3/8 -9.6) / 9.6
R#30 (X_3)	8.4	17.6	X_3_coded=(R#30 -13) / 4.6
P#200 (X_4)	1.7	5.9	X_4_coded=(P#200 -3.8) / 2.1

Three separate RSM models were developed, one for each performance response. Model selection was determined by statistical validity and physical/engineering interpretability. The full second-order model, containing 15 terms (intercept, 4 linear, 4 quadratic, and 6 two-way interactions), could not be estimated for all responses due to the limited dataset. Accordingly, reduced models were adopted where a full second-order model exhibited aliasing.

Table 4.14: Summary of Models for Three Different Responses

Response	Model type	R^2	Adj. R^2	F (p-value)	RMSE
MPD (mm)	RSM SO (R#3/8, P#200)	0.964	0.955	2.18×10^{-14}	0.093 mm
$\log_{10}(k)$	lm: AV+R#3/8+R#30+P#200+AV×P200	0.989	0.986	$< 2.2\times10^{-16}$	0.103 log
RT Index	RSM SO (AV, P#200)	0.868	0.835	1.58×10^{-8}	19.29

4.5.1 Surface Texture Model (MPD)

A second-order RSM, shown in Equation 4.2, was fitted to the MPD data using two input variables (R#3/8 and P#200). The analysis was performed using the RSM package in R (Lenth, 2009), and equivalent results can be obtained using the RSREG procedure in SAS (SAS Institute Inc., 2018). These two variables best represent the main gradation features controlling surface texture. Coarse aggregates retained on the 3/8" (9.5 mm) sieve (R#3/8) help create surface peaks and increase macrotexture. On the other hand, materials passing US No. 200 (0.075 mm) (P#200) fill surface voids and reduce texture depth. R#3/8 showed a correlation of $r = +0.884$ with MPD (more coarse aggregates create surface texture peaks), and P#200 showed $r = -0.909$ (fines fill voids and reduce texture depth). AV and R#30 were not included in this model because the preliminary analysis showed they were not independently significant for MPD ($p > 0.05$).

$$\hat{Y}_{MPD} = 0.8034 + 0.2997X_2 - 0.2774X_4 - 0.0117X_2X_4 - 0.1583X_2^2 + 0.2216X_4^2 \quad (4.2)$$

where $X_2 = (R\#3/8 - 9.600) / 9.600$ and $X_4 = (P\#200 - 3.800) / 2.100$.

Table 4.15: ANOVA for the Second-Order Response Surface Model

	D_f	Sum Sq	Mean Sq	F value	Pr(>F)
FO(S38_c, P200_c)	2	4.5147	2.25733	260.1313	1.522e-15
TWI(S38_c, P200_c)	1	0.0696	0.06955	8.0152	0.0100057
PQ(S38_c, P200_c)	2	0.2538	0.12690	14.6239	0.0001051
Residuals	21	0.1822	0.00868		
Lack of fit	2	0.0074	0.00368	0.3996	0.6760989
Pure error	19	0.1749	0.00920		

ANOVA results, presented in Table 4.15, show that the linear, interaction, and quadratic terms are all statistically significant. Table 4.15 also shows that the lack-of-fit test was not significant ($F = 0.40$, $p = 0.676$), indicating that the second-order polynomial adequately represents the true response surface and no higher-order terms are required. Figure 4.15 shows the diagnostic plots for MPD. The Q-Q plot of residuals showed points closely aligned with the reference line. The residual plots exhibited random scatter around zero with no systematic pattern. The residual plots show normality and constant variance. The histogram of residuals was approximately bell-shaped and centered at zero, although it was not perfectly aligned with the normal curve. The histogram shows slight skew due to a small sample size ($n = 27$). Finally, the fitted response surface was further examined to interpret the combined effects of coarse aggregate and fines content on MPD.

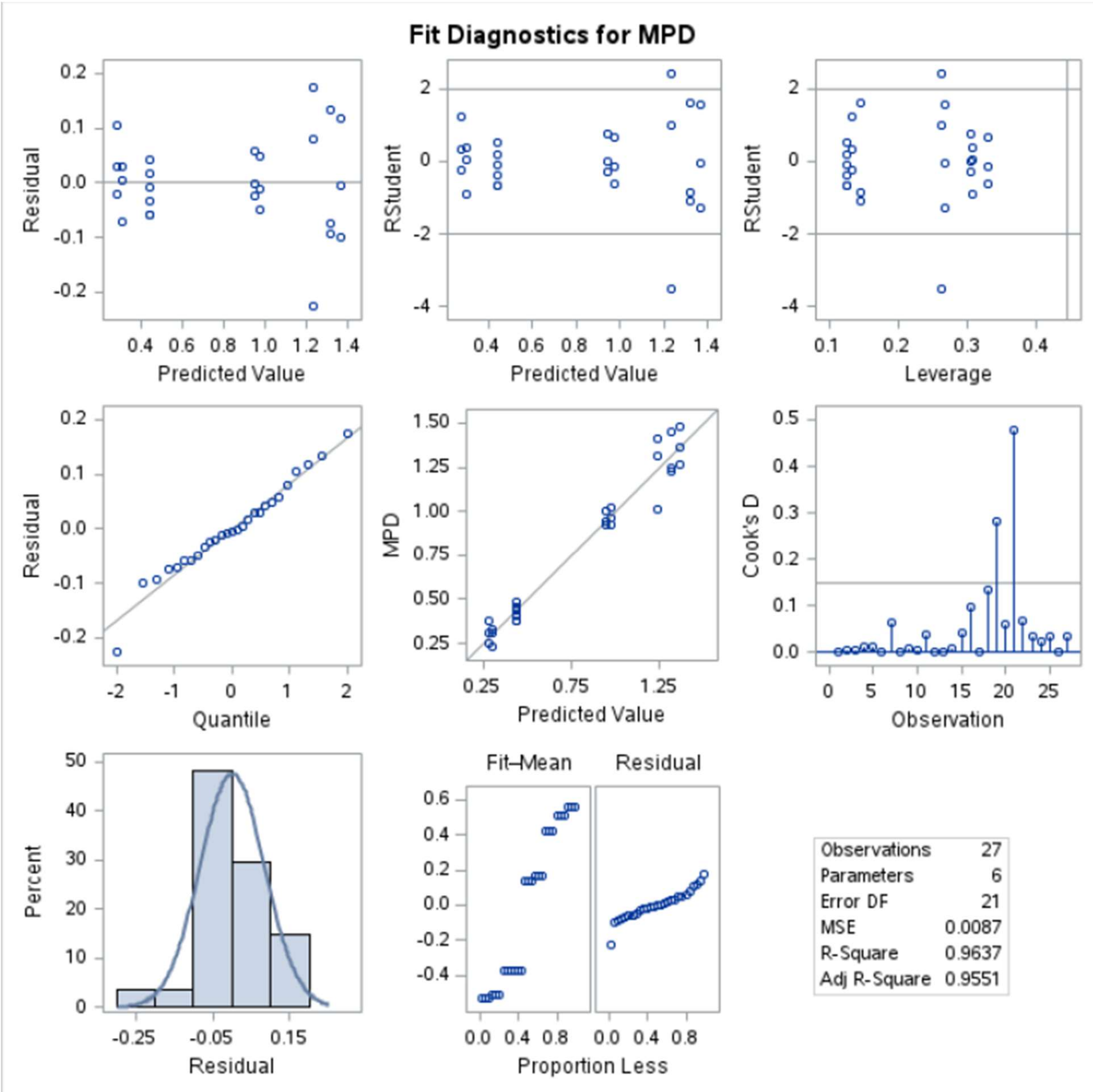

Figure 4.15: MPD diagnostic plot

The response surface plots indicate that MPD varies nonlinearly with the variables. The plot has a saddle-shaped surface. The stationary point, located at R#3/8 = 18.46% and P#200 = 5.17%, corresponds to a predicted MPD of 0.034 in. (0.852 mm). Eigenvalues of opposing signs (+0.222 and −0.158) were obtained using eigen analysis of the second-order coefficient matrix. The point indicates that it is a saddle point rather than a maximum or minimum point. The graph indicates that MPD increases in one direction and decreases in another, and therefore, no optimal solution exists within the interior of the design space. The contour plot further shows that higher

MPD is concentrated in regions with higher coarse aggregate content and lower fine content. The optimal MPD is achieved toward the boundary of the design space rather than at an interior point. The plot concludes that coarse aggregate enhances macrotexture while fines reduce it.

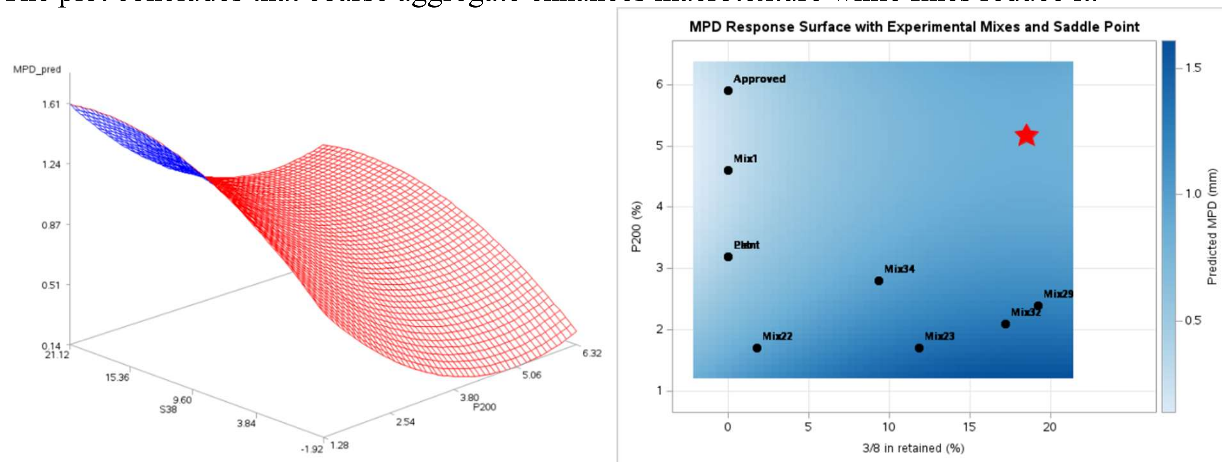

Figure 4.16: MPD 3D surface and contour plot

4.5.2 Permeability Model

A response surface methodology (RSM) approach similar to that used for MPD was initially attempted for permeability (k) using a full second-order model based on the two most strongly correlated predictors, materials retained on the 3/8 in (9.5 mm) sieve (R#3/8) ($r = +0.74$ with log k) and percentage passing US No. 200 (0.075 mm) sieve (P#200) ($r = -0.65$ with log k). However, the lack-of-fit test was highly significant ($F = 240.74$, $p < 0.0001$). Moreover, the Variance Inflation Factor (VIF) exceeded 30 when multiple terms were included, indicating multicollinearity. These results demonstrate that permeability cannot be validly represented as a response surface.

Accordingly, an alternative modeling approach was required. A reduced multiple linear regression model was developed for $\log_{10}(k)$ using four physically independent predictors. The four predictors are Air voids (AV), Percentage retained on a 3/8 in. (9.5 mm) sieve (R#3/8), percentage on US No. 30 (0.6 mm) sieve (R#30), percentage passing No. 200 (4.75 mm) sieve (P#200), and the AV×P#200 interaction term. The interaction term (AV×P#200) was included in the model, thereby increasing R^2 and reducing the root-mean-squared error (RMSE). Permeability is also governed by the interconnected voids, not only by the design air voids. Therefore, the interaction term is important. The fitted model achieved R^2=0.9886 (adjusted R^2=0.9859, RMSE=0.103 log units), and was highly significant overall (F=365.12, p<0.0001).

All five predictors were individually significant. Both R#3/8 (β=+1.225, p<0.0001) and R#30 (β=+1.185, p<0.0001) showed positive effects on permeability, indicating that larger particles tend to open the inter-particle pore structure and allow water to flow. In contrast, materials passing the No. 200 (0.075 mm) sieve (P#200) have a negative effect (β = -3.006, p < 0.0001). The finer particles or dust fill the voids and reduce connectivity. Mixtures with higher air voids at 50 gyrations also tended to contain higher fines content. As a result, the AV coefficient does not fully represent permeability. Therefore, the interaction term (AV × P#200) is added, which has the strongest effect in the model (β = -4.969). This interaction term indicates that fines fill the interconnected voids. Thereby, permeability sharply decreases. In contrast, when AV is high but P#200 is low, the voids are more connected, increasing permeability substantially. This behavior is consistent with the concept that permeability depends not only on total void content but also on whether those voids form a continuous flow network.

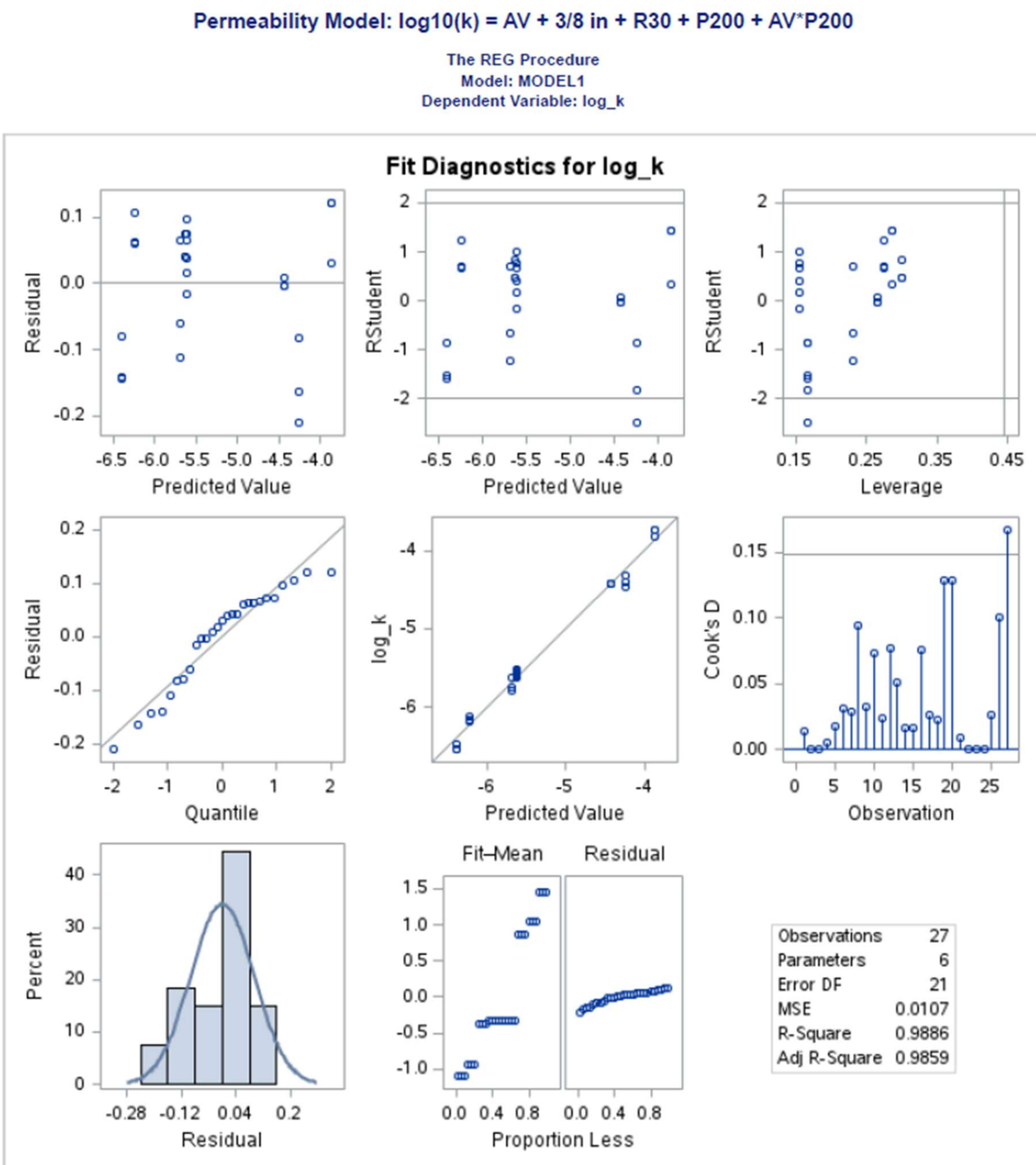

Figure 4.17: Permeability diagnostic plot

The Q-Q plot and residual histogram indicated normality of residuals with minor deviation at the tail. No observation exceeded the Cook's distance threshold of 4/n (0.15), which indicates that no single data point exerted undue influence on the model (Kutner et al., 2005; Montgomery et al., 2012). Because this model contains more than two predictors, it cannot be represented as a conventional three-dimensional response surface. Therefore, it is presented as a regression equation. The Shapiro–Wilk test ($p = 0.039$) indicates a slight deviation from normality. However, the Kolmogorov–Smirnov test did not reject the null hypothesis of normality ($D = 0.150$, $p = 0.116$).

4.5.3 IDEAL-RT Model

As with MPD, a full second-order response surface model was fitted to the Rutting Index. The predictors were air voids (AV) and percentage passing No. 200 (0.075 mm) sieve (P#200). The model indicated that $R^2 = 0.868$, adjusted $R^2 = 0.835$, and RMSE = 16.90. The overall model was highly significant ($F = 27.72$, $p < 0.0001$). The ANOVA confirmed that both the linear ($F = 58.62$, $p < 0.0001$) and quadratic ($F = 9.53$, $p = 0.0011$) terms were statistically significant. However, the interaction term was marginally non-significant ($F = 2.30$, $p = 0.144$). The lack-of-fit test was highly non-significant ($F = 0.13$, $p = 0.879$). Therefore, the second-order polynomial was adopted to represent the response surface.

$$\hat{Y}_{RTIndex} = 108.54 - 8.83X_1 + 22.84X_4 - 61.48X_1X_4 - 25.52X_1^2 + 22.76X_4^2 \tag{4.3}$$

where $X_1 = (AV - 2.735)/1.845$ and $X_4 = (P200 - 3.8)/2.1$.

The Q-Q plot of residuals showed close alignment with the reference line. All four formal normality tests (Shapiro–Wilk $p = 0.295$, Kolmogorov–Smirnov $p > 0.15$, Cramer–von Mises $p > 0.25$, Anderson–Darling $p > 0.25$) failed to reject normality. The residual plots showed random scatter around zero with no systematic patterns. In the Cook's distance plot, no observation exceeded the threshold.

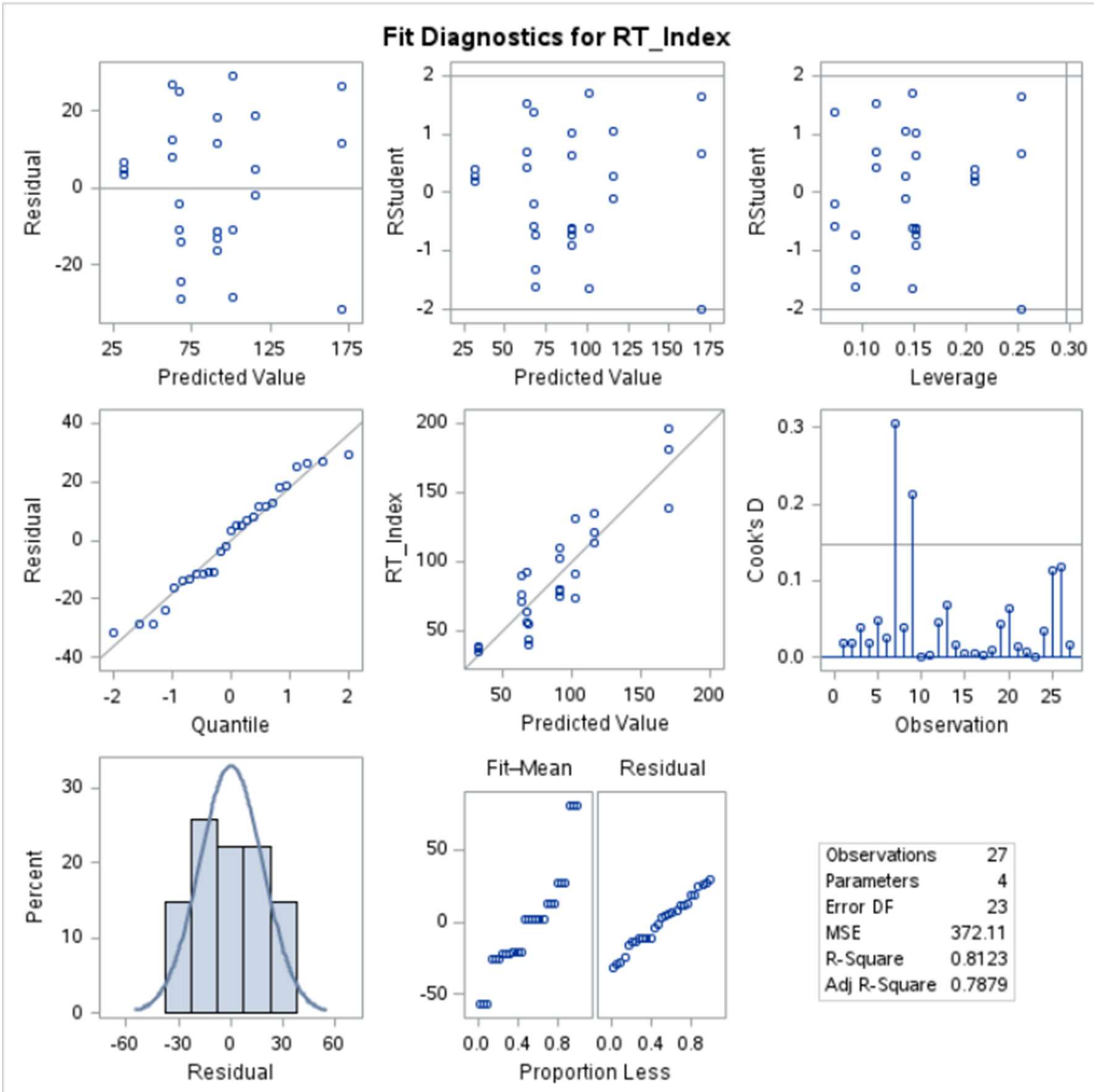

Figure 4.18: IDEAL-RT Index diagnostic plot

To further explain the RTIndex fit, a canonical analysis was performed. In canonical analysis, the stationary point is located at AV = 3.05% and P#200 = 3.20%, with a predicted RT Index of 104.5. Eigenanalysis yielded +36.89 and −40.66; the opposite signs indicate the stationary point is a saddle rather than a true maximum or minimum. This indicates that the RT Index response surface exhibits opposing curvature in two perpendicular directions, similar to MPD. The saddle point, therefore, represents a trade-off region in the mix design area rather than an optimum. The results indicate that the effect of AV and P#200 on rutting resistance is not uniform across the design. Instead, the RT Index changes differently depending on the combination of the two variables. Higher rutting resistance occurs in the regions associated with relatively high fine content and moderately low air voids. In contrast, a lower RTIndex was observed when high air voids were combined with low fine materials. RSM results indicate that densely graded and well-compacted mixtures, where sufficient fine materials and low air voids are present, contribute to a stiffer internal structure and improved resistance to permanent deformation.

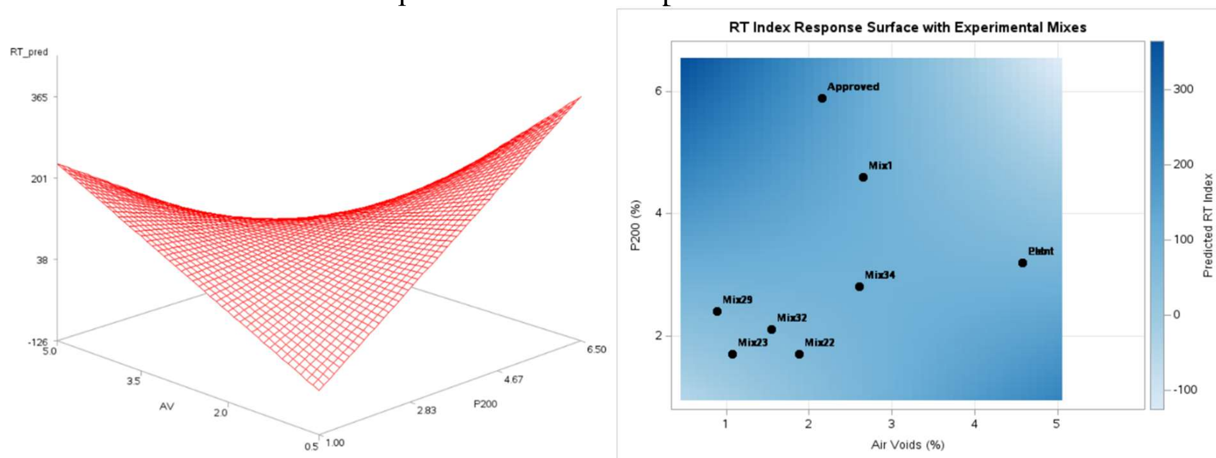

Figure 4.19: IDEAL-RT Index surface and contour plot

These three models show that different mechanisms control each performance. MPD and RT Index could both be well described by two-variable response surface models, and both showed saddle-point behavior. The fitted RSM model indicates that improving one variable of the mix can reduce performance in another. Permeability behaved differently. Only two variables could not explain it, because it depends on the internal void structure of the mix, not just surface gradation. Therefore, permeability was studied using multiple linear regression with five predictors. The MPD response surface identified a saddle point at 3/8 in (9.5 mm) = 18.46% and P#200 = 5.17%, while the RT Index response surface saddle point at AV = 3.05% and P200 = 3.20%. Achieving high MPD requires high coarse aggregate content (approximately 17–19%), while achieving high RT Index requires moderate air voids (approximately 2–3%) with moderate fines. The results indicated that the models suggested a balanced combination of coarse aggregate content (17-19%), air voids (2-3%), and fines (3-5%) is needed to achieve good texture, low permeability, and strong rutting resistance simultaneously.

4.5.4 Optimization

To identify the optimal mix design that simultaneously satisfies all three performance criteria, a constrained multi-response optimization was performed using Derringer's desirability function (Derringer & Suich, 1980). The threshold was MPD ≥ 0.039 in. (1.0 mm) (adequate surface macrotexture), k ≤ 1.97 × 10^{-5} in./s (5 × 10^{-5} cm/s) (acceptable impermeable range), and RT Index ≥ 65 (acceptable rutting resistance for PG 70-XX). A four-dimensional grid of approximately 761,000 candidate mixes was generated across the experimental ranges of AV, R#3/8, R#30, and P#200, and the three fitted models were used to predict each response at every grid point. Candidates failing any threshold were disqualified. The overall desirability (D) was computed as the geometric mean of the three individual desirability scores and was used to rank the remaining feasible candidates. Figure 4.20 shows the pass/fail results for each of the nine experimental mixes against the three thresholds. Mix 32 (Venture 5/8") was the only mix that could simultaneously pass all three thresholds. Mix 32 reported MPD = 0.051 in. (1.306 mm), k = 1.47 × 10^{-5} in./s (3.73 × 10^{-5} cm/s), and RT Index = 70.3. The mathematical optimum located at AV = 1.99%, R#3/8 = 7.5%, R#30 = 8.4%, and P#200 = 1.7%. The optimal predicted performance is MPD = 0.048 in. (1.23 mm), k = 4.21 × 10^{-6} in./s (1.07 × 10^{-5} cm/s), and RT Index = 82.0 (Figure 4.20). The feasible region forms a narrow diagonal band in the low-AV, low P#200, moderate R#3/8 corner of the design area. The design area confirms that no single variable can be optimized independently.

Pass/Fail Check for Each of Your 9 Mixes
MPD>=0.039 in., k<=1.97E-05 in./s, RT>=65

MixDesign	PrimaryAgg	AV	S38	R30	P200	MPD	k	RT_Index	pass_MPD	pass_k	pass_RT	result
Approved	Approved	2.16	0.0	16.7	5.9	0.011	2.72178E-07	172.2	0	1	1	FAIL
Lab	Lab	4.58	0.0	15.6	3.2	0.016	1.10892E-06	96.4	0	1	1	FAIL
Mix1	CS-2A	2.65	0.0	16.8	4.6	0.012	1.18766E-07	122.9	0	1	1	FAIL
Mix22	Dolese	1.88	1.8	9.3	1.7	0.038	1.04987E-06	79.0	0	1	1	FAIL
Mix23	TrapRock	1.07	11.8	9.0	1.7	0.054	7.61155E-07	36.6	1	1	0	FAIL
Mix29	Limestone	0.89	19.2	10.9	2.4	0.049	6.71916E-05	45.7	1	0	0	FAIL
Mix32	Venture	1.55	17.2	8.2	2.1	0.051	1.46982E-05	70.3	1	1	1	ALL PASS
Mix34	Huber	2.61	9.3	11.8	2.8	0.038	1.58793E-05	98.1	0	1	1	FAIL
Plant	Plant	4.58	0.0	15.6	3.2	0.018	9.94751E-07	77.9	0	1	1	FAIL

Figure 4.20: Pass/fail results for all nine experimental mixes against three thresholds

Mathematical Optimum (MPD>=0.039 in., k<=1.97E-05 in./s, RT>=65)

AV	S38	R30	P200	MPD_pred	k_pred	RT_pred	d_MPD	d_k	d_RT	D	pass_all
1.99	7.5	8.4	1.7	0.048	4.20053E-06	82.0	0.453	0.249	0.126	0.242	1

Figure 4.21: Mathematically optimum mix identified by constrained multi-response optimization

The statistical analysis showed that distinct physical mechanisms govern the three bridge deck overlay properties, so each response required a different model. Surface macrotexture (MPD) and rutting resistance (RT Index) were both modeled using second-order response surface models. The saddle-shaped response surfaces showed trade-offs among gradation and volumetric variables, indicating that improving one variable condition can reduce another. Permeability behaved differently because it depends more on the connected internal void structure of the mix than on the two surface-related variables. Therefore, permeability was studied using a multiple linear regression model. Moreover, the multi-response optimization showed that only Mix 32 (Venture 5/8) satisfied all three performance requirements simultaneously. The optimization threshold is MPD $\geq$ 0.039 in. (1.0 mm), k $\leq 1.97 \times 10^{-5}$ in./s (5×10^{-5} cm/s), and RT Index $\geq$ 65. The mathematical optimum was found at AV = 1.99%, R#3/8 = 7.5%, R#30 = 8.4%, and P#200 = 1.7%. Overall, the narrow feasible region in the design space shows that bridge deck overlay mix design requires a careful balance of coarse aggregate, fines, and air voids, rather than trying to improve only one variable at a time. These findings suggest that traditional dense-graded mixes are not suitable for bridge deck overlays without modification. The recommended coarse aggregate and fine particle gradations are consistent with the general open-graded friction concept used by agencies such as Georgia DOT and Florida DOT. The DOTs emphasize coarse aggregate structure and very low fines to promote drainage and macrotexture. However, the present study identified a much narrower and denser feasible region than a conventional OGFC. Because Mix 32 (Venture 5/8”) satisfied all three performance thresholds at R#3/8 = 17.2% and P#200 = 2.1%, the results suggest that Kansas bridge deck overlay specifications may need a hybrid design approach.

Chapter 5 Conclusions and Recommendations

5.1 Conclusions

This study evaluated asphalt mixtures for bridge deck applications with respect to surface texture, permeability, and rutting resistance. Several mixtures were tested using the Laser Texture Scanner (LTS), the permeameter, the IDEAL-RT setup, and the Hamburg Wheel Tracking Device (HWTD). Analysis of the test results led to the following conclusions.

- The most promising five mixtures achieved MPD values of about 0.039 in. (1 mm) or higher. The LTS results showed that the Trap Rock–Dolese and Venture 5/8” aggregate mixtures had the highest macrotexture, ranging from 0.055 to 0.071 in. (1.4 to 1.8 mm). In contrast, the Dolese and Huber 3/4” aggregate mixtures showed lower texture than the other mixtures. However, all five aggregates can increase the MPD value of the mix from 0.012 in. (0.3 mm) to 0.039 in. (1 mm) due to coarser aggregates.
- Based on the permeability test results, mix design Dolese and Trap Rock–Dolese fell within the impermeable range. Mix designs with Venture 5/8” and Huber 3/4” aggregates indicated low permeability coefficients; however, their coefficients remain within the range of 0 to 1.97×10^{-5} in./s (0 to 5×10^{-5} cm/s). In contrast, the limestone aggregate mixture had the highest permeability and did not meet the impermeability criteria due to coarse aggregate content.
- IDEAL-RT test results showed that the Huber 3/4” aggregate mixture had the highest IDEAL-RT index, followed by the Dolese aggregate mixture. While the Trap Rock–Dolese and Limestone mix designs had relatively low IDEAL-RT indices, their design air voids and dust-to-binder (D/B) ratios were much lower than those of the other three mix designs. HWTD also validated the IDEAL-RT test results. The HWTD results indicated that none of the candidate mixtures reached the target value of 15,000 wheel passes at 0.5 in. (12.5 mm) rut depth. Among the mix designs, Venture 5/8” aggregate and Huber 3/4” aggregate had the highest wheel passes, whereas the Trap Rock–Dolese mixture had the lowest. These results indicate that the 5/8” Venture and 3/4” Huber aggregate mixes demonstrated better rutting resistance in the HWTD and IDEAL-RT

tests. However, all mixtures remained below the specified highway mix criterion in the HWTD tests.

- Overall, no mixture performed the best across all three performance parameters. Trap Rock–Dolese aggregate mixture provided high texture and low permeability, but poor rutting resistance. The limestone aggregate mixture was the least favorable because its structure produced higher permeability and lower rutting resistance. Although the Huber ¾" aggregate mix design passed all criteria except MPD ≥ 0.039 in. (1 mm), which was about 2.6% lower than the target MPD. Based on the combined results, the mixtures with Venture 5/8" aggregates provided balanced overall performance.
- Statistical analysis using Response Surface Methodology (RSM) and constrained multi-response optimization quantified the relationships between mix design variables (AV, R#3/8, R#30, and P#200) and the three performance responses (MPD, k, and RT Index). Among the nine experimental mixtures, only the Venture 5/8" aggregate mixture simultaneously satisfied all three performance thresholds (MPD ≥ 0.039 in. (1.0 mm), $k \leq 1.97 \times 10^{-5}$ in./s (5×10^{-5} cm/s), RT Index ≥ 65), confirming it as the best-balanced mixture for bridge deck overlay applications. The mathematical optimum identified within the design space (AV = 2.0%, R#3/8 = 7–17%, R#30 = 8.4%, P#200 < 2.5%) also indicated that achieving all three performance targets simultaneously requires a coarse, near-gap-graded mixture with low fines and air voids.
- Conventional dense-graded Superpave mixtures (Plant, Lab, Approved, and the Mix design 1) failed to meet the MPD threshold due to insufficient coarse aggregate content, while open-graded mixtures with excessive coarse aggregate (Limestone) failed the permeability. These results confirm that typical highway surface mix designs are not directly transferable to bridge deck overlay applications and must be modified toward a hybrid composition combining moderate-to-high coarse aggregate content, low fines, and carefully controlled air voids.

5.2 Recommendations

Based on this study, the following recommendations are made:

- Since none of the mixtures satisfied the HWTD requirement of 15,000 wheel passes at 0.5 in. (12.5 mm) rut depth for highway mixes, further improvement in rutting resistance is needed before final mixture selection for bridge deck applications. Although Venture 5/8" aggregate mixture showed promising results in three performances, it could not be compacted properly at 7% air voids. Future studies should investigate its gradation and mixture stability in more detail to determine whether it can be produced and compacted reliably for field application.
- Future studies should also evaluate other important performance properties, such as bond behavior, cracking resistance, chloride resistance, and long-term durability, because these are critical for bridge deck wearing surface courses in Kansas. A suitable bridge deck mixture must not only provide adequate texture, low permeability, and rutting resistance, but also maintain strong bonding, resist reflective and thermal cracking, limit chloride penetration from deicing salts, and perform well under long-term environmental and traffic loading.

References

Ahmad, A. S. (2011). Bridge preservation guide: Maintaining a state of good repair using cost-effective investment strategies (FHWA-HIF-11-042). Federal Highway Administration.

American Association of State Highway and Transportation Officials. (2020). AASHTO LRFD bridge design specifications (9th ed.).

American Road & Transportation Builders Association (ARTBA). (2024). Kansas bridge report. https://artbabridgereport.org/state/profile/KS

American Society of Civil Engineers. (2021). *2021 report card for America's infrastructure: Bridges*.

Ames Engineering. (2024). *Rapid Laser Texture Scanner 9500.* Ames Engineering.

Asphalt Institute. (2024, May 27). Reflective cracking relief interlayer for composite pavements. Asphalt Magazine. https://www.asphaltmagazine.com/reflective-cracking-relief-interlayer-for-composite-pavements/

ASTM International. (2018). *Standard test method for measuring surface frictional properties using the British pendulum tester (ASTM E303-93(2018)).* ASTM International, West Conshohocken, PA.

ASTM International. (2021). ASTM D8360-21, Standard test method for determination of asphalt mixture rutting resistance using the indirect tensile rutting test (IDEAL-RT).

ASTM International. (2023). ASTM E1845-23, Standard practice for calculating pavement macrotexture mean profile depth.

ASTM International. (2024). ASTM E965-15(2024), Standard test method for measuring pavement macrotexture depth using a volumetric technique.

Babaei, K., & Hawkins, N. M. (1987). Evaluation of bridge deck protective strategies (NCHRP Report 297). Transportation Research Board.

Bear, J. (1972). *Dynamics of fluids in porous media*. Dover Publications.

Bennert, T., Sheehy, M., Blight, R., & Gresavage, J. (2015). Bridge deck wearing surface course. In *Application of asphalt mix performance-based specifications* (TRB E-Circular E-C189). Transportation Research Board.

Bennert, T., & Pezeshki, D. (2015). *Performance testing for HMA quality assurance* (FHWA-NJ-2015-010). Rutgers Center for Advanced Infrastructure and Transportation; New Jersey Department of Transportation.

Blankenship, P. E. (2007). Reflective cracking relief interlayer for composite pavements. Asphalt.

Bollendorf, E. (2021). Bridge deck thermography: Revisiting “bridges freeze before roadway” from a safe salt perspective [Poster presentation, Minnesota State University Undergraduate Research Symposium].

Bukovatz, J. E. (1984). Kansas’ experience with interlayer membranes on salt-contaminated bridge decks. Transportation Research Record, 962, 67–74.

California Department of Transportation. (2013). Division of design policy updates: Approval delegations [Memorandum]. https://dot.ca.gov/-/media/dot-media/programs/design/documents/2013-06-07-division-of-design-policy-updates-a11y.pdf

Carman, P. C. (1937). Fluid flow through granular beds. *Transactions, Institution of Chemical Engineers, 15*, 150–166.

Chavel, B. (2022). Steel bridge design handbook: Chapter 17, bridge deck design—American Institute of Steel Construction.

Chen, S., Liu, X., Luo, H., Yu, J., Chen, F., Zhang, Y., Ma, T., & Huang, X. (2022). *A state-of-the-art review of asphalt pavement surface texture and its measurement techniques*. Journal of Road Engineering, 2(2), 156–180. https://doi.org/10.1016/j.jreng.2022.05.003

Cooley, L. A., Jr., & Brown, E. R. (2000). Selection and evaluation of field permeability device for asphalt pavements. *Transportation Research Record, 1723*, 73–82. https://doi.org/10.3141/1723-10

Cooley, L. A., Jr., Brown, E. R., & Maghsoodloo, S. (2001). Development of critical field permeability and pavement density values for coarse-graded Superpave pavements (NCAT Report 01-03). National Center for Asphalt Technology, Auburn University.

Cooley, L. A., Jr., Prowell, B. D., & Brown, E. R. (2002). Issues about the permeability characteristics of coarse-graded Superpave mixes (NCAT Report 02-06). National Center for Asphalt Technology, Auburn University.

Corun, R. (2020, January 22). Polymer-modified bridge deck waterproof surface mix [Conference presentation]. Pennsylvania Asphalt Pavement Association 60th Annual Paving Conference, Hershey, PA.

Darwin, D., Browning, J., O'Reilly, M., & Xing, L. (2020). *Survey of bridge decks in Kansas and assessment of deterioration*. Kansas Department of Transportation.

Derringer, G., & Suich, R. (1980). Simultaneous optimization of several response variables. *Journal of Quality Technology, 12*(4), 214–219. https://doi.org/10.1080/00224065.1980.11980968.

ElBatanouny, M. K., Hawkins, K. A., Abdelrahman, M. A., Lawler, J. S., Nelson, T. D., & Krauss, P. D. (2022). *Guide to remediate bridge deck cracking* (Report No. TR-782)—Iowa Department of Transportation.

Federal Highway Administration. (1978). Latex-modified concrete overlay for bridge decks (FHWA-RD-78-035).

Federal Highway Administration. (2006). Freeze-thaw resistance of concrete with marginal air content (FHWA-HRT-06-117).

Federal Highway Administration. (2011). A guide to cost-effective bridge preservation (FHWA-HRT-11-017).

Federal Highway Administration. (2014a). *Assessment of LTPP friction data*. U.S. Department of Transportation.

Federal Highway Administration. (2014b). Long-term bridge performance: high-priority bridge performance issues (FHWA-HRT-14-043).

Federal Highway Administration. (2017). FHWA LTBP summary: Current information on the use of overlays and sealers (FHWA-HRT-16-079). https://www.fhwa.dot.gov/publications/research/infrastructure/structures/bridge/16079/index.cfm.

Federal Highway Administration. (2019). Concrete pavement texturing (FHWA-HIF-17-011).

Federal Highway Administration. (2022a). High-friction surface treatment site selection and installation guide.

Federal Highway Administration. (2022b). Laser texture scanner (LTS). Mobile Asphalt Technology Center.

Federal Highway Administration. (2022c). Service life design reference guide (FHWA-HIF-22-052).

Federal Highway Administration. (2023). Peer exchange report on corrosion prevention and mitigation for highway bridges (FHWA-HIF-23-064).

Federal Highway Administration (FHWA). (2025). National Bridge Inventory: Owner-based bridge tables.

Florida Department of Transportation. (2003). Section 334: Superpave asphalt concrete.

Florida Department of Transportation. (2015). FM 5-565: Measurement of water permeability of compacted asphalt paving mixtures.

Gao, C., & Fam, A. (2024). Fatigue behavior of reinforced concrete bridge decks under moving wheel loads: A state-of-the-art review. Journal of Bridge Engineering, 29(11), 03124003.

Giles, C. G. (1969). The nature of tire-road friction. Wear, 14(2), 223–239.

Gillespie, T. D. (1992). Fundamentals of vehicle dynamics. Society of Automotive Engineers.

Gode, K., & Paeglitis, A. (2014). Concrete bridge deterioration caused by de-icing salts in high traffic volume road environment in Latvia. The Baltic Journal of Road and Bridge Engineering, 9(3), 200–207.

Hall, J. W., Smith, K. L., Titus-Glover, L., Wambold, J. C., Yager, T. J., & Rado, Z. (2009). Guide for pavement friction (NCHRP Report 640). Transportation Research Board.

Haynes, M. A., Coleri, E., Sreedhar, S., & Obaid, I. A. (2020). Bridge deck asphalt concrete pavement armoring (FHWA-OR-RD-20-04; SPR 815). Oregon Department of Transportation.

Hanson, D. I., & Prowell, B. D. (2004). *Evaluation of Circular Texture Meter for Measuring Surface Texture of Pavements*. NCAT Report 04-05. National Center for Asphalt Technology, Auburn University.

Henry, J. J. (2000). Evaluation of pavement friction characteristics (NCHRP Web Document 35). Transportation Research Board.

Hu, N., Haider, S. W., & Burgueño, R. (2013). Development and validation of deterioration models for concrete bridge decks—Phase 2: Mechanics-based degradation models (RC-1587B; CEE-RR-2013/02). Michigan State University/Michigan Department of Transportation.

International Organization for Standardization. (2019). ISO 13473-1:2019, Characterization of pavement texture by use of surface profiles—Part 1: Determination of mean profile depth.

Izeppi, E. de León, Flintsch, G. W., & McGhee, K. K. (2010). Field performance of high friction surfaces (VTRC 10-CR6). Virginia Transportation Research Council.

Keeney, J. N. (2017). *Evaluation of the circular texture meter for measuring pavement surface texture* (Master's thesis, Virginia Polytechnic Institute and State University). Virginia Tech.

Koch, G. H., Brongers, M. P. H., Thompson, N. G., Virmani, Y. P., & Payer, J. H. (2002). *Corrosion cost and preventive strategies in the United States* (Report No. FHWA-RD-01-156): Federal Highway Administration, U.S. Department of Transportation.

Kutner, M. H., Nachtsheim, C. J., Neter, J., & Li, W. (2005). *Applied linear statistical models* (5th ed.). McGraw-Hill/Irwin.

Lane, S., & Jalinoos, F. (2017). FHWA LTBP summary: Current information on the use of overlays and sealers. Federal Highway Administration. https://www.fhwa.dot.gov/publications/research/infrastructure/structures/bridge/16079/index.cfm

Lenth, R. V. (2009). Response-surface methods in R, using rsm. *Journal of Statistical Software*, 32(7), 1–17. https://doi.org/10.18637/jss.v032.i07

Li, S., Noureldin, S., & Zhu, K. (2010). *Macrotexture and microtexture testing using laser sensors*. Joint Transportation Research Program, Purdue University. https://doi.org/10.5703/1288284314251

Luo, X., Hu, S., Zhou, F., Crockford, W., & Karki, P. (2022). *Simple asphalt mixture shear rutting test and mechanical analysis*—Journal of Materials in Civil Engineering.

Maupin, G. W., Jr. (2003). Additional asphalt to increase impermeability of selected Virginia mixes (VTRC 03-R15). Virginia Transportation Research Council.

Meggers, D. A. (1998). Crack sealing and repair of older serviceable bridges using polymer sealers (Report No. FHWA-KS-98-4)—Kansas Department of Transportation, Materials and Research Center.

Montgomery, D. C., Peck, E. A., & Vining, G. G. (2012). *Introduction to linear regression analysis* (5th ed.). John Wiley & Sons.

Myers, R. H., Montgomery, D. C., & Anderson-Cook, C. M. (2016). *Response surface methodology: Process and product optimization using designed experiments* (4th ed.). Wiley.

National Academies of Sciences, Engineering, and Medicine. (2017). Control of concrete cracking in bridges (NCHRP Synthesis 500). The National Academies Press.

National Transportation Safety Board. (2024). *Maintenance and oversight failures led to 2022 Fern Hollow Bridge collapse*.

New Jersey Department of Transportation. (2018, August 8). *2018 standard input changes to the 2015 standard specifications for road and bridge construction: Section 504—Bridge deck waterproof surface course (BDWSC)* (BDC17S-05)—State of New Jersey.

New York State Department of Transportation. (2015). Waterproofing bridge deck hot mix asphalt (HMA) overlay (Item 402.90720208 F2 / 402.90730208 F3).

New York State Department of Transportation. (2024). Waterproofing bridge deck overlay (WBDO) (EB 24-040).

New York State Department of Transportation. (2025). Comprehensive pavement design manual (Chapter 6).

Okada, K., Okamura, H., & Sonoda, K. (1978). Fatigue failure mechanism of reinforced concrete bridge deck slabs. Transportation Research Record, 664, 136–144.

PIARC (World Road Association). (2015). *Road surface characteristics and skid resistance.*

Pulugurtha, S. S. (2008). Relationship between pavement macrotexture and crash incidences on North Carolina roads (FHWA/NC/2007-12). North Carolina Department of Transportation.

Rahman, F., Flintsch, G., & Dawson, A. (2014). Review and analysis of Hamburg wheel tracking device testing for asphalt concrete (VCTIR 14-R6). Virginia Center for Transportation Innovation and Research.

Rahman, F., & Hossain, M. (2014). Review and analysis of Hamburg wheel tracking device test data (KS-14-1). Kansas State University Transportation Center.

Russell, H. G. (2012). Waterproofing membranes for concrete bridge decks (NCHRP Synthesis 425). Transportation Research Board.

Reed, J. (2013). History of polymer overlays in Kansas. Joint Midwestern Bridge Preservation Partnership.https://pavementvideo.s3.amazonaws.com/2013_JointMidwest_Bridge/PDF/17%20-%20Polymer%20Overlays%20in%20Kansas%20-%20Reed.pdf

SAS Institute Inc. (2018). *SAS/STAT® 15.1 user's guide: The RSREG procedure*. SAS Institute Inc.

Sprinkel, M. M., & Özyıldırım, C. (2007). Investigation of materials for thin bonded overlays on bridge decks (FHWA/VTRC 07-R17). Virginia Transportation Research Council.

Tabatabai, H., Sobolev, K., Ghorbanpoor, A., Nabizadeh, A., Lee, C.-W., & Lind, M. (2016). Evaluation of thin polymer overlays for bridge decks. University of Wisconsin–Milwaukee / Wisconsin Highway Research Program.

Texas Department of Transportation. (2019). Tex-242-F: Hamburg wheel-tracking test.

Thomas, J., Rahman, F., & Hossain, M. (2013). *Investigation of aged hot-mix asphalt pavements* (Report No. K-TRAN: KSU-09-2). Kansas State University Transportation Center. https://rosap.ntl.bts.gov/view/dot/26450

Transportation Research Board (TRB). (1974). Corrosion and Kansas bridges. Transportation Research Record, 500.

Varamini, S., Tighe, S., Baaj, H., Esenwa, M., Kucharek, A. S., & Kennedy, M. (2019). Development and field experience of performance-based low-permeability asphalt mixture used to overlay bridge decks. *Proceedings of the Canadian Technical Asphalt Association*.

Virginia Transportation Research Council. (2022). Pavement friction management program demonstration—Virginia (VTRC 22-R14). Virginia Transportation Research Council.

Virmani, Y. P., Clemena, G. G., & Schutt, J. D. (2004). *Long-term performance of epoxy-coated reinforcing steel in Virginia bridge decks* (FHWA-HRT-04-090): Federal Highway Administration, U.S. Department of Transportation.

Washington State University Transportation Research Program & TriDurLE Research Initiative. (2022). Development of IDEAL-RT rutting criteria aligned with Hamburg wheel tracking performance [TriDurLE report]. https://wpcdn.web.wsu.edu/wp-voiland/uploads/sites/2442/2024/09/TriDurLE-report_asphalt-mix-durability.pdf

West, R., Timm, D., Willis, J. R., Powell, B., Tran, N., Watson, D., Sakhaeifar, M., Brown, R., Robbins, M., Nordbeck, A. V., Leiva-Villacorta, F., Guo, X., & Nelson, J. (2012). (NCAT Report 12-10). National Center for Asphalt Technology, Auburn University.

Williams, S. G., Schmitt, R. L., Buss, A., & Rindt, C. (2010). Development of in-place permeability criteria for HMA pavement in Wisconsin (WisDOT Highway Research Project 06-02). Wisconsin Department of Transportation.

Willis, J., Timm, D., & Kluttz, R. (2016). Performance of a highly polymer-modified asphalt binder test section at the National Center for Asphalt Technology Pavement Test Track. Transportation Research Record: Journal of the Transportation Research Board, 2575, 1–9. https://doi.org/10.3141/2575-01

Wu, Z., & King, B. (2012). Development of surface friction guidelines for LADOTD (FHWA/LA.11/485). Louisiana Transportation Research Center.

Yildirim, Y., Jayawickrama, P. W., Hossain, M. S., Alhabshi, A., Yildirim, C., Smit, A. F., & Little, D. N. (2006). Hamburg wheel-tracking database analysis (FHWA/TX-05/0-1707-7). Texas Department of Transportation.

Yin, F., Chen, C., West, R., Epps Martin, A., & Arambula-Mercado, E. (2020). Determining the relationship among Hamburg wheel-tracking test parameters and correlation to field performance of asphalt pavements. *Transportation Research Record: Journal of the Transportation Research Board, 2674*(4), 281–291. https://doi.org/10.1177/0361198120912430

Zahir, M., Flintsch, G. W., de León Izeppi, E., & Katicha, S. W. (2017). Friction management on Kansas Department of Transportation pavements (KSU Report No. KSU-14-5). Kansas State University, Kansas Department of Transportation.

Zhou, F., Scullion, T., & Sun, L. (2020). Development and application of the IDEAL rutting test for asphalt mixtures. Texas A&M Transportation Institute.

Zhuo, W., Yan, Q., Yang, Z., Lin, S., Lin, K., & He, F. (2019). Chloride penetration in coastal concrete structures: Field investigation and model development. Advances in Materials Science and Engineering, 2019, Article No. 4537283.